

University of Alberta

**Development of New Wear-resistant Material:
TiNi-based composite**

by Haizhi Ye



A thesis submitted to the Faculty of Graduate Studies and Research in partial fulfillment
of the requirements for the degree of Doctor of Philosophy

in

Materials Engineering

Department of Chemical and Materials Engineering

Edmonton, Alberta

Fall 2002



National Library
of Canada

Acquisitions and
Bibliographic Services

395 Wellington Street
Ottawa ON K1A 0N4
Canada

Bibliothèque nationale
du Canada

Acquisitions et
services bibliographiques

395, rue Wellington
Ottawa ON K1A 0N4
Canada

Your file Votre référence

Our file Notre référence

The author has granted a non-exclusive licence allowing the National Library of Canada to reproduce, loan, distribute or sell copies of this thesis in microform, paper or electronic formats.

The author retains ownership of the copyright in this thesis. Neither the thesis nor substantial extracts from it may be printed or otherwise reproduced without the author's permission.

L'auteur a accordé une licence non exclusive permettant à la Bibliothèque nationale du Canada de reproduire, prêter, distribuer ou vendre des copies de cette thèse sous la forme de microfiche/film, de reproduction sur papier ou sur format électronique.

L'auteur conserve la propriété du droit d'auteur qui protège cette thèse. Ni la thèse ni des extraits substantiels de celle-ci ne doivent être imprimés ou autrement reproduits sans son autorisation.

0-612-81286-3

Canada

University of Alberta

Library Release Form

Name of Author: Haizhi Ye

Title of Thesis: Development of new wear-resistant material: TiNi-based composite

Degree: Doctor of Philosophy

Year this Degree Granted: 2002

Permission is hereby granted to the University of Alberta Library to reproduce single copies of this thesis and to lend or sell such copies for private, scholarly or scientific research purpose only.

The author reserves all other publication and other rights in association with the copyright in the thesis, and except as herein before provided, neither the thesis nor any substantial portion thereof may be printed or otherwise reproduced in any material form whatever without the author's prior written permission.



Haizhi Ye

Apt. 4-11, 6th Building

52 Middle Section, Jiu Li Di Road

Chengdu City, Sichuan Province


P. R. China 610031

2002, 04, 22

University of Alberta

Faculty of Graduate Studies and Research

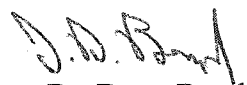
The undersigned certify that they have read, and recommend to the Faculty of Graduate Studies and Research for acceptance, a thesis entitled Development of new wear-resistant material: TiNi-based composite submitted by Haizhi Ye in partial fulfillment of the requirements for the degree of Doctor of Philosophy in Materials Engineering.


Dr. Dongyang Li


Dr. Reg Eadie


Dr. Douglas Ivey


Dr. Don Raboud


Dr. Doug Boyd

The thesis was approved by
Committee on March 28, 2002

Abstract

Key words: TiNi, Composite, Pseudoelasticity, Wear

In this research, a new type of wear-resistant composite was developed using a TiNi alloy as the matrix reinforced by hard TiC or TiN particles. Due to its pseudoelasticity and good wear resistance, the TiNi alloy is a desirable matrix for high-performance composites. The TiNi-based composite was fabricated using a vacuum sintering process. The effects of powder metallurgy processing and hard particles on the microstructure and mechanical properties of the composite were studied. It has been demonstrated that the TiNi alloy matrix composite can be obtained by sintering elemental Ti and Ni powders with the hard TiC or TiN particles. However, high porosity is typical for such a sintered composite. 52 vol% was found to be the best fraction for TiC particles, and 1500°C and 6 hours were the optimum sintering parameters for making such a composite. Even with high-density porosity, the sintered TiNi-based composite showed a wear resistance that is about three orders of magnitude higher than that of 304 stainless steel, one order of magnitude higher than that of a Ti-51at%Ni alloy, and comparable to that of WC/NiCrBSi, a commercial hardfacing material. In order to further improve the composite's wear resistance, the effects of porosity on the composite's mechanical properties and wear resistance were investigated, and accordingly, hot isostatic pressing (HIP) was used to reduce the porosity of the composite for enhanced wear resistance. Finally, the pseudoelasticity of the TiNi matrix in the composite and corresponding phase transformation were investigated, using nano-indentation, differential scanning calorimetry (DSC), X-ray diffraction (XRD) and transmission electron microscopy

(TEM) techniques, respectively. It was demonstrated that a reversible R-phase transformation induced by the wearing stress was mainly responsible for the pseudoelasticity of the composite. The pseudoelasticity of the composite affected its wear performance over a relatively wide temperature range.

Acknowledgement!

During my studies and research, I have obtained painstaking instructions from my supervisors Dr. Dongyang Li and Dr. Reg Eadie. In addition, Natural Science and Engineering Research Council of Canada (NSERC) and Syncrude Canada Ltd. have offered financial support for this project. I deeply appreciate these help!

Table of Contents

Chapter 1. Introduction

| | |
|------------------------------------------------------------------------|----|
| 1. 1. Wear of material | 1 |
| 1. 1. 1. Mechanical wear modes and mechanisms..... | 4 |
| 1. 1. 1. 1. Abrasive wear | 4 |
| 1. 1. 1. 2. Adhesive wear | 7 |
| 1. 1. 1. 3. Erosive wear | 9 |
| 1. 1. 1. 4. Surface fatigue wear | 10 |
| 1. 1. 2. Measurement and analysis of wear | 12 |
| 1. 1. 3. Wear-resistant materials..... | 16 |
| 1. 2. Wear behavior and pseudoelasticity of TiNi alloy..... | 23 |
| 1. 2. 1. Mechanical properties and wear behavior of TiNi alloy..... | 23 |
| 1. 2. 2. Phenomena and mechanism of TiNi alloy's pseudoelasticity..... | 25 |
| 1. 2. 3. Mechanism of TiNi alloy's wear behavior..... | 28 |
| 1. 2. 4. The application of TiNi alloy..... | 32 |
| 1. 3. TiNi-based composites and the objective of this research | 33 |
| 1. 3. 1. TiNi composite..... | 33 |
| 1. 3. 2. Objective of the study..... | 34 |

Chapter 2. Development of TiNi-based Composite Using P/M Processing

| | |
|----------------------------------|----|
| 2. 1. Experimental procedure | |
| 2. 1. 1. Materials..... | 36 |
| 2. 1. 2. Sample preparation..... | 38 |

| | |
|--------------------------------------------------------------------------------------------------------|----|
| 2. 1. 3. Specimen structure analysis..... | 39 |
| 2. 1. 4. Mechanical property testing..... | 39 |
| 2. 1. 5. Wear and friction testing..... | 40 |
| 2. 2. Experimental results and discussion | |
| 2. 2. 1. Composition and microstructure..... | 41 |
| 2. 2. 2. Pseudoelasticity and wear behavior of TiNi-based composite..... | 44 |
| 2. 2. 3. Friction behavior of TiNi-based composite..... | 49 |
| 2. 2. 4. The effects of secondary phase particles on the wear behavior of TiNi based composite..... | 53 |
| 2. 2. 4. 1. Effect of TiC fraction on the wear behavior..... | 54 |
| 2. 2. 4. 2. The effect of the reinforcing particle hardness on the wear behavior..... | 56 |
| 2. 2. 5. Processing and wear behavior of TiNi-based composite..... | 61 |
| 2. 2. 6. Wear mechanism of the TiNi-based composite..... | 66 |
| 2. 3. Conclusions..... | 70 |

Chapter 3. Influences of Porosity on Mechanical and Wear Performance of TiNi-based Composites

| | |
|--------------------------------------------------------------------------------------|----|
| 3.1. Experimental procedure | |
| 3. 1. 1. Powder mixing and compaction..... | 75 |
| 3. 1. 2. Sintering of the composite..... | 76 |
| 3. 1. 3. Composition and phase structure analyses of the samples..... | 76 |
| 3. 1. 4. Examination on mechanical properties and wear behavior of TiNi composites.. | 77 |
| 3. 2. Experimental results and discussion | |

| | |
|--------------------------------------------------------------------------------------------------------------------------------------------------|-----|
| 3. 2. 1. Composition and microstructure of the TiNi composite..... | 77 |
| 3. 2. 2. Effects of the sealing of pores on the mechanical properties and wear behavior of the TiNi composite..... | 79 |
| 3. 2. 3. Influence of lubrication in powder mixing and compaction on the mechanical properties and wear behavior of TiNi-based composite..... | 90 |
| 3. 2. 4. Effects of compaction load on the mechanical properties and wear behaviors of the TiNi composite..... | 94 |
| 3. 2. 5. Porosity and processing of the TiNi-based composite..... | 99 |
| 3. 3. Conclusions..... | 101 |

Chapter 4. Improvement in Wear Resistance of TiNi-based Composite by
Hot Isostatic Pressing

| | |
|---------------------------------------------------------------------------------|-----|
| 4. 1. Experimental procedure | |
| 4. 1. 1. Powder mixing and compaction..... | 104 |
| 4. 1. 2. The sintering of the composite..... | 104 |
| 4. 1. 3. The Hot Isostatic Pressing (HIP) of the composite..... | 104 |
| 4. 1. 4. The composition and microstructure examination of the composite..... | 106 |
| 4. 1. 5. The mechanical property and wear resistance test of the composite..... | 106 |
| 4. 2. Experimental results and discussion | |
| 4. 2. 1. The HIP densification mechanisms..... | 106 |
| 4. 2. 1. 1. The diffusion HIP densification mechanism..... | 107 |
| 4. 2. 1. 2. The creep HIP densification mechanism..... | 108 |

| | |
|-------------------------------------------------------------------------------------|-----|
| 4. 2. 2. Effects of HIP on the structure of the sintered TiNi matrix composite..... | 110 |
| 4. 2. 3. Effects of HIP on the mechanical behaviors of the TiNi composites..... | 116 |
| 4. 2. 4. Effects of HIP on the wear behavior..... | 119 |
| 4. 3. Conclusions..... | 122 |

Chapter 5. The Phase Transformation and Wear Behavior of TiNi-based Composite

5. 1. Experimental procedure

| | |
|---------------------------------------------------------------------------|-----|
| 5. 1. 1. Sample preparation..... | 123 |
| 5. 1. 2. Microstructure analysis and mechanical property examination..... | 124 |
| 5. 1. 3. Phase transformation characterization..... | 124 |
| 5. 1. 3. 1. DSC analysis..... | 124 |
| 5. 1. 3. 2. X-ray diffraction | 125 |
| 5. 1. 3. 3. TEM analysis..... | 126 |
| 5. 1. 4. Wear of the composite with respect to the temperature | 127 |

5. 2. Experimental results and discussion

| | |
|--------------------------------------------------------------------------------------|-----|
| 5. 2. 1. Microstructure and composition of the 52vol%TiN/TiNi composite..... | 128 |
| 5. 2. 2. The mechanical properties..... | 128 |
| 5. 2. 3. Phase transformation in Ti-Ni binary system..... | 131 |
| 5. 2. 4. The phase transformations in 52vol%TiN/TiNi composite | 140 |
| 5. 2. 5. Wear behavior and the phase transformation of the TiNi-based composite..... | 149 |
| 5. 3. Conclusions..... | 153 |

Chapter 6. Summary and Future Work

| | |
|-------------------------------------------------------------------------------------------------|-----|
| 6. 1. Summary of the thesis | 155 |
| 6. 2. Possible future work | |
| 6. 2. 1. Control of the matrix composition and optimization of the composite processing..... | 158 |
| 6. 2. 2. Heat treatment..... | 159 |
| 6. 2. 3. Amorphization..... | 161 |
| 6. 2. 4. Investigation of the interface between the matrix and second phase particles... | 164 |
| Publications..... | 165 |
| References..... | 165 |

List of Tables

| | |
|----------------------------------------------------------------------------------|----|
| Table 1-1. Canadian economic losses due to wear in 1986..... | 2 |
| Table 1-2. Mechanical properties of some conventional engineering materials..... | 18 |
| Table 2-1. Composite nominal compositions and reinforcing particle data..... | 37 |

List of Figures

| | |
|-----------------------------------------------------------------------------------|----|
| Fig. 1-1. Some examples of wear in industry..... | 2 |
| Fig. 1-2. Studies involved in wear process..... | 3 |
| Fig. 1-3. The formation of abrasive wear in industry..... | 5 |
| Fig. 1-4. Asperity deformation and fracture | 5 |
| Fig. 1-5. Material's surface and adhesive force formation..... | 7 |
| Fig. 1-6. Erosion of a pipe wall..... | 10 |
| Fig. 1-7. The tearing damage on a rolling aluminum cylinder..... | 11 |
| Fig. 1-8. The structure of some tribometers..... | 13 |
| Fig. 1-9. Worn surface analysis by SEM image | 16 |
| Fig. 1-10. The structure of cast iron..... | 18 |
| Fig. 1-11. Microstructure of a high Cr white cast iron | 20 |
| Fig. 1-12. Austenite in the high Mn steel | 21 |
| Fig. 1-13. SEM image of a WC/Co structure | 22 |
| Fig. 1-14. Wear loss of TiNi in comparison with other engineering materials..... | 25 |
| Fig. 1-15. The pseudoelasticity of TiNi alloy..... | 25 |
| Fig. 1-16. A DSC curve of Ti-50.3at%Ni alloy in cooling and heating process | 26 |
| Fig. 1-17. TEM analysis of stress-induced phase transformation in TiNi alloy..... | 28 |
| Fig. 1-18. Demonstration of pseudoelasticity and wear behavior of TiNi alloy..... | 29 |
| Fig. 1-19. Loading and unloading curves of TiNi alloys in the tensile test..... | 30 |
| Fig. 1-20. Wear test results of the TiNi alloys..... | 31 |
| Fig. 2-1. Schematic of powder mixing..... | 38 |
| Fig. 2-2. The schematic of the powder compaction..... | 39 |

| | |
|-----------------------------------------------------------------------------------------------|----|
| Fig. 2-3. The cantilever system of measuring the friction coefficient..... | 41 |
| Fig. 2-4 Microstructure of 52vol%TiC/TiNi composite..... | 42 |
| Fig. 2-5. SEM image taken in the vicinity of the TiC/TiNi interface..... | 43 |
| Fig. 2-6. (Co-K α 1) X-ray pattern of 52vol%TiC/TiNi sintered at 1500°C for 6 hours... | 44 |
| Fig. 2-7. The Load-depth curves during indentation under a maximum load of 20 mN. | 45 |
| Fig. 2-8. Wear losses of different materials against the applied loads..... | 46 |
| Fig. 2-9. Friction coefficients of TiNi alloy, TiN/TiNi, TiC/TiNi and Steel 304..... | 50 |
| Fig. 2-10. Wear losses of samples with different TiC fractions..... | 54 |
| Fig. 2-11. Worn surface of 52vol% TiC/TiNi under 0.05 kN..... | 55 |
| Fig. 2-12. Worn surface of 52vol%TiC/TiNi under 0.167 kN | 55 |
| Fig. 2-13. Wear losses of 52vol%TiN/TiNi and 52vol%TiC/TiNi with respect to the load..... | 57 |
| Fig. 2-14. Scratch track of 52vol%TiN/TiNi at a normal force of 35 N..... | 58 |
| Fig. 2-15. Scratch track of 52vol%TiC/TiNi at a normal force of 35 N..... | 58 |
| Fig. 2-16. The influence of graphite on the wear behavior of TiNi-based composite..... | 60 |
| Fig. 2-17. Wear losses of samples sintered at different temperatures for 6 hours..... | 66 |
| Fig. 2-18. The adhesive wear morphology of TiNi alloy..... | 68 |
| Fig. 2-19. The abrasive wear morphology of TiNi alloy..... | 68 |
| Fig. 2-20. The surface fatigue wear morphology of TiNi alloy | 68 |
| Fig. 2-21. The brinelling wear morphology of TiNi alloy | 69 |
| Fig. 3-1. The voids in the sintered composite..... | 78 |

| | |
|-----------------------------------------------------------------------------------------------|-----|
| Fig. 3-2. (Co-K α 1) X-ray diffraction pattern of a TiN/TiNi specimen before HIP..... | 79 |
| Fig. 3-3. The wear losses of samples at different loads..... | 80 |
| Fig. 3-4. Worn surface of TiN/TiNi under load of 0.05 kN..... | 81 |
| Fig. 3-5. Worn surface of TiN/TiNi under load of 0.243 kN..... | 81 |
| Fig. 3-6. (Co-K α 1) X-ray diffraction pattern of TiN/TiNi pre-worn at 0.243 kN..... | 82 |
| Fig. 3-7. The new unwaxed TiN/TiNi sample surface..... | 84 |
| Fig. 3-8. The worn surface of pre-worn TiN/TiNi specimen..... | 85 |
| Fig. 3-9. The wear loss rate of unwaxed TiC/TiNi specimen..... | 85 |
| Fig. 3-10. The load-displacement curves during indentation under a 4500 μ N load..... | 87 |
| Fig. 3-11. The maximum depth versus the nano-indentation load..... | 87 |
| Fig. 3-12. η values of a new sample, a worn sample and a double-wear treated sample..... | 88 |
| Fig. 3-13. The new waxed TiN/TiNi sample surface..... | 91 |
| Fig. 3-14. The tensile and yield strength and the porosity of a Fe-Mo-C alloy..... | 92 |
| Fig. 3-15. The elongation and porosity of a Fe-Mo-C alloy..... | 93 |
| Fig. 3-16. The wear loss of the waxed and unwaxed TiN/TiNi specimens..... | 93 |
| Fig. 3-17. The wear loss and compaction load of TiC/TiNi..... | 95 |
| Fig. 3-18. Indentation depth of samples compacted at 4000, 5000 and 7000 pounds..... | 96 |
| Fig. 3-19. The η value of the samples compacted under 4000, 5000 and 7000 pounds..... | 96 |
| Fig. 3-20. The influence of porosity on the indentation depth and η value..... | 98 |
| Fig. 4-1. The setup of the samples in HIP process..... | 105 |
| Fig. 4-2. The HIP procedure..... | 105 |
| Fig. 4-3. Paths for mass transport during neck growth in sintering | 107 |
| Fig. 4-4. The closure treatment of the open pores before HIP..... | 110 |

| | |
|----------------------------------------------------------------------------------------------|-----|
| Fig. 4-5. The SEM image of the 1300°C hipped 52vol%TiC/TiNi | 111 |
| Fig. 4-6. The pore structure of 52vol%TiC/TiNi after hipped at 1300°C | 112 |
| Fig. 4-7. The matrix of hipped 52vol%TiC/TiNi | 112 |
| Fig. 4-8. (Co-K α 1) X-ray diffraction pattern of TiN/TiNi after 1300°C HIP..... | 113 |
| Fig. 4-9. The Load-displacement curves of one indentation under 4500 μ N..... | 117 |
| Fig. 4-10. The average maximum depth versus the nano-indentation load..... | 117 |
| Fig. 4-11. η values of TiN/TiNi specimen before and after HIP..... | 118 |
| Fig. 4-12. HIP and mechanical properties of a Ni-Al alloy | 118 |
| Fig. 4-13. Wear loss of 52vol%TiC/TiNi and 52vol%TiN/TiNi before and after HIP.. | 120 |
| Fig. 4-14. Worn surface of hipped 52vol%TiN/TiNi composite under 0.05 kN..... | 121 |
| Fig. 4-15. Worn surface of hipped 52vol%TiN/TiNi composite under 0.243 kN..... | 121 |
| Fig. 5-1. The η value of the tested materials over the whole indentation load range.... | 129 |
| Fig. 5-2. The η value of the tested materials under low load range in Fig. 5-1..... | 129 |
| Fig. 5-3. The maximum depth of the materials in the indentation test..... | 130 |
| Fig. 5-4. The ordered BCC structure of the TiNi austenite..... | 132 |
| Fig. 5-5. The structure of TiNi alloy martensite phase..... | 133 |
| Fig. 5-6. The structure of TiNi alloy R phase..... | 133 |
| Fig. 5-7. The high temperature X-ray pattern of TiNi alloy | 134 |
| Fig. 5-8. The low temperature X-ray pattern of TiNi alloy | 135 |
| Fig. 5-9. DSC curve of the martensite and R phase transformation of TiNi alloy..... | 135 |
| Fig. 5-10. The 1/3 diffraction spots in TEM diffraction pattern of the R-phase..... | 136 |
| Fig. 5-11. The DSC curves of the prealloyed TiNi powder..... | 137 |
| Fig. 5-12. XRD pattern of the TiNi alloy at high temperature..... | 139 |

| | |
|-----------------------------------------------------------------------------------------------------|-----|
| Fig. 5-13. XRD pattern of the TiNi alloy at low temperature..... | 139 |
| Fig. 5-14. The XRD patterns of TiNi alloy during heating and cooling cycles..... | 140 |
| Fig. 5-15. The DSC curve of TiN/TiNi composite..... | 141 |
| Fig. 5-16. Low temperature XRD pattern of TiN/TiNi cooled with solid CO ₂ | 143 |
| Fig. 5-17. Low temperature XRD pattern of TiN/TiNi cooled with liquid N ₂ | 143 |
| Fig. 5-18. High and low temperature XRD pattern of TiN/TiNi cooled with liquid N ₂ | 144 |
| Fig. 5-19. The TEM image of the wear debris..... | 145 |
| Fig. 5-20. The composition of a selected area for TEM examination..... | 146 |
| Fig. 5-21. The TEM diffraction pattern of the wear debris..... | 146 |
| Fig. 5-22. R* and M* versus annealing time | 148 |
| Fig. 5-23. The weight loss versus temperature of TiN/TiNi..... | 150 |
| Fig. 5-24. The pseudoelasticity due to the R-phase transformation..... | 151 |
| Fig. 5-25. The pseudoelasticity due to the martensite phase transformation..... | 151 |
| Fig. 6-1. The wear losses of the aged TiNi alloys..... | 160 |
| Fig. 6-2. The stress-strain curves under different irradiation intensities | 162 |

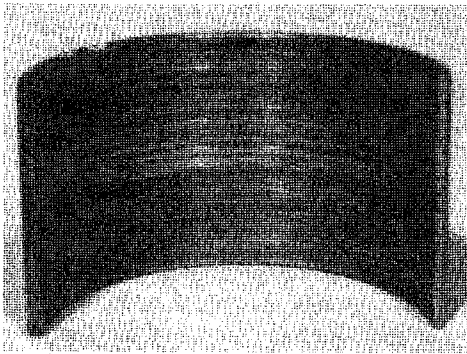
Chapter 1. Introduction

In Chapter 1, an introduction concerning the wear process is provided in the first section, the second discusses the wear performance and pseudoelasticity of TiNi alloys, and the third presents the objectives of this study.

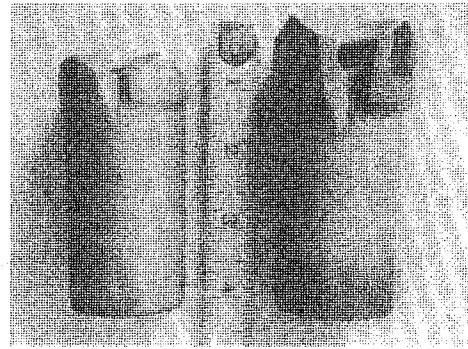
1. 1. Wear of material

Wear is one of the major failure modes of materials. It happens in almost every industry such as mining, petroleum, manufacturing and chemical processing. Some worn machine parts are shown in Fig. 1-1. Fig. 1-1A illustrates a steel bearing worn by adhesion, Fig. 1-1B a new steel drill bit with a cemented WC insert (right) and a worn-out one (left), Fig. 1-1C a ball mill showing its partially worn end and shell liners, and Fig. 1-1D a worn steel pin.

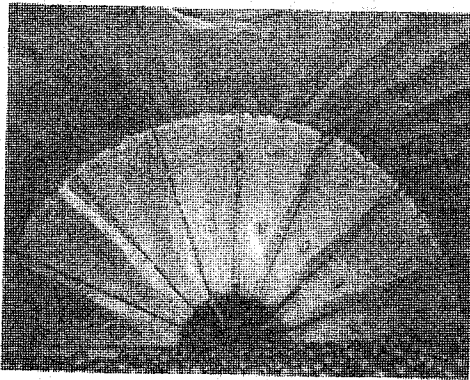
The extensive occurrence of wear results in serious economic loss. The cost of abrasive wear (one kind of wear, as discussed in Section 1.1.1) in industrialized countries was about 1% ~ 4% of the total gross national product in the 1960s [1]. Canadian economic losses due to wear in 1986 are listed in Table 1-1. The total cost exceeded \$ 5 billion [2], and this economic loss has continuously increased due to industrial expansion. As a result, there has been an increasing demand for wear-resistant materials. In order to develop superior wear-resistant materials, a systematic knowledge of friction and wear is essential.



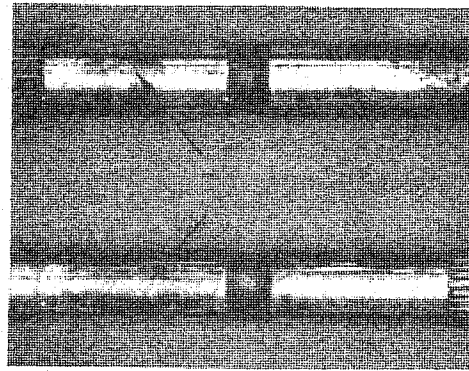
(A). Wear on a steel bearing



(B). Wear on a drill bit



(C). Wear on a ball mill liner



(D). Wear on a steel pin

Fig. 1-1. Some examples of wear in industry.

| Industries | Friction Losses | Wear Losses | Total Losses |
|---------------------|-----------------|-------------|--------------|
| Agriculture | 321 | 940 | 1261 |
| Electric utilities | 54 | 189 | 243 |
| Forestry | 111 | 158 | 269 |
| Mining | 211 | 728 | 940 |
| Pulp and paper | 105 | 382 | 487 |
| Rail transportation | 284 | 467 | 750 |
| Truck and buses | 126 | 860 | 986 |
| Wood Industry | 14 | 189 | 203 |
| Totals | 1226 | 3913 | 5139 |

Table 1-1. Canadian economic losses due to wear in 1986 (millions of dollars) [Ref. 2].

Wear is a process in which surface material is gradually removed from two or more bodies interacting with each other, and thus the material eventually fails in service. This is a complicated occurrence involving a number of disciplines, as illustrated in Fig. 1-2 [3]. Accordingly, environment, loading conditions and material properties all can significantly affect the wear performance of a material. Environmental factors such as temperature, lubrication and corrosion can change the wear process dramatically. Generally, at high temperatures, materials show lower wear resistance, and the synergistic attack of wear and corrosion usually accelerates the removal of material.

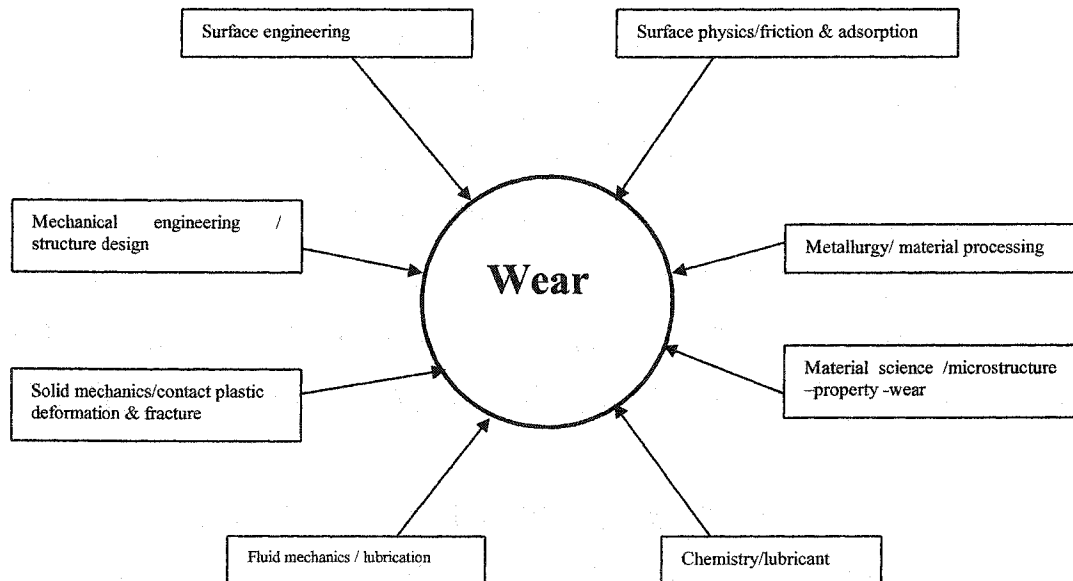


Fig. 1-2. Studies involved in wear process.

Loading conditions include factors such as the load value, loading speed and direction. A load of the same value can cause totally different wear on the same material when applied slowly or suddenly. The material's properties are factors related to the material itself, and they also determine the wear performance of a system to a great extent. Environmental and loading conditions are an essential part of tribological study, but as a result of the

complexity of these factors, very little has been understood about these aspects. However, many studies have been conducted on the effects of a material's mechanical properties on its wear resistance.

1.1.1. *Mechanical wear modes and mechanisms*

Due to its complexity, there are various classifications of the wear process. According to the wear mechanisms, mechanical wear is generally divided into abrasive wear, adhesive wear, erosive wear and surface fatigue wear [4].

1.1.1.1. *Abrasive wear*

Abrasive wear is the removal of material due to hard asperities or particles that are forced against and move along a solid surface, as illustrated in Fig. 1-3 [4]. It is the most common mode, with 50% of all wear estimated to be in this category [5]. Several mechanisms are responsible for abrasive wear. The first is asperity deformation and fracture [6]. This process is described in Fig. 1-4. Any surface is microscopically rough, with many small protrusions. When two surfaces come into contact, these small protrusions with velocities V_A and V_B touch each other first. In Fig. 1-4, when surfaces A and B , moving in opposite directions, contact each other, the asperities a and b contact each other first. Due to the relative motion, a stress field will be built up in the a and b asperities. If the stresses in the a and b asperities reach a certain level, the a and b asperities will deform and finally fracture.

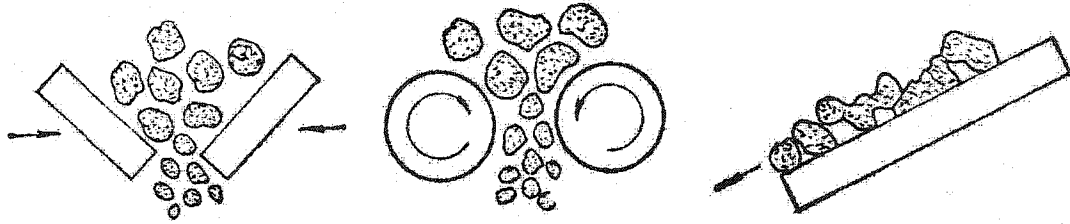


Fig. 1-3. The formation of abrasive wear in industry.

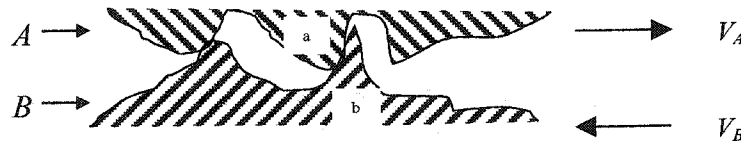


Fig. 1-4. Asperity deformation and fracture [Ref. 6].

The fractured *a* and *b* asperities are removed from the bulk material but remain between the *A* and *B* surfaces. The severe deformation of the fractured *a* and *b* asperities can greatly strain harden these particles and thus initiate the second abrasive wear mechanism, the plowing and cutting of hard particles on the solid surface [7]. When these sharp and hard particles scratch a material's surface, the materials beside the hard particles will plastically deform. After a number of such cutting cycles, the plastically deformed material will fracture, and the wear of material is thus spread (these sharp particles can be produced internally such as the above fractured *a* and *b* particles or can result from external sources). If the material is brittle, it can be easily fractured instead of undergoing plastic deformation.

A couple of factors can influence abrasive wear. Abrasive particle hardness and shape are outside influences [7]. Usually, hard and sharp particles produce greater wear on the same material. The hardness and microstructure of the material are internal influences

[7]. Generally, the harder the material, the less the abrasive wear. The finer the grain and second phase sizes in the material, the less the abrasive wear. The role of a material's hardness on its resistance to abrasive wear is understandable. Abrasive wear always begins with local plastic deformation. Regardless of whether fractures of the small asperities on the worn surface or plowing and cutting of the worn surface by abrasive particles occurs, wear takes place through the expansion and accumulation of local plastic deformation. The hardness is simply the property of the material to resist local plastic deformation. Material that has a higher hardness is more resistant to abrasive wear because it is more difficult for it to develop local plastic deformation. However, this does not mean that hardness is the only mechanical property that determines the wear resistance of a material. If the material is too hard, it may become too brittle. In this case, if there is an impact from the loading, the material can fracture without plastic deformation, and thus it has a poor resistance to abrasive wear. Accordingly, the optimum balance between the hardness and toughness of a material depends on its working conditions, especially the loading conditions.

Abrasive wear loss can be approximately predicted with the following equation [8]:

$$V=KWL/H \quad (1. 1)$$

where V is the volume wear loss, K a wear coefficient, W the normal load, L the total distance of relative motion, and H the hardness of the worn material. So the wear loss is proportional to the wearing load and distance, but inversely proportional to the material's hardness.

1.1.1.2. Adhesive wear

Adhesive wear is removal of material caused by adhesive (attractive) forces [9]. It occurs on two contact surfaces in relative motion under a normal or tangential load. A material's surface usually has some adsorbed and oxidation layers, as shown in Fig. 1-5 [10]. When the two surfaces are close to each other (usually within 1 nm), the short-range force comes into play, and atomic bonds can be formed between the two surfaces in contact, thus generating an adhesive force [9]. If the adhesive force is greater than the strength of the soft material, the soft material will be broken by the relative motion, and thus the material is worn. At the same time, when the asperities on two surfaces push on each other, as shown in Fig. 1-4, because the contact area between the two asperities is very small, the stress around the two asperities could be very high, even greater than the yield strength of the materials. This large contact stress can deform the asperities in contact and even weld them together. This is especially true when the temperature of the contact area increases. If the weld strength is greater than the shear strength of the soft asperity material, the soft asperity will also be cut by the shear stress and removed from the surface of the soft material.

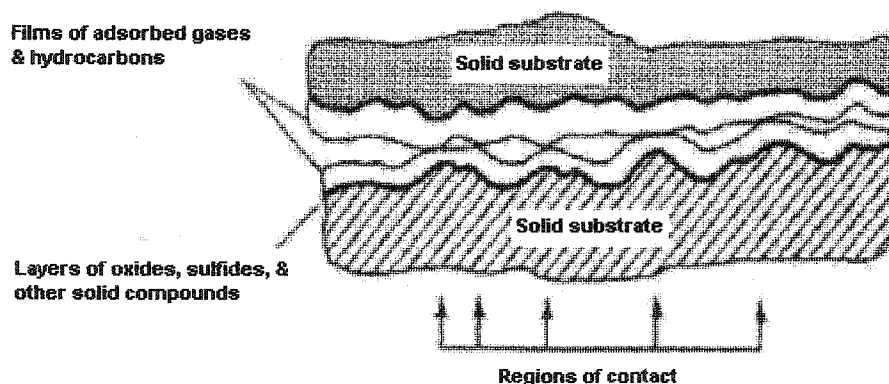


Fig. 1-5. Material's surface and adhesive force formation [Ref. 10].

Adhesive wear is also affected by several factors. The first is the material's compatibility [9]. The compatibility is the similarity between the materials' physical and mechanical properties. The more compatible the two materials, the more similar physical and mechanical properties these two materials have. Generally speaking, materials with a higher compatibility have a larger solubility in each other. Therefore, the wear couple with a higher solubility has an increased likelihood of forming atomic bonds, and thus more adhesive wear will happen. Following this principle, wear couples are usually made from materials of lower mutual solubility. Another factor influencing the materials' compatibility is atomic interaction. It has been observed that some metals with low mutual solubility may also have strong adhesion resulted from their electronic structure. Among the transition metals, the *d* band is usually not fully filled by electrons, and it is also easy for these materials' atoms to form bonds [11]. Thus adhesive wear can easily occur on these materials. The second factor that affects adhesive wear is the crystal structure of the material [9]. In general, the wear on a face centered cubic structure (FCC) has a larger adhesive wear component than on an hexagonal closely packed (HCP) structure. FCC structures have more slip systems, and thus the FCC material couple usually has a larger contact area, which creates more possibilities for bonding. The material microstructure is the third influence on its adhesive wear. This primarily involves the grain size of the material. The finer the grain size, the higher the yield strength of the material, and thus the greater resistance of the material to the shear stress caused by the relative motion. So fine grained materials usually have lower adhesive wear than coarse grained ones. The last major influence on adhesive wear is lubrication. Apparently, if the wear couple is lubricated and separated by the lubricant, it is difficult

or even impossible for atomic bonds to form between these material couples, and thus the adhesive wear will be negligible.

Adhesive wear loss can be approximately depicted with the following equation [12]:

$$V=QWL/(3H) \quad (1. 2)$$

where V is the volume wear loss, Q a wear coefficient, W the normal load, L the total distance of relative motion, and H the hardness of the material. The wear loss is still proportional to the wearing load and sliding distance, but inversely proportional to the material's hardness. In the case of adhesive wear, the hardness is not mentioned among the above four influencing factors. But the role of hardness in resisting adhesive wear is explicable. Since adhesive wear is caused by fracture of the atomic bonds inside the material instead of the atomic bonds between the wear couple materials, the stronger the atomic bonds that the material has, the less adhesive wear it will experience. On the other hand, hardness reflects the strength of the atomic bonds of the material and is proportional to its yield strength. Therefore, hardness also indicates the material's resistance to adhesive wear.

1.1.1.3. *Erosive wear*

Erosion is wear damage resulting from the impingement of liquid or sharp particles on the surface of a material [9]. The sharp particles are usually transported in a moving fluid. An example of erosion in a pipeline is provided in Fig. 1-6. Two mechanisms are responsible for the formation of erosion wear. The first is abrasive erosion, which is caused by the micromachining action of the abrasive particles. In this type of erosive

wear, the particles are usually at a small incident angle to the surface and thus do not produce a large stress around the impingement area. Therefore, cutting is the major cause of abrasive erosion. If the particles are at a large incident angle to the surface and moving at a high speed, they can generate a stress that may be great enough to break the material and thus speed up the wear damage [9]. Accordingly, the particle shape, particle velocity, impact angle, particle quantity and density are important in determining erosive wear. Simultaneously, the material's mechanical properties, mainly its hardness and toughness, are also critical in resisting erosive wear as they help to resist the cutting and fracturing of the material.

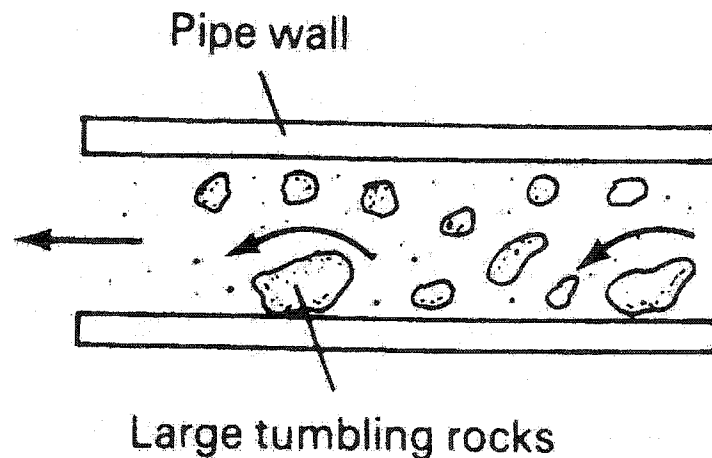


Fig. 1-6. Erosion of a pipe wall.

1.1.1.4. *Surface fatigue wear*

Surface fatigue wear is a type of material removal caused by cyclic loads such as occurs in gears and rolling contact bearings [9]. In these wear couples, even if the two materials do not directly contact each other, an alternating stress field will be established inside the materials. Moreover, calculations show that at the subsurface, there is usually a shear stress, which is large in quantity [13]. This high shear stress can initiate and then

propagate microcracks, particularly if there are inclusions in these high stress areas. When a microcrack reaches the surface of the material, a chunk of material will fall off, resulting in wear. Fig. 1-7 shows the tearing damage occurring on a rolling aluminum cylinder by such a mechanism [14]. Several factors affect surface fatigue wear. The first is the material microstructure. If the material has defects, such as incoherent inclusions, the stress concentration can be high enough to initiate microcracking and thus surface fatigue wear. The second influence is the hardness of the material. A high hardness usually corresponds to a high fatigue resistance in the material [15] and thus indicates a better resistance to surface fatigue wear. Surface roughness is the third important effect on surface fatigue wear. Clearly, a smooth surface has fewer chances to initiate microcracking and thus has a higher surface fatigue resistance [16].

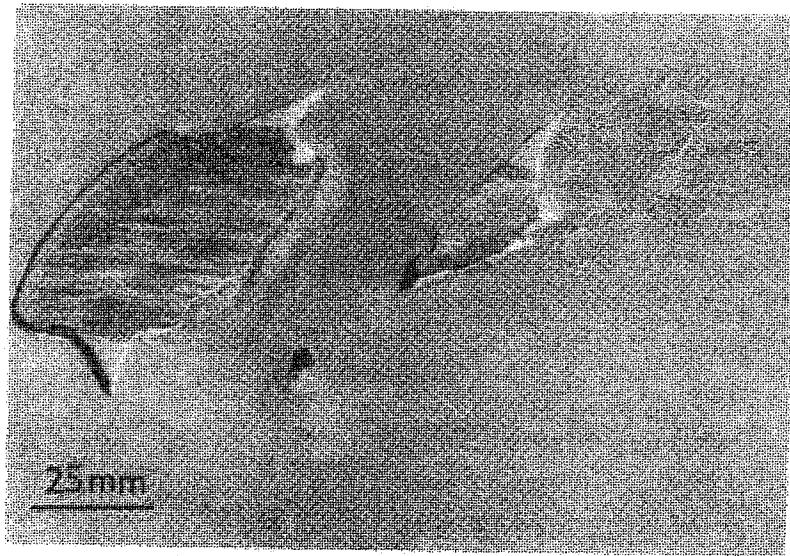


Fig. 1-7. The tearing damage on a rolling aluminum cylinder [Ref. 14].

These above four mechanisms are the fundamental ones governing a material's mechanical wear. They evince that the wearing of a material is influenced by a number of

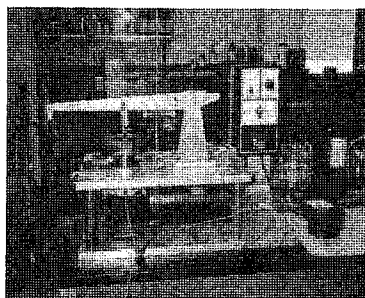
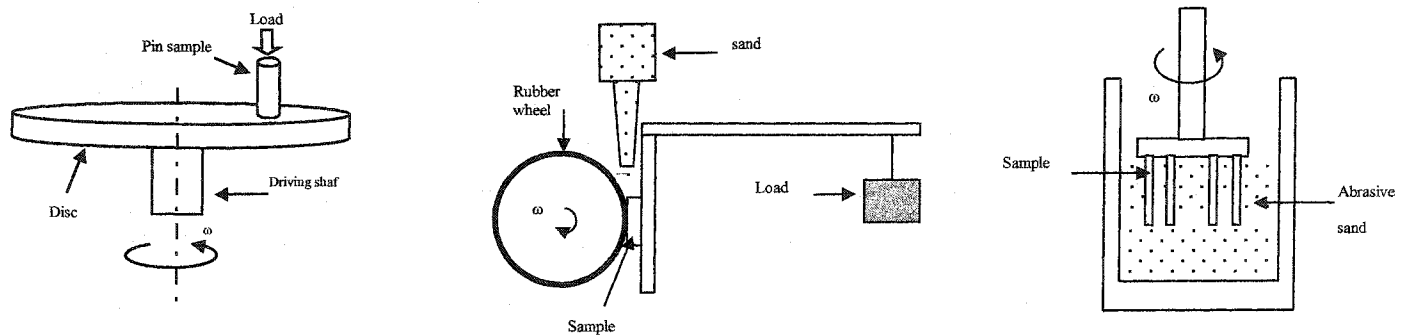
factors, but the material's hardness is a very important influence in almost each case. Generally, the harder the material, the less the wear. This is because hardness directly resists cutting, that is, the abrasive wear, or reflects a material's other capabilities to resist external attacks. Simultaneously, toughness is another important parameter in the wear performance of a material. How to increase the hardness of a material without a significant loss of its toughness has become a major focus in wear-resistant material design.

1.1.2. Measurement and analysis of wear

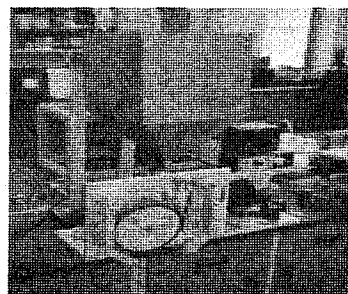
In order to examine the wear resistance and characteristics of different materials, some testing and characterizing methods have been widely used.

In the laboratory, pin-on-disc, rubber wheel, and slurry tribometers are frequently employed to test the wear resistance of materials. The structures of these devices are schematically shown in Fig. 1-8A, 1-8B, and 1-8C respectively. The pin-on-disc wear tester is basically composed of a disc and a pin. The pin is usually made of the sample material, and the disc of another material chosen to be the wear couple. During the testing, the disc spins at different speeds, and the sample pin is pushed onto the disc under different vertical loads. Thus, the wear testing can be performed under a series of combinations of sliding speeds and loads. The pin-on-disc tester is generally used to conduct testing on the wear of a sample material directly against another disc material. Because of the tight contact and high temperature, adhesive wear often takes place in this type of wear testing. At the same time, wear debris are formed and strain hardened during

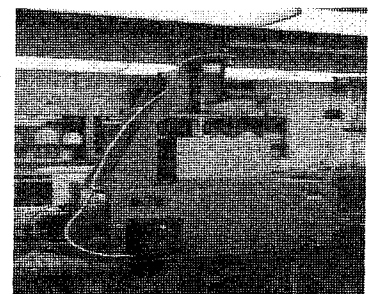
the wear process. Subsequently, the surfaces of materials are also cut by the hard debris, and thus abrasive wear features are also quite common in this type of wear testing. In addition to adhesive and abrasive wear, the wearing conditions can be modified to carry out wear tests under different circumstances. For example, if a solution is placed on the disc, corrosive wear testing becomes possible. More details of the pin-on-disc wear testing are offered in The American Society of Testing Materials (ASTM) standard ASTM G99.



A. Pin-on-disc tester



B. Rubber wheel tester



C. Slurry tester

Fig. 1-8. The structure of some tribometers.

The rubber wheel apparatus is usually used to perform abrasive wear tests. The wheel is surrounded by a thick rubber layer, and the sample is pushed against the rubber wheel by a horizontal force. During the test, the wheel spins at various velocities, and abrasive

particles drop into the space between the wheel and sample from an upper sand hopper. When the sand particles pass through the sample material and wheel, the sample is worn by the abrasive particles. Since the horizontal load, wheel spin speed, and sand particle hardness, size and shape are also controllable, abrasive wear testing can be carried out according to the desired conditions. More details of the rubber wheel wear testing are described in The American Society of Testing Materials (ASTM) standard ASTM G65.

The slurry tribometer is a good tester for erosion wear examination. The pin specimens made of the tested material are fastened onto a plate. Along with the specimens, the plate is then buried into abrasive sand and rotates at different speeds. The rotation of specimens in the abrasive sand results in severe erosive wear on the pin specimens. Erosion wear testing is also totally controllable as the specimen rotation and abrasive sand properties are all fully adjustable.

After wear testing, the samples are weighed to obtain the weight loss of the different materials. The weight loss can be used as a criterion to judge the wear resistance of materials having the same density. The greater the weight loss, the less wear resistant the material is. For materials of different densities, it is important to convert the weight loss to volume loss, the latter of which is then utilized to evaluate the material's wear resistance. There are some other methods for assessing a material's wear performance, but in any testing, it is essential in comparison tests to ensure that no change occurs in the nature of the wear process between the two sets of wear conditions. Even a small change

in the testing conditions can sometimes lead to a significant difference in the material's wear performance.

Along with the wear loss, an understanding of a material's structural change during the wear process is indispensable to completely comprehending the material's wear behavior. For this purpose, worn surface and wear debris analyses are often practiced in the investigation on the wear of a material. After wearing, the surface and subsurface of the material have been greatly deformed, and many wear features are present on the worn surface including microcracks and wear tracks of various lengths and configurations and element transfer. Scanning electron microscopy (SEM), optical microscopy (OM), energy dispersive X-ray analysis (EDX) and Auger electron analysis are some typical methods for worn surface characterization. Fig. 1-9 offers an example of illustrating how to identify wear mechanisms through SEM worn surface analysis [17]. The figure indicates surface damage caused by chip formation, plastic deformation, and pickup of fragments of a ceramic particle abrading the material's surface. Wear debris analysis is another productive source for information on a material's structural alteration during the wear process. When deformed and removed from the bulk material, surface material degrades into wear debris of various shapes. This wear debris can present substantial data about the material's structural change during the wear process such as dislocation multiplication and phase transformation. Transmission electron microscopy (TEM) and X-ray diffraction (XRD) are routinely adopted in this field.

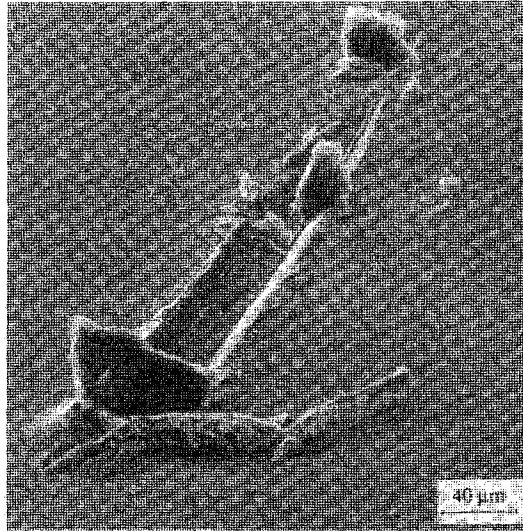


Fig. 1-9. Worn surface analysis by SEM image [Ref. 17].

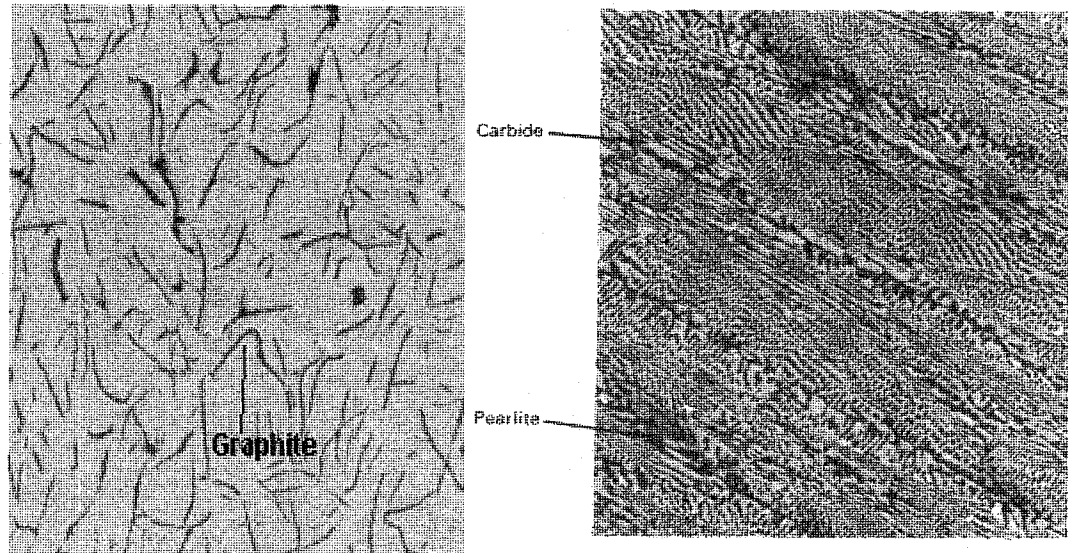
1.1.3. Wear-resistant materials

Since the various wear mechanisms have clearly revealed that a material's mechanical properties, especially its hardness and toughness, play a paramount role in wear process, altering a material's hardness and toughness has become a key technique in the development of wear-resistant materials. Actually, in the past, a large number of wear-resistant materials have been developed by enhancing their hardness while maintaining their toughness as much as possible. The following wear-resistant materials embody this development logic.

Graphitic cast iron, white cast iron, alloy steel/iron and cemented ceramic materials have been developed for wear applications. Currently, cemented WC is the most prevalent wear-resistant material worldwide. These wear-resistant materials ordinarily consist of two phases. One is the matrix, which is relatively ductile to bind the second phase and

accommodate deformation. The other is a kind of hard phase dispersed in the matrix, serving to resist wear and protect the matrix.

Graphitic cast iron has an iron matrix and a graphite second phase, as shown in Fig. 1-10A [18]. The matrix can be heat treated into different structures such as ferrite, pearlite and martensite. Graphite has very poor mechanical properties. At the load of 100 g, the knoop hardness of graphite, ferrite and pearlite in cast iron is 15-40, 215-270 and 300-390 respectively [19]. Consequently, the dispersed graphite is sometimes considered as being like holes or cracks inside the metal, and it greatly reduces the strength and ductility of the material. However, graphite has a very small friction coefficient with metals. The iron ~ iron friction coefficient is about 0.50, while the graphite ~ steel friction coefficient is merely around 0.10 [20]. Thus, the graphite in the cast iron can lubricate the worn surface. Due to its low hardness, however, graphite can barely protect the matrix, and graphitic cast iron usually has a low overall hardness, as shown in Table 1-2 [21]. Therefore, graphitic cast iron generally has poor wear resistance and is seldom used as a wear resistant material except when graphite lubrication is preferred.



A. Graphitic cast iron ($\times 75$) [Ref. 18]. B. White cast iron ($\times 80$) [Ref. 22].

Fig. 1-10. The structure of cast iron.

| Materials | Graphitic cast iron | White cast iron | High Cr white cast iron | High Mn steel | Stainless steel | TiNi |
|-----------|---------------------|-----------------|-------------------------------|-----------------|-----------------|--------------------------------------------------|
| UTS (MPa) | 120~1600 | --- | --- | 400~700 | 480~2000 | 895 |
| Hardness | 170HB~ 555HB | 400HB~ 650HB | 60HRC ~ 69HRC (> 650HB) | 140HB~ 190HB | 130HB~ 400HB | 200HV~ 320HV (≈ 250 HB ~320HB) |

Table 1-2. Mechanical properties of some conventional engineering materials.

White cast iron has an iron matrix and a carbide second phase, as shown in Fig. 1-10B [22]. The matrix can also be heat treated to form different structures, with the most common carbide in white cast iron being cementite, Fe_3C . Fe_3C is hard compared with the graphite and even the iron matrix. The average hardness of pearlite and carbide is 200

HV ~ 300 HV and 900 HV ~ 1200 HV respectively [23]. Accordingly, white cast iron has high bulk hardness, as shown in Table 1-2 [24]. So white cast iron possesses much higher wear resistance than graphitic cast iron does.

Based on the wear performance of white cast iron, alloy steel or iron is developed by adding alloying elements into the Fe-C system to generate more and harder carbides inside the matrix. The most frequently selected alloying element is Cr, which can form Cr_7C_3 , Cr_{21}C_7 and even more complicated $(\text{Fe}, \text{Cr})_m\text{C}_n$ type carbides [25]. Fig. 1-11 is a high Cr white cast iron SEM structure image, which shows a large number of carbides embedded in the matrix [26]. All these carbides are extremely hard. For instance, the hardness of $(\text{CrFe})_7\text{C}_3$ is 1700 HV [27]. This increase in hardness remarkably augments the wear resistance of the material. However, there is an optimum hardness of the carbide in a particular case. In general, the harder the carbide, the more protective it is to the matrix. Nevertheless, if it is too hard, the carbide can be easily broken under an external impact force and thus accelerate the wear process. So in certain situations, it is important to choose an appropriate carbide as the reinforcing phase of the matrix and thus to obtain the optimum balance between hardness and toughness of the material.

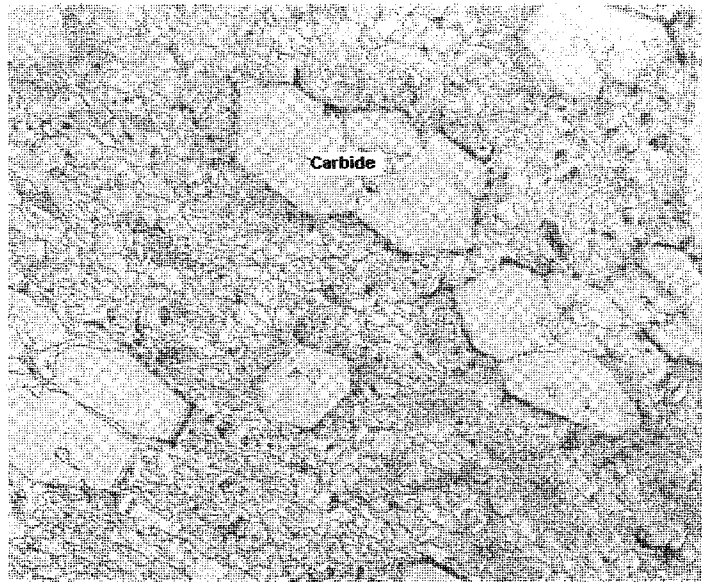


Fig. 1-11. Microstructure of a high Cr white cast iron ($\times 300$) [Ref. 26].

Apart from the Cr alloying white cast iron, high Mn alloying steel (Hadfield steel) is another typical wear-resistant alloy in the Fe-C system. This steel primarily contains C (normally around 1.0 wt%) and Mn (normally around 15 wt%) [25]. The high concentration of Mn stabilizes the austenite phase, and thus the steel has an austenitic structure at room temperature, as displayed in Fig. 1-12 [28]. When undergoing a severe impact, the steel experiences strong work hardening [21], which imparts to the steel very high hardness and wear resistance. However, from this mechanism, it can be deduced that when the material works in a low stress condition, where the stress is not high enough to harden the material, the steel may not display wear resistance as good as that in the high stress wearing condition. So this material's good wear resistance also originates from its high hardness.

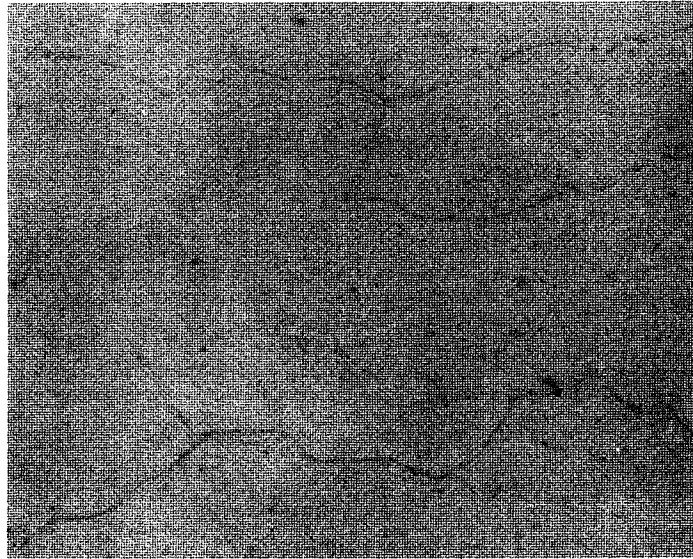


Fig. 1-12. Austenite in the high Mn steel ($\times 600$) [Ref. 28].

In order to further enhance the hardness of the material and reduce its cost, cemented ceramic materials have been produced for wear applications. In the alloy steel/iron, the hard second phases are generated inside the material when the Fe-C alloy is being melted. These internally formed second phases have a very strong interface with the matrix, but solubility limit and cost have made it increasingly difficult to add more alloying elements. For the Cr-alloyed white cast iron, the commonly maximum addition of Cr is about 30 wt% of the total iron [7]. Such an addition has greatly limited the application of this material because of the increasing price of Cr. Meanwhile, the cemented ceramic materials possess a very high wear resistance and also have a relatively low production cost. They are formed by sintering hard particles such as carbide and nitride with a certain amount of metal as a binding matrix. So in this kind of wear-resistant material, the hard second phase is formed externally, and the key point in its manufacturing is to introduce a good bond between the second phase and the metal matrix. In order to attain

this good bond, the selection of the appropriate base alloy and the sintering process are critical. Cemented WC/Co is a good representative of this type of hard material. The hardness of WC is 2400 HV [29]. The cemented WC hard alloy has extraordinarily high hardness and wear resistance compared with those Fe-C alloys. Normally the raw WC particles have a mesh size of 20 ~ 250, and the fraction of WC in the cemented WC hard material is from 30 wt% to 60 wt% [7]. The final structure of very hard WC grains in a binder matrix of tough cobalt metal is processed by liquid phase sintering. Fig. 1-13 shows a SEM image of a WC/Co alloy [30]. The WC particles having different sizes are dispersed in the matrix. The combination of WC and metallic cobalt as a binder is a well-adjusted system not only with regard to its properties, but also to its sintering behavior. The high solubility of WC in cobalt at high temperatures and a very good wetting of WC by the liquid cobalt binder result in an excellent densification during liquid phase sintering and in a pore-free structure. As a result, the obtained material combines high strength, good toughness and high hardness.

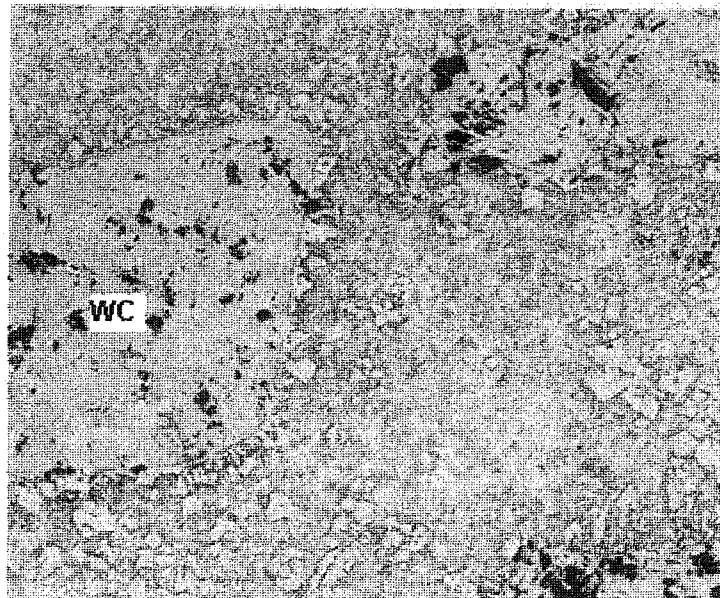


Fig. 1-13. SEM image of a WC/Co structure ($\times 120$) [Ref.30].

Besides the above-mentioned materials, some other materials are available for wear applications such as nonferrous alloys, polymers and ceramics [7, 25]. However, the materials described in this section are the principal ones for current industrial wear applications. They embody a general rule governing wear-resistant material's design: improving a material's hardness without too much loss of toughness. The material's overall hardness is usually attributed to both the second phase and matrix, while its average toughness primarily to the matrix. Accordingly, the wear resistance of a material relies on the balance between its matrix and hard phase. The hard phase usually lasts a long time unless it breaks. The failure of a wear-resistant material commonly initiates in the matrix. If too soft, the matrix cannot accommodate the strain caused by a large stress, and the hard phase can be easily pulled out. If too hard, the matrix can easily crack under a strong impact, and it thus also destroys the wear-resistant material. Accordingly, a kind of special matrix that can be both sufficiently strong and tough is a key point to the wear resistance of a composite material. (The strength of the interfacial bonding is also of importance to the overall wear resistance of the composite material.)

1. 2. Wear behavior and pseudoelasticity of TiNi alloy

1.2. 1. Mechanical properties and wear behavior of TiNi alloy

The previous sections have delineated the importance of hardness for conventional wear-resistant materials. The harder the material, the more wear resistant it is. However, recent studies [31-40] have noted an exception to this rule. The equiatomic (Ti-51at%Ni or Ti-56wt%Ni) TiNi alloy exhibits high wear resistance, even with low hardness. Table 1-2 lists TiNi alloy's mechanical properties compared with those of some other conventional

engineering alloys [41, 42]. The hardness of TiNi alloy is significantly less than that of stainless steel and other engineering alloys. Following the performance of conventional wear-resistant materials, the wear resistance of TiNi alloy is supposed to be inferior. However, Fig. 1-14 provides a comparison between the wear resistance of TiNi alloy and of some conventional wear-resistant alloys through erosion wear testing [32]. ST-6 and ST-21 are Stellite alloys with a hardness ranging from 30 HRC ~ 43 HRC [43]. IRECA, F255, 304L and CA6-NM are different stainless steels with a hardness ranging from 130 HB ~ 400 HB [44]. Relative wear loss is shown in Fig. 1-14. It can be seen that the wear loss of TiNi alloy is much lower than that of all the other alloys. Other studies have confirmed TiNi alloy's high wear resistance. Jin and Wang [37] found that TiNi alloy is more wear resistant than commercial wear-resistant Co45 alloy and nitrogenized 38CrMoAlA steel during dry sliding. J. Singh and A.T. Alpas [38] compared $Ti_{50}Ni_{47}Fe_3$ to SAE 52100 bearing steel and demonstrated that the former has significantly higher wear resistance than the latter. Since TiNi alloy is much softer than these materials, its good wear resistance has made it a subject of great interest in recent years. Studies have demonstrated that the high wear performance of the TiNi alloy is attributed to its pseudoelasticity, a special property associated with a reversible phase transformation inside the material, as discussed in Sections 1. 2. 2 and 1. 2. 3. The wear characteristics of the TiNi alloy have also been investigated, and adhesion, abrasion and surface fatigue are found to make large contributions to the wear of this alloy [42].

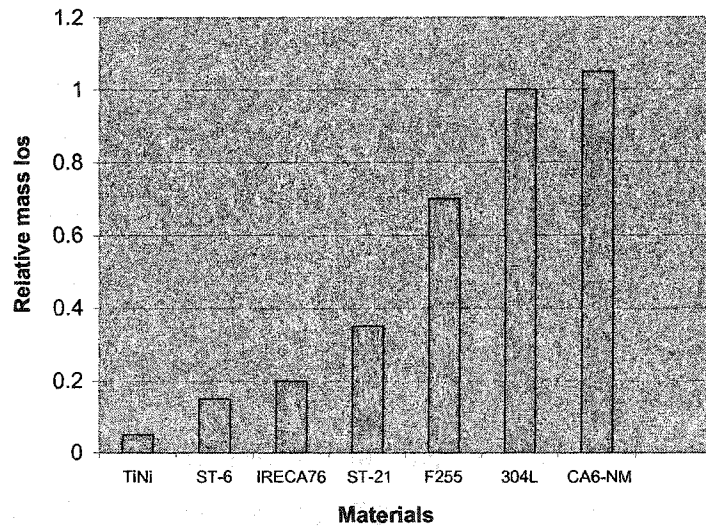


Fig. 1-14. Wear loss of TiNi and some other engineering materials [Ref. 32].

1. 2. 2. Phenomena and mechanism of TiNi alloy's pseudoelasticity

Pseudoelasticity is a special property of TiNi alloy, as depicted in Fig. 1-15. When subject to a stress, TiNi alloy initially deforms elastically. When the stress reaches a high level, corresponding to the point *A* in Fig. 1-15, the alloy's deformation begins to behave "plastically". The stress is no longer linear relative to the strain. After a certain period of such

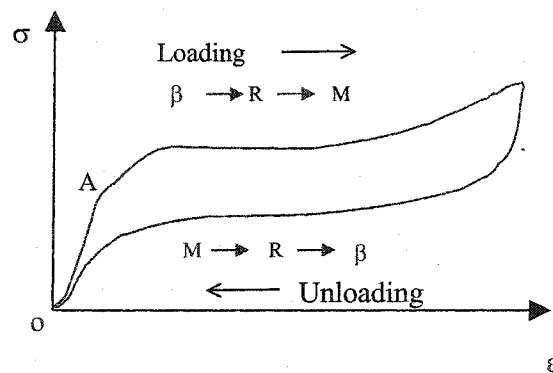


Fig. 1-15. The pseudoelasticity of TiNi alloy.

deformation, if the stress is removed, the "plastic" deformation reverts to zero. This great strain recovery from the large "plastic" deformation is called pseudoelasticity because the recovery results from a reversible phase transformation rather than the atomic recovery

associated with true elasticity.

The TiNi alloy has a low-temperature martensite phase (M) and a high-temperature austenite phase (β). Usually, the equiatomic TiNi alloy exists in the austenite β phase. TiNi alloy's martensite is coherent with its austenite phase, and thus these two phases have a low energy and glissile interface. This means that the martensite is thermoelastic, and the transformation between these two phases can be easily reversed by a certain temperature or stress condition. A differential scanning calorimetry curve of this reversible phase transformation in a Ti-50.3at%Ni alloy is provided in Fig. 1-16 [33].

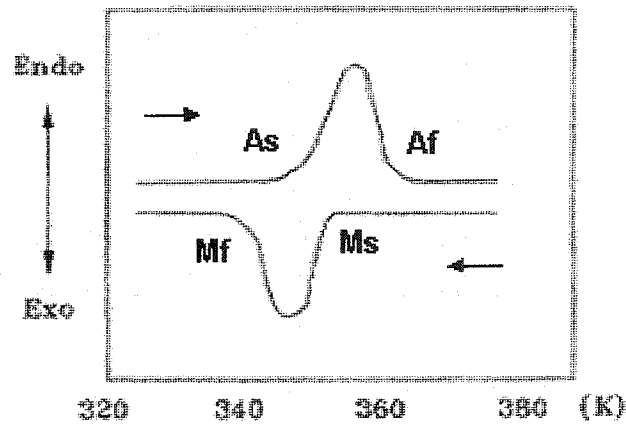


Fig. 1-16. A DSC curve of Ti-50.3at%Ni alloy in cooling and heating process [Ref. 33].

When the TiNi alloy is cooled to a certain temperature, the M_s point (the start temperature for the martensite formation), the austenite β phase transforms to the martensite M phase, a process which completes at the M_f point (the finish temperature for the martensite formation). Due to the reversibility, when the temperature increases to the A_s point (the start temperature for the austenite formation), the martensite M phase can partially or completely return to the austenite β phase, which ends at the A_f point (the finish temperature for the

austenite formation). Corresponding to the phase transformation is a reversible transformation in the crystal structure between these two phases. It is just this reversible structure transformation that engenders pseudoelasticity. The reversible phase transformation has been discovered to be a multiple step process. Between the two terminal β and M phases is an intermediate R phase. The R phase usually appears at a temperature higher than M_S point in the cooling process, and thus it is often referred as pre-martensitic phase. The R phase transformation is also reversible and contributes to the pseudoelasticity of TiNi alloy [45-48]. More information will be offered in Chapter 5 about the phase transformation of TiNi alloy.

This reversible phase transformation is also stress inducible. When stressed, martensite is generated in a TiNi alloy, corresponding to the loading process in Fig. 1-15. When released, the martensite reverts to austenite, corresponding to the unloading process. An *in situ* TEM diffraction analysis of this stress-induced reversible phase transformation is shown in Fig. 1-17 [33], in which a Ti-50.3at%Ni alloy underwent a tensile test. Fig. 1-17A depicts the original austenite β phase. Fig. 1-17B shows the occurrence of $\beta \rightarrow R$ transformation while the tensile stress is being applied. The small white spots, located about 1/3 of the distance between the parent phase diffraction spots, are the characteristic diffraction spots of the R phase. Fig. 1-17C indicates the formation of martensite phase during the tensile process. Fig. 1-17D illustrates the recovery to the parent austenite β phase after the test.

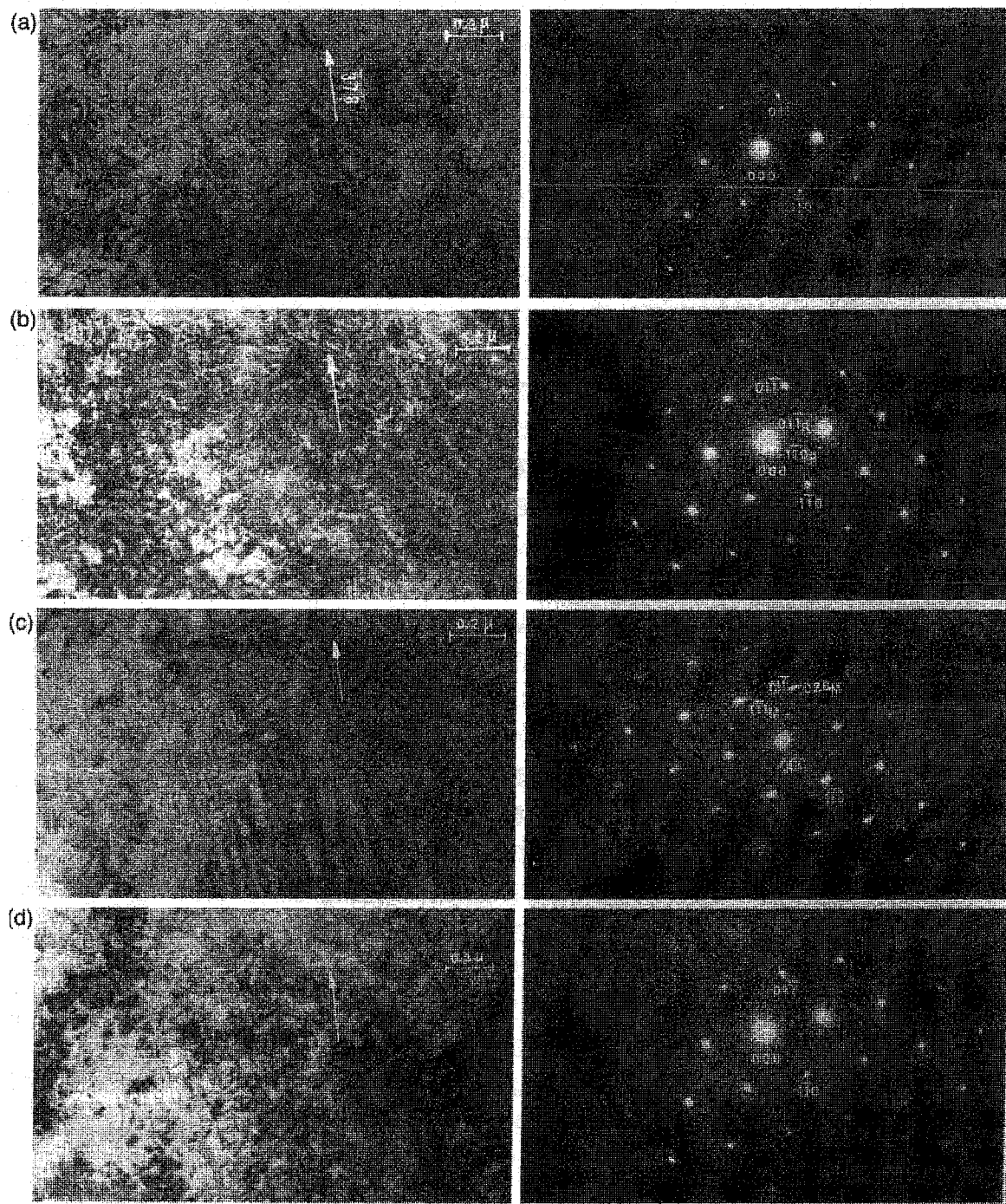


Fig. 1-17. TEM analysis of stress-induced phase transformation in TiNi alloy [Ref. 33].

1.2.3. Mechanism of TiNi alloy's wear behavior

It is its pseudoelasticity that primarily bestows the high wear resistance to TiNi alloy. Fig. 1-

18 schematically demonstrates the process by which pseudoelasticity may affect the wear behavior of this alloy. There are two asperities in Fig. 1-18, the lower one being TiNi alloy. When the upper asperity hits the TiNi alloy, a stress field is established around the contact area of the two surfaces. This process corresponds to the loading period in Fig. 1-15, and the martensitic phase transformation is activated when the stress amounts to a certain value.

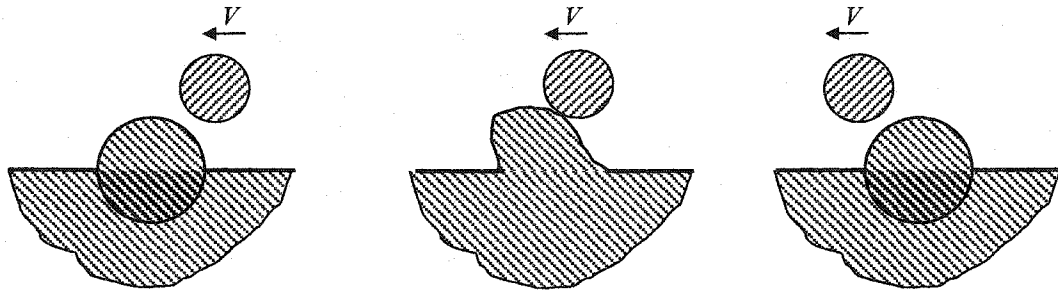


Fig. 1-18. Demonstration of pseudoelasticity and wear behavior of TiNi alloy.

Accompanying this phase transformation process is a large deformation of the TiNi alloy, which greatly enlarges the contact area and thus reduces the stress. When the upper asperity passes by, the stress built up inside the TiNi alloy vanishes, resulting in the reverse phase transformation from martensite to austenite. During the unloading process, because of the pseudoelasticity, the large deformation partially or completely recovers. As a result, there is little plastic deformation accumulating so that the damage to the material is diminished. Accordingly, the pseudoelasticity imparts to the TiNi alloy a rubber-like behavior with a relatively large recoverable strain (up to 8.5%) [41] and greatly benefits its wear resistance. This mechanism has been supported by some studies. Shida and Sugimoto [39] observed the remarkable resistance of TiNi alloy to water-jet erosion. They found that the erosion resistance of TiNi alloy strongly depends on its

chemical composition and microstructure. The optimal composition is from Ti-55wt%Ni to Ti-56.5wt%Ni, where the reversible martensitic phase transformation occurs. Liang *et al.* [40] investigated the wear behavior of TiNi alloy during sliding wear, impact abrasion and sandblasting erosion. They perceived a strong correspondence between the wear resistance and the recoverable strain resulting from the pseudoelasticity. Another recent study has directly related the wear resistance of TiNi alloy to its pseudoelasticity [49]. The pseudoelasticity of an as-received (cold worked) and a heat treated (aged and then water quenched) Ti-51.0at%Ni alloy was evaluated using a tensile test, as illustrated in Fig. 1-19. The aged TiNi alloy exhibited a higher pseudoelasticity. At a total strain of 4%, the aged TiNi alloy recovered almost all the 4% strain, while the as-received one only about 3%. Besides the tensile test, the same samples underwent wear testing with and without cooling. The results of the wear testing are shown in Fig. 1-20. The aged TiNi sample has better wear resistance, especially at low load. These tests further confirm the beneficial effects of the pseudoelasticity on TiNi alloy's wear resistance.

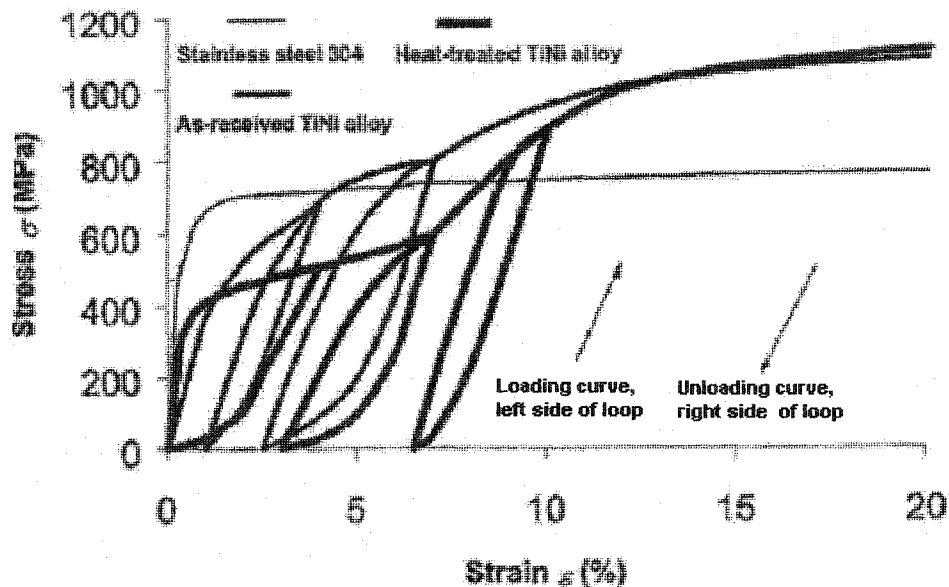


Fig. 1-19. Loading and unloading curves of TiNi alloys in the tensile test [Ref. 52].

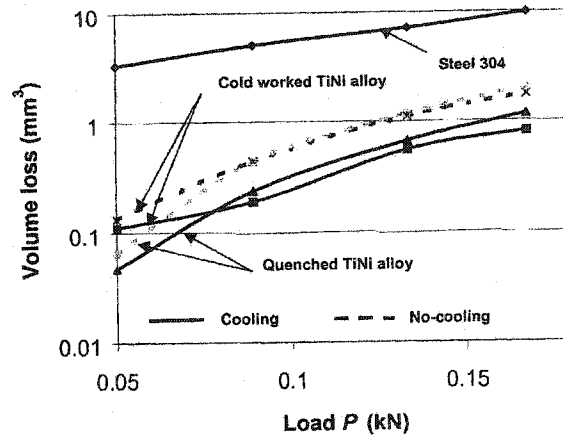


Fig. 1-20. Wear test results of the TiNi alloys [Ref. 52].

It was also noticed that the high wear resistance of TiNi alloy is not only ascribed to its pseudoelasticity but also to its strain-hardening capability. Clayton [50] investigated wear and rolling fatigue of a TiNi alloy having a composition beyond the range in which the martensitic transformation can occur. He correlated the good cyclic strain hardening capability of TiNi alloy to its high resistance to rolling fatigue. However, pseudoelasticity is still a great benefit to the high wear resistance of the TiNi alloy.

Since pseudoelasticity has a large influence on the wear behavior of TiNi alloy, it can be deduced that any factor that affects TiNi alloy's pseudoelasticity will alter its wear behavior. The pseudoelasticity of TiNi varies with the alloy's heat treatment, manufacturing, and especially composition. A variation of 0.1% in Ni content brings out about a 10°C change in the phase transformation temperatures [51]. The addition of a third element such as Co, Fe, or Nb also moves the phase transformation temperatures [52-54], which could be used to control the temperature range for application of this material.

TiNi alloy is typically manufactured by melting, during which composition control is paramount due to the dependence of pseudoelasticity on the alloy's composition. C and O₂ are easily entrapped into the melt and react with Ti. Therefore, reducing C and O content in the molten TiNi is a key operation. Recent studies have explored the sintering of TiNi alloy from prealloyed or elemental powders [55-57]. A TiNi alloy has been produced by hot isostatic pressing (HIP) using prealloyed powders. The obtained compact had a relative density of 99.6%, with no detectable increase in impurity content. The sintered TiNi alloy also exhibited the reversible stress-induced phase transformations and mechanical properties that were almost identical to those of the typical melted TiNi alloys [55]. The application of elemental Ti and Ni powders in the sintering of TiNi alloy has significantly lowered the manufacturing costs of this alloy.

1.2.4. The application of TiNi alloy

Since the 1960s, TiNi alloy, as a shape memory material, has found diverse applications. Typical examples include a temperature switch [58], a space shuttle antenna [59], a thermal machine [60], an artificial heart [61] and an artificial bone [62]. The good wear resistance of TiNi alloy has also led to its use in valves. Some water-flow valves made from Ti-51.8at%Ni TiNi alloy in a power station have demonstrated a lifetime that was four times longer than the valves made of 1Cr13 and nitrogenized 38CrMoAlA triboalloys [37]. However, compared with the large number of reports about TiNi alloy's applications in functional and bio-materials, reports on this metal's applications in structural materials are still quite rare.

1. 3. TiNi-based composites and the objective of this research

1.3.1. TiNi composite

Recently, TiNi alloy has been incorporated into composite materials. In an Al-based composite reinforced with TiNi fibers/particles, the Young's modulus, yield strength and work hardening rate of the material are all enhanced by the presence of TiNi alloy fibers/particles [63-68]. Compared with the composites reinforced by conventional hard phases, the TiNi reinforced composite has its own advantage, that is, the residual stress between the matrix and TiNi can be definitely controlled, which results from the shape memory effect of TiNi alloy.

Another type of TiNi composite is made by reinforcing a TiNi alloy matrix with hard particles such as TiC [69-76]. S. N. Kulkov *et al.* [69-71] probed the sintering behavior, structure and mechanical properties of TiC/TiNi composite sintered at 1300°C. They observed the dominance of solid-phase sintering in the 0 ~ 30% TiNi range, an intense recrystallization through a liquid phase in the 40% ~ 60% TiNi range, and the regrouping of carbide particles in the 70% ~ 90% TiNi range. The composite consists of TiC, TiNi and Ni₃Ti phases. When bent and compressed, the TiC/TiNi composite has conspicuously higher strength than TiC/Ni and WC/Co materials due to the reversible martensitic transformation in the matrix. Dunand *et al.* [72-76] examined the phase transformation and mechanical properties of the TiC/TiNi composite with a TiC fraction up to 20%. They found that the TiC particles tend to suppress the phase transformation, in particular, the R phase transformation, and lower the A_s and M_f temperatures with the M_s and A_f temperatures unchanged.

1.3.2. Objective of the study

The objective of this study is to develop a TiNi matrix composite for potential wear applications. There has been some research done on the TiC/TiNi composite, but the emphasis of the work was on investigating the effects of reinforcing particles on the sintering, phase transformation and mechanical properties of this material. No attempt has been made to scrutinize the composite's potential in wear applications, and thus it is unclear whether or not this type of composite is suitable for tribological applications. However, the previous research is valuable to our work, as it has indicated the feasibility of fabricating such a pseudoelastic composite. In addition, the development of such a pseudoelastic tribo-composite offers an opportunity to investigate how the combination of a material's hardness and pseudoelasticity affects its wear behavior. The preceding sections have stated two main factors for the wear resistance of a material. The dominant one is the material's hardness, which is valid for the majority of wear-resistant materials and has been intensively studied and applied. The other source of a material's wear resistance is the pseudoelasticity of special materials, such as TiNi alloy. This novel finding presents an alternative logic for the development of wear-resistant materials. Therefore, based on the TiNi alloy's pseudoelasticity and good wear resistance, we intend to develop a novel type of wear-resistant composite employing a TiNi alloy matrix reinforced by hard particles. Titanium carbide and titanium nitride were chosen as the reinforcing phase because of their high hardness, and TiNi alloy as the matrix due to its pseudoelasticity and toughness. The conventional metal matrix is either too soft or too brittle. But TiNi alloy exhibits both wear resistance and flexibility and thus becomes an ideal candidate matrix for a high performance tribo-composite. In the proposed

composite, TiC/TiN particles may sustain external loads, while the TiNi matrix may accommodate deformation, absorb impact energy, and retain the hard particles. Such a combination is expected to induce enhanced wear resistance, compared with the TiNi alloy and even conventional wear-resistant materials. A series of studies were performed centered on this point, and the results will be reported in the next chapters.

Chapter 2. Development of TiNi-based composite using P/M processing

In Chapter 1, the background information relevant to TiNi alloy's wear behavior and pseudoelasticity has been introduced. Chapter 2 reports the development of TiNi-based composite using powder metallurgical technique. Two types of TiNi-based composites were fabricated employing a vacuum sintering process. TiC and TiN particles were selected as reinforcing dispersoid at different fractions. The composites' structures were studied using optical microscopy (OM), scanning electron microscopy (SEM) and X-ray diffraction (XRD). The mechanical properties and pseudoelasticity of the composite matrix were preliminarily examined by indentation tests. The wear and friction performance of the composites were evaluated and compared to some other engineering alloys. The wear mechanisms of the TiNi-based composites are proposed through worn surface analysis. The effects of powder metallurgy processing were investigated, and the optimum sintering parameters were identified. This chapter reports the results of these tests and discusses some fundamental relationships between the powder metallurgy processing, structure, pseudoelasticity, and wear behavior of the TiNi-based composite.

2. 1. Experimental procedure

2.1.1. Materials

Two groups of TiNi-based composite samples were prepared by a vacuum sintering process. The nominal composition of these different composites and their reinforcing particles' data are listed in Table 2-1 [77]. The designation of "Ti+Ni" refers to synthesis of the composite's matrix from the elemental Ti and Ni powders. In order to investigate how the

fraction of the hard particles affects the composite's wear resistance, the first group of samples were prepared by the addition of TiC particles from 18 vol% to 70 vol%. Following the determination of the best TiC fraction, which was 52 vol%, came the investigation on the influences of second phase particle hardness on the composite's wear resistance. For this purpose, TiN particles were used to substitute for TiC particles in preparing the TiNi matrix composite, under the assumption that the optimum fraction of TiN hard particles be 52 vol%. Subsequently, the mechanical properties and wear performance of both 52vol%TiC/TiNi and 52vol%TiN/TiNi samples were investigated. Finally, different amounts of graphite particles were added into the 52vol%TiC/TiNi and 52vol%TiN/TiNi samples to study how the graphite particles influence the wear behavior of these composites. All the powders had a mesh size of -325 (< 45 μm) except the graphite particles, whose size was 1 μm ~ 2 μm . The Ti, Ni, TiC and TiN powders were ordered from Strem Chemical Inc. (Newburyport, MA) with a purity of 99%, 99.5%, 99%, and 99% respectively, while the graphite particles were from Aldrich Chemical Company Inc. (Milwaukee, WI) with a purity of 99%.

| Group | Sample Name | Particle Fraction | Particle Size (μm) | Particle Hardness (GPa) | Effect Investigated |
|-------|--------------|-------------------|---------------------------------|-------------------------|---------------------|
| 1 | TiC/ (Ti+Ni) | 18 vol% | < 45 | 20 ~ 30 | Particle Fraction |
| | | 35 vol% | | | |
| | | 52 vol% | | | |
| | | 70 vol% | | | |
| 2 | TiN/(Ti+Ni) | 52 vol% | < 45 | 20 | Particle Hardness |
| | TiC/(Ti+Ni) | | | 20 ~ 30 | |

Table 2-1. Composite nominal compositions and reinforcing particle data.

2.1.2. Sample preparation

The elemental Ti and Ni powders and the corresponding reinforcing particles were placed into a plastic bottle with a size of 60 mm in diameter and 120 mm in height. A few sintered WC balls, having a diameter of about 5 mm, were put into the plastic bottle with the mixed powders, and then the bottle was rotated at a speed of 155 rpm on a mill apparatus in air for 2 hours. The mixing process is illustrated in Fig. 2-1. The mixed powders were then manually loaded into a compaction die with a v-shaped spoon and pressed into pin specimens with a Carver laboratory press under a pressure of 787 MPa for 30 seconds, as illustrated in Fig. 2-2. Before loading the powders, both the internal wall and punches of the compaction die were lubricated with SILCHEM mould release spray for easy removal of the compacted sample from the die. The cylindrical green specimens were 8 mm long with a diameter of 6 mm. Thereafter, the specimens were sintered in vacuum of about 6.7×10^{-2} Pa (5.0×10^{-4} torr) in a BREW vacuum furnace. The vacuum was obtained and maintained by a mechanical and a diffusion pump. The heating rate was automatically controlled at around $12^\circ\text{C}/\text{min}$ by the furnace. After the determined period of sintering time, the samples were furnace cooled to room temperature and ready for testing. In order to identify the optimal sintering condition, different sintering temperatures and times were tried from 900°C to 1800°C and from 2 hours to 18 hours.

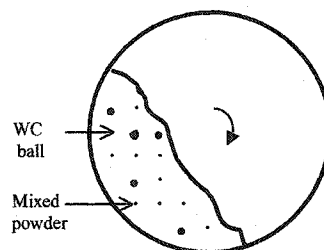


Fig. 2-1. Schematic of powder mixing.

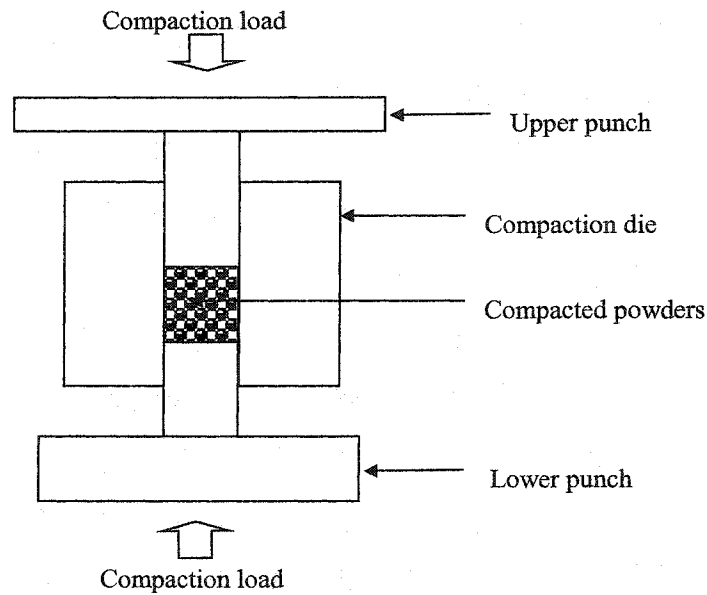


Fig. 2-2. The schematic of the powder compaction.

2.1.3. Specimen structure analysis

The nominal composition of the composite's matrix was Ti-51at%Ni (Ti-56wt%Ni). The microstructure of the composite was examined by an optical microscope and a JEOL 6301F field emission scanning electron microscope. The matrix composition of the composite was analyzed by EDX. The sintered specimens were examined with a Rigaku Geigerflex powder diffractometer to check the phase constitution of the composite, especially the matrix. The scanning was performed from 20 degrees to 80 degrees for 2θ at a rate of 0.5 degree/minute with a Co-K α 1 X-ray incident beam.

2.1.4. Mechanical property testing

Hardness is the most important mechanical property that affects the wear resistance of a material. In TiNi matrix composite, the pseudoelasticity of the matrix also plays a key role in this material's wear behavior. Therefore, the hardness and pseudoelasticity of the

composite were investigated prior to the study of its wear resistance. Since an indentation test offers information on both the material's hardness and pseudoelasticity, it was employed to conduct the investigation through a triboscope - a combination of mechanical indentation and scratch instrument. The indentation load was 20 mN, and scratch load 35 N.

2.1.5. Wear and friction testing

The wear behavior of the composite was evaluated using a pin-on-disc tribometer. During the pin-on-disc wear testing, the pin sample was slid against a 304 stainless steel disc under a normal load in the range of 0.050 to 0.25 kN, and a sliding speed of 60 m/min over 600 meters. A copper tube was attached to the stainless steel disc, through which cooling water passed to carry away frictional heat. Following the wear testing, the samples were washed in alcohol and dried with warm air. The cleaned samples were then weighed with an OHAUS analytical balance to an accuracy of 0.1 mg, and the weight losses were converted to volume losses for assessing the wear resistance of each sample. Each wear loss data point was an average of 4 or 5 measurements. The wear resistance of the 52vol%TiC/TiNi composite was compared to that of 304 stainless steel, as-received Ti-51at%Ni alloy, heat-treated Ti-51at%Ni alloy (aged at 500°C for 5 minutes followed by water quench) and WC/NiCrBSi hardfacing overlay. The fraction of WC in the WC/NiCrBSi hardfacing overlay was 50 vol%.

The friction behavior was tested with a pin-on-disc tribometer by employing a cantilever approach, as illustrated in Fig. 2-3. The surface of the tested samples was ground and polished before the test. Under a normal load of 50 N, pin samples of different materials

were slid against a 304 stainless steel disc for 600 m in oil lubrication. The oil was vegetable-based, and the sliding speed was 30 m/min. The friction coefficients of the materials were determined by measuring the ratio of frictional force to the normal load. The value of the friction coefficient μ was calculated from the equation

$$F = \mu N \quad (2.1)$$

where F was the frictional force between the 304 stainless steel disc and pin sample, while N the normal load applied on the pin specimen. N was known, and F was obtained by measuring the displacement of the end of the pin sample (see Fig. 2-3). The relationship between the frictional force and pin sample displacement was calibrated in advance. After the calibration, when the relationship between the frictional force and pin sample displacement was established, a strain sensor was attached on the specimen to monitor its lateral displacement, and thus the friction force was determined. The entire friction measurement was automated, in which the friction coefficient was recorded by a data-logging system during the whole sliding process.

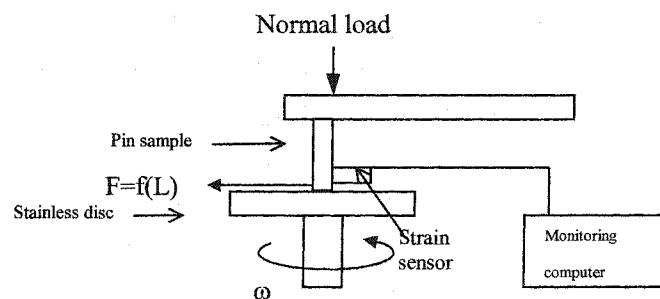


Fig. 2-3. The cantilever system of measuring the friction coefficient.

2. 2. Experimental results and discussion

2. 2. 1. Composition and microstructure

The TiC/TiNi specimens containing 18 vol%, 35 vol%, 52 vol% and 70 vol% TiC particles

were sintered at various temperatures from 900°C to 1800°C for 6 hours, respectively. The specimen sintered at 1500°C exhibited the best wear performance, as discussed later. Fig. 2-4 is a SEM microstructure image of a 52vol%TiC/TiNi composite specimen sintered at 1500°C for 6 hours. The dark areas were TiC particles (the black pits in the TiC particles were porosity of the raw TiC powders), and the lighter ones were matrix. TiC particles were distributed homogeneously. The average size of the raw TiC particles was 45 μm. The SEM image shows a larger size for some TiC particles, say, 100 μm. This may be due to agglomeration of TiC particles occurring during the mixing and sintering process or the existence of some large TiC particles among the raw powders. Additionally, many voids, networking along grain boundaries, were observed in some areas, especially in the central region of the specimen. The porosity will be discussed in detail in the subsequent chapters.

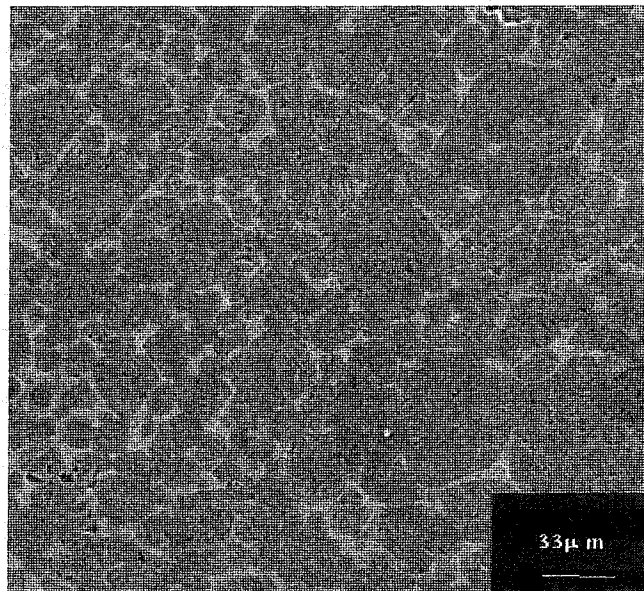


Fig. 2-4. The microstructure of 52vol%TiC/TiNi composite.

The composition of the matrix was analyzed by EDX. The results evince some fluctuation in the matrix's composition with a typical value around Ti-54at%Ni. A local area of the TiNi

matrix between two TiC particles is displayed in Fig. 2-5. The darker region corresponded to a high Ti concentration (Ti-22at%Ni). The particles and the matrix appeared to be well bonded. Since the composition was not very uniform, the mixing or sintering process needs further improvement, although such a specimen has already shown very good wear resistance, as demonstrated later. In order to make sure that the matrix was a TiNi alloy rather than a mixture of the elemental Ti and Ni powders, the specimens underwent X-ray diffraction analysis. Fig. 2-6 is the X-ray diffraction pattern of a 52vol%TiC/TiNi specimen sintered at 1500°C for 6 hours. The XRD detected no dissociated Ti or Ni powders and indicated the formation of the desired TiNi austenite β phase in the matrix. Thus the matrix was in an alloyed state.

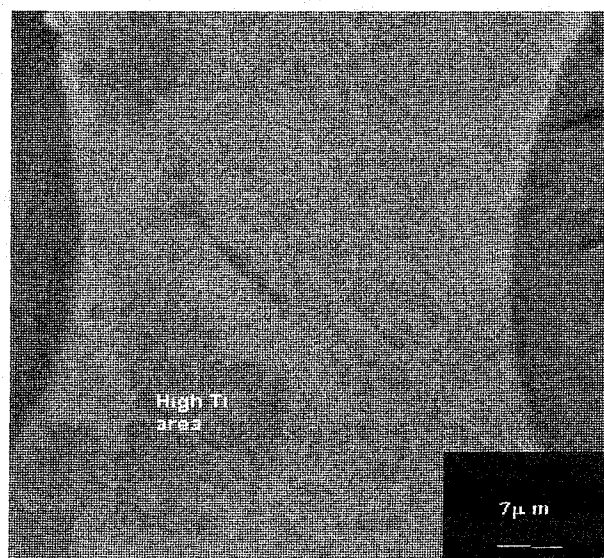


Fig. 2-5. SEM image taken in the vicinity of the TiC/TiNi interface.

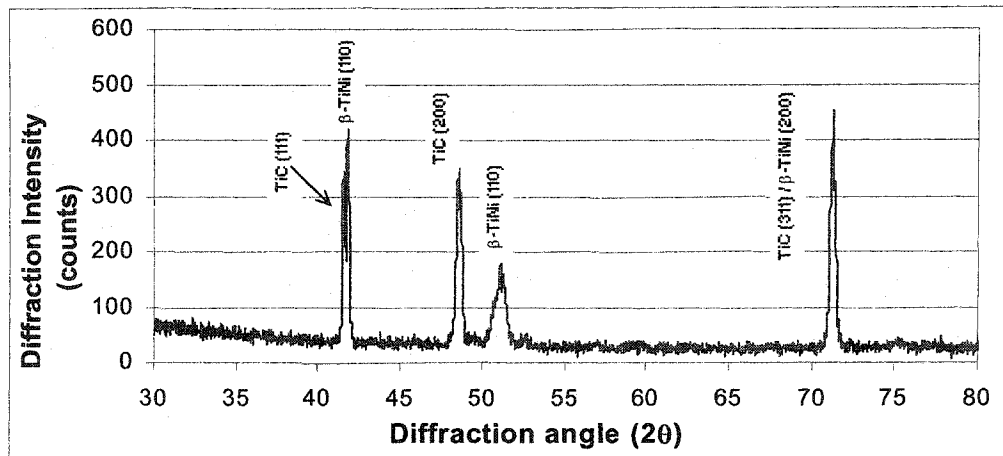


Fig. 2-6. (Co-K α 1) X-ray pattern of 52vol%TiC/TiNi sintered at 1500°C for 6 hours.

2. 2. 2. Pseudoelasticity and wear behavior of TiNi-based composite

Since pseudoelasticity underlies the wear performance of such a designed TiNi-based composite, the pseudoelasticity of the composite was studied along with the as-received, heat-treated (aged at 500°C for 5 minutes and then water quenched) Ti-51at%Ni alloys and 304 stainless steel. Tensile testing is the typical method used to examine pseudoelasticity of a material. However, it is difficult to perform tensile test on such small specimens. Furthermore, the pseudoelasticity of the composite originates from its matrix. So, the matrix is the area of interest. In order to examine the selected areas, indentation testing was employed in this work to investigate the material's pseudoelasticity, and the corresponding load ~ depth curves are displayed in Fig. 2-7. There are two important parameters that can be determined from the indentation test curves. One is the penetration depth, d , a measure of a material's hardness. The smaller the depth, the harder the material. The other one is the ratio (η) of the recoverable deformation energy (the area enclosed in the unloading curve and maximum penetration depth) to the total deformation energy (the area enclosed in the

loading curve and the maximum depth). Fig. 2-7 demonstrates that the 304 steel had little recoverable displacement, where the ratio of the recoverable deformation work to the total deformation work, η , was 11%. The heat-treated TiNi alloy had a considerably larger recoverable displacement with an η value of 47% due to its pseudoelasticity. The as-received TiNi alloy had an η of 36%. Compared to the TiNi alloys, the matrix of the 52vol%TiC/TiNi composite showed medium pseudoelasticity, corresponding to a smaller recoverable displacement with a η value of 33%. It is thus anticipated that an improvement in the matrix's pseudoelasticity will enhance the wear resistance of the material. In addition, it was noticed that the deformation of the 52vol%TiC/TiNi composite's matrix was the lowest, and this is obviously due to the particle strengthening by TiC.

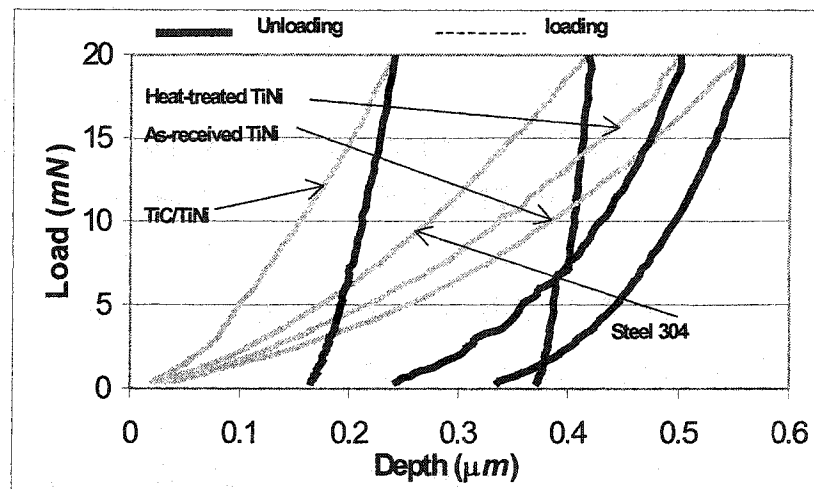


Fig. 2-7. The Load-depth curves during indentation under a maximum load of 20 mN.

In order to investigate the relationship between the composite's pseudoelasticity and wear behavior, dry sliding wear testing was conducted with the pin-on-disc tribometer on the 52vol%TiC/TiNi composite sintered at 1500°C for 6 hours, because it showed the highest

wear resistance among the processed TiNi matrix composites, as reported later. The other materials tested in the dry sliding wear included 304 stainless steel, the as-received TiNi alloy, the heat-treated TiNi alloy and WC/NiCrBSi overlay. The comparison with the Ti-51at%Ni alloys may provide information about the efficiency of TiC particles in improving the wear resistance. It is also worth comparing the TiC/TiNi composite to 304 stainless steel and WC/NiCrBSi hardfacing overlay. The 304 stainless steel is a widely used industrial material, and substantial information about this steel is available. The WC/NiCrBSi overlay is a specially designed hardfacing material widely used in mining and oilsand industries. Comparison of the TiC/TiNi composite with these two standard materials provides evidence that this type of composite is a promising wear-resistant material. The volume losses of the above materials were measured, and results are illustrated in Fig. 2-8. The data shown in Fig. 2-8 was an average of 4 measurements with a variation of 20%. Since the data are plotted at a log scale, this 20% error does not reduce the credibility of the test.

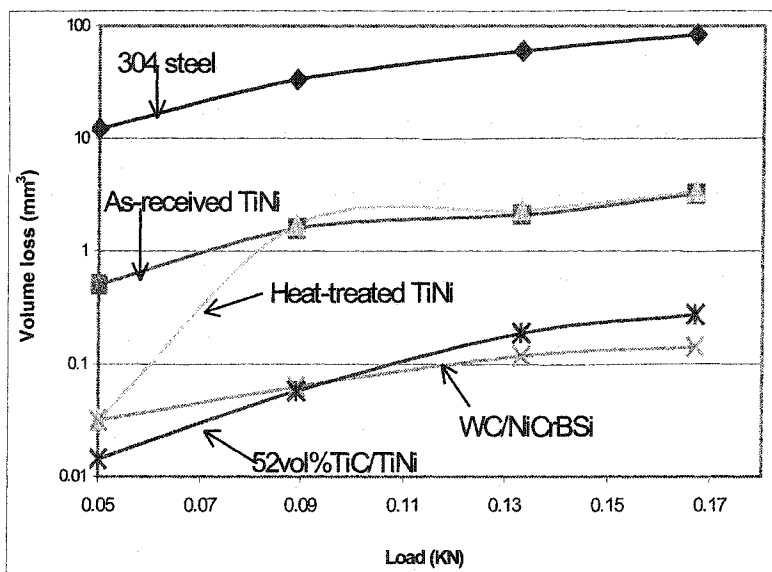


Fig. 2-8. Wear losses of different materials against the applied loads.

The as-received TiNi alloy exhibited wear resistance that was about one order of magnitude higher than that of the 304 stainless steel. The heat-treated TiNi alloy displayed wear resistance similar with that of the as-received TiNi alloy at high wearing loads and superior wear resistance at low wearing loads. The superiority of the TiNi alloy's wear resistance compared with the stainless steel can be explained by its pseudoelasticity, as discussed in Section 1. 2. During a tensile test, the as-received TiNi alloy had a recoverable strain around 3%, while the heat-treated TiNi alloy's recoverable strain reached 4% [49], which means the heat-treated TiNi alloy had a better pseudoelasticity. These two recoverable strains were compatible with the indentation test shown in Fig. 2-7, where the calculated η value of the as-received TiNi alloy was 36% and the heat-treated TiNi alloy 47%. The pseudoelasticity enables the TiNi alloy to accommodate a larger deformation and show a higher wear resistance. It was also interesting to notice that, under low loads, the heat-treated TiNi alloy specimens had considerably higher wear resistance than the as-received TiNi, while under higher loads this discrepancy in the two TiNi alloys' wear resistance was eliminated. This happened because the pseudoelasticity may not accommodate the very large deformations introduced by great loads. As a result, the as-received and heat-treated TiNi alloy specimens behaved similarly when heavily loaded. Furthermore, under higher loads the increased frictional heat may raise the material out of the temperature range for the martensitic transformation to occur, and this could further diminish the difference in these two TiNi alloys. The wear behavior of the stainless steel, as-received and heat-treated TiNi alloys once again demonstrates the beneficial effect of pseudoelasticity on the wear resistance of the material.

For the TiNi-based composite, compared to the volume loss ~ load curves of the as-received and the heat-treated TiNi alloys, it seems that the TiNi matrix of the TiC/TiNi composite did not possess a high degree of pseudoelasticity. This may be seen from the trend of the composite's volume loss with respect to load, which was closer to the trend of the as-received TiNi alloy. This conclusion is supported by the indentation test, where the TiC/TiNi composite matrix TiNi alloy showed a η value of 33%, close to that of the as-received TiNi alloy at 36%. Simultaneously, it was observed that the wear resistance of the 52vol%TiC/TiNi composite was more than one order of magnitude higher than the as-received TiNi alloy for the entire loading range. Compared to the heat-treated TiNi alloy, the TiC/TiNi composite also showed significantly higher wear resistance under high loads. However, under low loads, this advantage of the composite in terms of wear resistance decreased, as Fig. 2-8 illustrates. This could be due to the superior pseudoelasticity of the heat-treated TiNi alloy, which made this TiNi alloy very resistant to wear under low loads. Accordingly, the decrement in the superiority of the TiC/TiNi's wear resistance compared with the heat-treated TiNi alloy at low loads still results from the material's pseudoelasticity. It is also interesting to compare the wear loss curves of the TiC/TiNi composite and WC/NiCrBSi. At low load, the TiC/TiNi outperformed WC/NiCrBSi, and as the load exceeded 0.09 kN, the WC/NiCrBSi began to exhibit a more competitive wear performance. WC has a hardness of 24 GPa and TiC 20 GPa ~ 30 GPa [77]. The fraction of WC in the overlay was 50 vol%, and TiC in the composite 52 vol%. The similar values of the hardness and fraction of TiC and WC particles in the composites exclude the possibility that the second phase particles differentiated the wear behaviors of these materials. Thus, the reasons for such alternative wear performances of these two materials involve the material's density,

pseudoelasticity and interphase bonding. A high porosity was uncovered in the sintered TiC/TiNi, which would reduce the wear resistance of the composite at high loads. The influences of porosity will be discussed with more details in Chapter 3 and interphase bonding in Chapter 6. Compared with the density of the material, pseudoelasticity is thought to be less determinant, as the load had reached a high value. Under high load, with the generation of a high-density of dislocations, the pseudoelasticity becomes less influential. As a result, the pseudoelasticity's contribution to the wear resistance is limited. The critical load that can overwhelm the pseudoelasticity must exist, and it was regarded to be around 0.09 kN in this specific case not only because the TiC/TiNi became inferior to the WC/NiCrBSi, but also because the heat-treated TiNi alloy began to show similar wear performance with the as-received TiNi alloy around this value.

The above sections form a preliminary discourse on the importance of pseudoelasticity to the wear behavior of the TiNi-based composite. More investigation of the relationship between the composite's pseudoelasticity and wear performance was conducted, and will be reported in Chapter 5. In addition to the pseudoelasticity, a material's hardness is another source for its wear resistance. The effects of the hard TiC or TiN particles on the wear performance of the TiNi based composite are discussed in Section 2.2.4.

2.2.3. Friction behavior of TiNi-based composite

The friction behavior of the 52vol%TiC/TiNi and 52vol%TiN/TiNi composites was investigated and compared to those of the as-received and heat-treated TiNi alloys as well as 304 stainless steel under an oil lubricated sliding condition. The surface of the tested

samples were ground and polished before the test, and the lubricant was vegetable-oil based, without petroleum and mineral components or heavy metals. Fig. 2-9 illustrates the friction coefficients of these materials during the continuous sliding process. Under the lubrication condition, the temperature of the pin samples did not change much. It was determined using a laser thermometer that the sample's temperature at the side near its bottom was around 26°C, close to the initial room temperature. The friction coefficients were continuously measured over a sliding distance of 600 m, as shown in Fig. 2-9. The heat-treated TiNi alloy had a friction coefficient (about 0.01) close to that of the stainless steel. The as-received TiNi alloy, however, had a considerably higher friction coefficient around 0.09. The test showed that the 52vol%TiC/TiNi and 52vol%TiN/TiNi composites had a medium friction coefficient between those of the as-received and the heat-treated TiNi alloys.

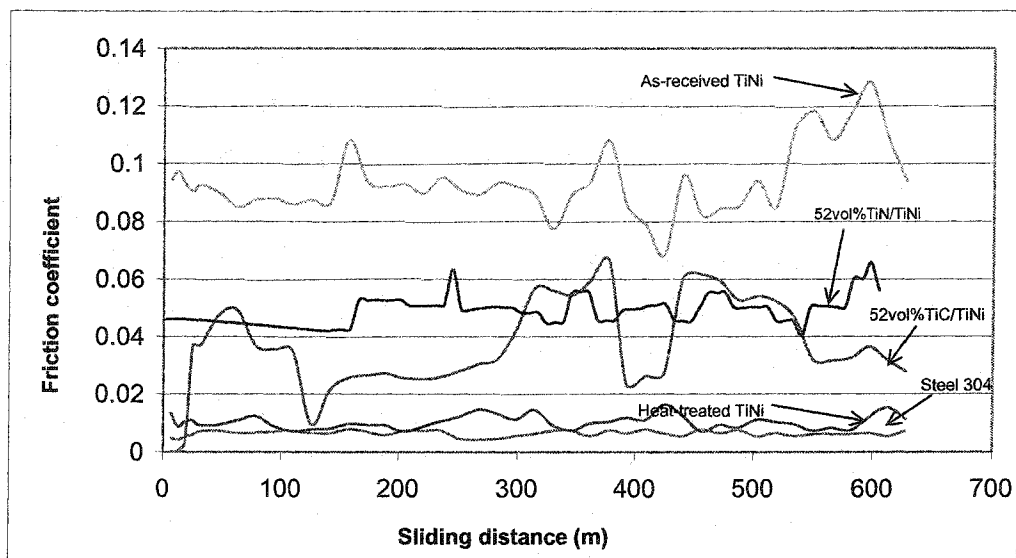


Fig. 2-9. Friction coefficients of TiNi alloy, TiN/TiNi, TiC/TiNi and Steel 304.

Fig. 2-9 shows the friction coefficients of different materials versus 304 stainless steel. It was interesting to observe the large difference in the friction coefficients of the as-received

TiNi alloy and the heat-treated TiNi alloy. It is known that the friction is influenced by two major forces: one is adhesion force from the atomic interaction between two sliding surfaces in contact, and the other from the force needed to deform interacting asperities or plough the surface by wearing particles and asperities [6, 78]. The friction coefficient, μ , may therefore be approximately expressed as a sum of two components:

$$\mu = \mu_a + \mu_d \quad (2.2)$$

where μ_a and μ_d represent contributions from the adhesion and deformation/ploughing, respectively. The adhesion contribution is largely dependent on the pair of materials in contact, especially on their chemical compositions, which strongly affect the atomic interaction. It is expected that pseudoelasticity may not drastically influence the adhesion force (per unit area), since it is unlikely for pseudoelasticity to influence the atomic interaction and thus considerably change the adhesion force. However, pseudoelasticity may raise μ_a because of the resultant increase in contact area. Adhesion significantly diminishes in oil lubrication because of the oil film between the sliding surfaces. Therefore, the disparity in μ between the heat-treated and as-received TiNi alloy specimens should mainly result from the difference in μ_d . Thus it can be deduced that pseudoelasticity greatly affects the μ_d value. The heat-treated TiNi alloy had a lower "yield" strength with the recoverable deformation resulting from its better pseudoelasticity, compared to the as-received TiNi alloy [79]. This property will enable the alloy to exhibit lower μ_d , since the superior pseudoelasticity facilitates the deformation of asperities in contact. Furthermore, when sliding under the lubrication condition, the frictional heating is greatly reduced (the measured sample temperature was only 26°C), thus obliterating the temperature rise and

consequent loss of the pseudoelasticity. Thus the heat-treated TiNi alloy should have a significantly lower friction coefficient because of its superior pseudoelasticity to that of the as-received TiNi alloy.

In the case of TiNi-based composite, both the matrix and particles can affect the material's friction coefficient. The generally low adhesion between unlike materials [9] may impart to the ceramic/metal contact, *i. e.* TiC/steel or TiN/steel, a smaller friction coefficient than that of a metal/metal contact, *i. e.* TiNi/steel contact. However, under the oil-lubrication condition, the adhesion may not be a predominant factor in determining the friction coefficient. Therefore, the lower pseudoelasticity of the TiNi matrix of the TiNi-based composites could be a major cause for a rise in friction coefficients, compared with that of the heat-treated TiNi alloy. However, the situation dissimilates from that of the as-received TiNi alloy. As demonstrated earlier, the TiNi-based composite had its local pseudoelasticity close to that of the as-received TiNi alloy. Therefore, the lower friction coefficient of the TiNi-based composite, compared to that of the as-received TiNi alloy, might be attributable to its higher hardness, which would result in less asperity penetration and deformation. However, the lowest friction coefficient of the heat-treated TiNi alloy among the TiNi alloys and TiNi-based composites implies the importance of pseudoelasticity to friction under the oil-lubrication condition.

2. 2. 4. The effects of secondary phase particles on the wear behavior of TiNi based composite

In the composite materials, hard particles are important in resisting wear through modification of the mechanical properties of the material. Wear often takes place from the material's cracking or fracturing in the heavily deformed subsurface region [9]. During the wear process, fresh dispersoids are exposed to the surface and interact with the counter-wearing material. This shift of the role in directly withstanding the external load from metal matrix to ceramic particles significantly alters the wearing process, since the hardness of ceramic particles is much higher, compared to that of the metal matrix and even the external loading material. Thus the hard particles can protect the composite material's matrix. Generally, if the hard particle does not fragment, wear on the matrix is greatly reduced. At the same time, even if some wear happens in the matrix area, that is, there is plastic deformation or microcrack propagation, the motion of dislocations during the plastic deformation or the propagation of microcracks can be blocked by the hard particles if they form a strong bond with the matrix. From this point of view, the hard particles will remarkably improve the material's wear resistance. The mechanical and tribological properties of the metal matrix composite depend on the amount, size, shape and distribution of the dispersed phase, and the nature of the interface formed between the dispersoids and matrix [7]. In the particular case of TiNi-based composite, the hard dispersoid will also affect the matrix's pseudoelasticity. Accordingly, the effects of the dispersoids in the TiNi-based composite on its mechanical properties and wear performance are a combination of their protection to the composite matrix, as in conventional wear-resistant metal matrix composite, and their influences on the matrix's

pseudoelasticity. The dispersoid's effects on the pseudoelasticity of the composite will be discussed in Chapter 5. In this chapter, the focus is put on the conventional influences of the hard particles on the wear resistance of the TiNi-based composite.

2.2.4.1. Effect of TiC fraction on the wear behavior

The volume losses of the TiC/TiNi specimens with 18 vol%, 35 vol%, 52 vol% and 70 vol% TiC particles were evaluated under the loads of 0.05, 0.133 and 0.167 kN respectively, and the results are illustrated in Fig 2-10. The volume loss decreased with increasing TiC content up to 52 vol%. The 70vol%TiC/TiNi specimens, however, were too brittle and showed a lot of voids visible to the naked eye. They were worn out quickly during the wear testing even under a low load. It turned out that the optimum content of TiC particles was 52 vol% among the selected fractions.

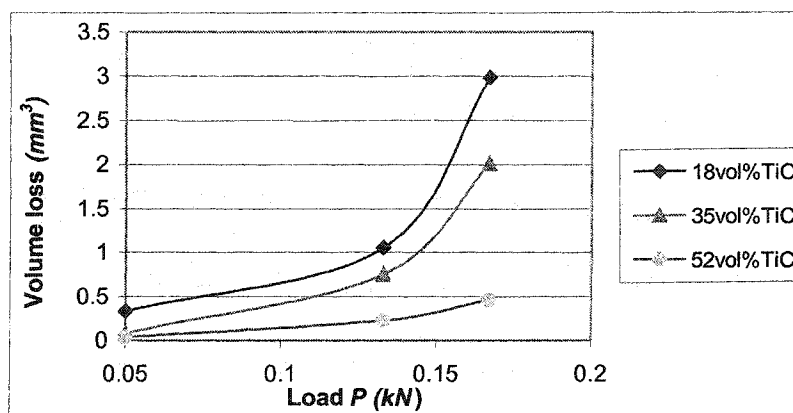


Fig. 2-10. Wear losses of samples with different TiC fractions.

The surfaces of the 52vol%TiC/TiNi specimens worn under 0.05 and 0.167 kN loads were examined and are illustrated in Fig. 2-11 and Fig. 2-12 respectively. Under the low load, the worn surface showed sliding wear characteristics, where the major damage was microcutting on the surface material by the external force. Under the high load, the wear

was more severe. The specimen was striped, and TiC particles were torn out (see the left-hand side of Fig. 2-12.)

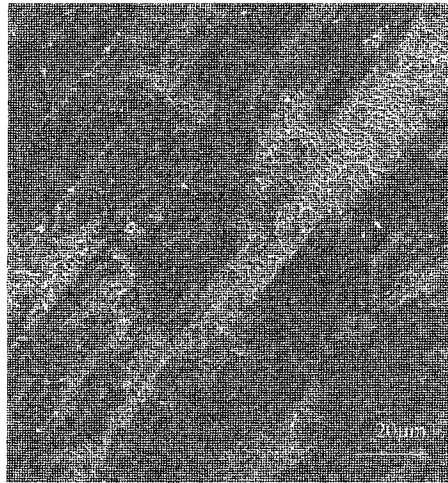


Fig. 2-11. Worn surface of 52vol%TiC/TiNi under 0.05 kN.

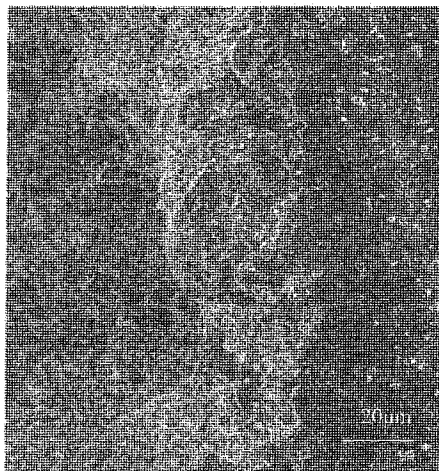


Fig. 2-12. Worn surface of 52vol%TiC/TiNi under 0.167 kN.

The hard particles have been proved to be very beneficial for the TiNi base composite to improve its wear resistance. Generally, in conventional metal matrix composite, with an increase in the volume fraction of the hard particles, the tensile strength and wear resistance of the composite increase, and the fracture toughness and ductility of the composite decrease

[7]. Fig. 2-10 shows the TiC fraction's influence on the wear resistance of the TiC/TiNi composite. A critical TiC fraction existed among the tested fraction values. Under 52 vol%, the composite's wear resistance increased when more TiC particles were added into the composite, and after 52 vol%, the wear resistance decreased with the addition of the TiC particles. This critical fraction of the secondary hard particles primarily depends on the loading conditions and hardness of the particles. Usually, when the loading has an impact force, the critical fraction of the second phase particle decreases, as the hard and brittle particles cannot sustain large impact loads. On the contrary, if the loading is applied smoothly. The critical fraction increases as the hard particles can sustain a high abrading force. So in the composite design, a series of investigations have to be conducted to find out the critical fraction according to the loading conditions. The critical fraction will also influence the matrix's pseudoelasticity of the composite, as discussed in Chapter 5, and powder metallurgy processing.

2. 2. 4. 2. *The effect of the reinforcing particle hardness on the wear behavior*

In order to study the effects of dispersoid's hardness on the wear performance of TiNi matrix composite, both 52vol%TiN/TiNi and 52vol%TiC/TiNi samples underwent wear testing over a wider range of loads, as illustrated in Fig. 2-13. The 52vol%TiN/TiNi had wear resistance comparable to that of the 52vol%TiC/TiNi at low loads and higher wear resistance at high loads. A scratch experiment was performed to investigate the scratch resistance of both the 52vol%TiN/TiNi and 52vol%TiC/TiNi composites. The scratched surfaces of 52vol%TiN/TiNi and 52vol%TiC/TiNi composites are shown in Fig. 2-14 and Fig. 2-15 respectively. No crack was found on the 52vol%TiN/TiNi specimen, while cracks appeared on the 52vol%TiC/TiNi specimen.

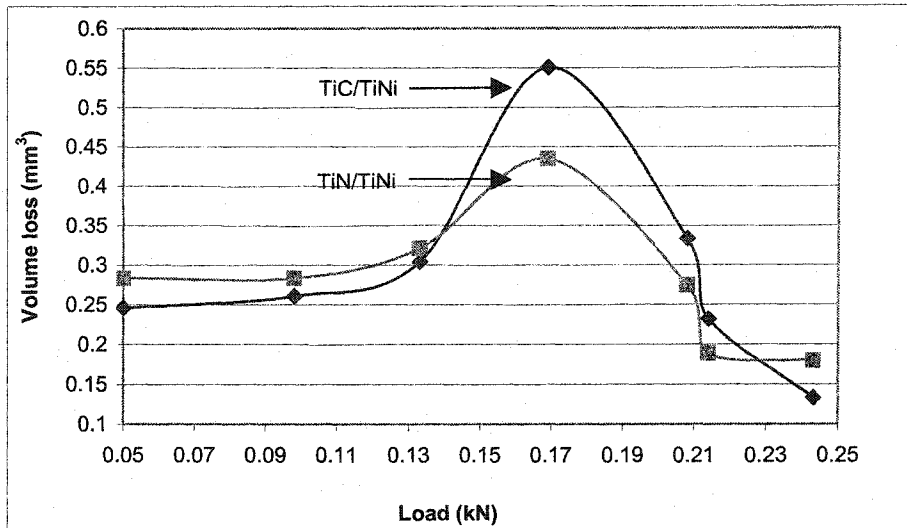


Fig. 2-13. Wear losses of 52vol%TiN/TiNi and 52vol%TiC/TiNi with respect to the load.

The comparison between the 52vol%TiC/TiNi and 52vol%TiN/TiNi scratch tests in Fig. 2-14 and Fig. 2-15 implies that the wear resistance of 52vol%TiC/TiNi was poorer under higher loads. One possible mechanism responsible for this difference is that TiN particles are tougher than TiC. TiN has a hardness of 20 GPa, while TiC has a hardness of 20 GPa ~ 30 GPa [77]. Thus 52vol%TiN/TiNi may sustain higher stresses without cracking, leading to higher wear and scratch resistances under larger external forces. Under low loads, the 52vol%TiC/TiNi composite showed slightly higher wear resistance, as Fig. 2-13 illustrates. This could be attributed to the higher hardness of TiC phase, since under low-stress wear condition, hardness plays a predominant role in resisting wear. Fig. 2-13 reveals another interesting phenomenon that when the load exceeded 0.17 kN, the wear losses of both the TiC/TiNi and TiN/TiNi specimens decreased with increasing the load. Studies have found that the decrease in the wear loss of the sintered TiNi-based composites under high loads is attributed to self-healing of pores. A decrease in the density of voids enhances the wear resistance of the TiNi composites. Details of the studies are reported in the upcoming

chapters.

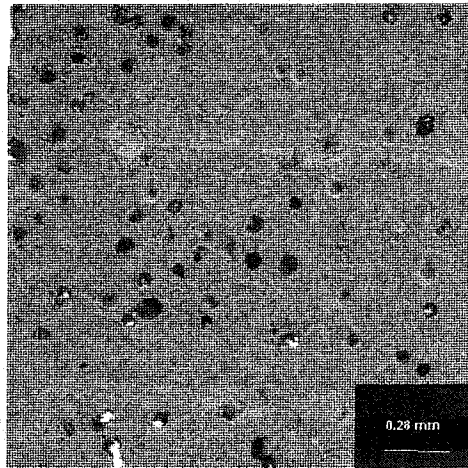


Fig. 2-14. Scratch track of 52vol%TiN/TiNi at a normal force of 35 N.



Fig. 2-15. Scratch track of 52vol%TiC/TiNi at a normal force of 35 N.

Along with the hard TiC and TiN particles, some graphite particles were also added into the TiNi matrix to investigate how soft particles will influence the wear performance of the TiC(N)/TiNi composite. Graphite particles are sometimes beneficial to the wear resistance of a material because they may act as a kind of solid lubricant. Roy *et al.* found that, in a dry sliding wear test, the composites containing SiC, TiC, TiB₂ or B₄C particles exhibit a lower wear rate when compared with the base metal. However, the aluminum alloy base

composite containing both hard particles and graphite has the lowest wear rate because of the lubrication from graphite [80].

Different amounts of graphite were added into the 52vol%TiC/TiNi and 52vol%TiN/TiNi composites to investigate the graphite's effect on the wear resistance of the TiNi-based composite. The graphite is expected to lubricate the wearing surface, suppress the worn surface temperature, help the composite's matrix to hold its pseudoelasticity, and thus finally enhance the material's wear resistance. The common addition of graphite in composite materials is between 3 wt% and 5 wt% [81, 82]. In our studies, 1 wt%, 3 wt% and 6 wt% graphite additions were implemented. The wear performances of these graphite-containing TiNi-based composites were studied by a dry sliding wear testing on the pin-on-disc tribometer at a wearing load of 0.133 kN and a sliding speed of 60 m/min for 600 m. The wear test results are shown in Fig. 2-16. It can be seen that the graphite decreased the wear resistance of both the TiC/TiNi and TiN/TiNi composites. The deleterious effect of graphite increased with its concentration in the composite. When the graphite content reached 6 wt%, the wear losses were hundreds of times larger than that of the graphite-free composites. Therefore, graphite does not help the TiC/TiNi and TiN/TiNi to resist wear.

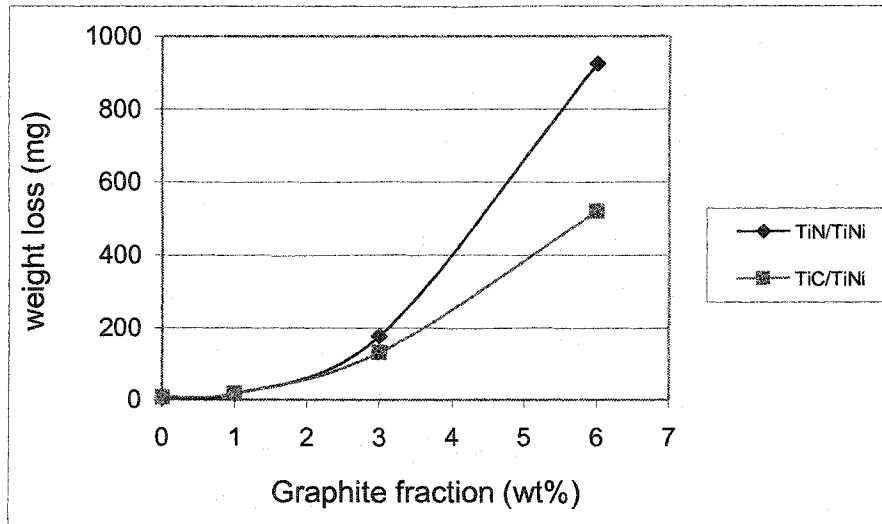


Fig. 2-16. The influence of graphite on the wear behavior of TiNi-based Composite.

There are a few reasons that may be responsible for the reduction of the wear resistance of TiC/TiNi and TiN/TiNi by graphite. The first is that since the graphite has a very low hardness and strength, the graphite added into the TiNi composite also acts as a “hole” in the material. These “holes” not only cannot sustain load but also raise stress concentration around them. This can significantly degrade the mechanical properties and wear resistance of the material. The second possible reason is that the graphite may adversely affect the bonding between TiC/TiN and TiNi matrix and thus reduce the composite’s wear resistance. The last possible reason is that the graphite may react with Ti in the TiNi matrix and change the matrix’s composition. This reaction would certainly destroy the pseudoelasticity of matrix and thus the wear resistance of the composite. This preliminary study shows that the graphite decreases the wear resistance of the TiNi base composite, although more work is needed to make a sound conclusion about the effects of soft particles on the mechanical properties and wear resistance of the TiNi-based composite.

In addition to the hard particle's fraction and hardness, in the composite material, there are some other factors that can affect the composite's wear performance, including second phase particle size and the interface between the matrix and reinforcing phase. However, since the current work was primarily aimed to demonstrate that the incorporation of the second hard particles into TiNi matrix can improve the alloy's wear resistance, these factors were not studied, even though they greatly influence the composite's properties.

2.2.5. Processing and wear behavior of TiNi-based composite

Since pseudoelasticity has been shown to be very important to the TiNi-based composite's wear performance, and the former relies on the composite's composition and structure, the composite's processing becomes critical as it affects both the composite's final composition and structure. Two important aspects of the composite are determined during its processing. One is its composition and phase constitution, and the other one is the density of the composite. The study associated with the density will be reported in the next chapters, and the dependence of the composition and phase constitution on its processing is presented here.

The composition of the composite is affected from the onset of its processing. Powder mixing, sintering and after-treatment all have a large influence on the composite's composition. From Fig. 2 - 4 and Fig. 2 - 5, it can be seen that the second phase particles basically had a uniform distribution in the matrix except that some particles had a size larger than the mean size. The presence of these large size particles may be due to the existence of some big individual raw particles or agglomeration of the TiN powders happening in the mixing and sintering process. The raw TiC or TiN powders were examined. Not many large

particles were found. Therefore, the large second phase particles were produced during the processing of the material. The matrix shown in Fig. 2 - 4 and Fig. 2 - 5 also did not have good homogeneity in its composition. Some areas had a higher Ni content and others had a lower Ni content. The variation from the nominal composition of the analyzed location in Fig. 2 - 5 was 29at%Ni. Since a change of 0.1% in the Ni concentration produces a 10°C's change in the martensitic phase transformation temperature [51], this composition variation is detrimental to the composite's pseudoelasticity and wear performance at a particular temperature, even though the composite has exhibited a reasonable pseudoelasticity and wear resistance. This composition fluctuation means the material's processing needs to be improved.

In the experiment, the Ni, Ti and TiC or TiN powders were mixed in a plastic bottle with a spinning speed of 155 rpm. There are two parameters in the mixing process that have an important effect on the homogeneity of the mixed powders. The first is the ratio of the mixed powders' volume over the total mixing container's volume. Some studies have discovered that the powder volume between 20% and 40% of the mixer capacity usually produces a high mixing efficiency [83]. The ratio for the mixing of the TiNi base composite's powders was in this range. The second important parameter affecting the mixing proficiency is the rotational speed of the mixer. During the mixing process, the spinning speed of the mixing bottle introduces a force to diffuse the individual powders into the powder lot. In Fig. 2 - 1, an inclined plane of the powder bed breaks down at the outer edge, which allows flow over the surface. The continuous rotation of the bottle provides the inclined plane with fresh powder and thus gives intermixing of particles. If the rotation of

the mixer is too slow, the powder plane cannot break in time, thus reducing the mixing efficiency. If the speed is too high, there is a centrifugal force that will interfere with the mixing. The best spinning speed corresponds to a small centrifugal force to produce those conditions where turbulence of the powders can take place. Some research has established an empirical relationship between the cylindrical mixer diameter and its optimal rotational speed, as shown in the equation below [83].

$$N=32/(d^{0.5}) \quad (2.3)$$

where d is the cylindrical mixer diameter in meters, and N is the optimal rotational speed of the mixer in rpm. According to equation 2.3, the optimum spinning speed of the mixing bottle in this work should be 130 rpm. However, due to facility availability, the actual rotational speed of the mixing bottle was 155 rpm. Since the mixer rotated at a speed close to the optimum mixing speed, it is quite possible that the fluctuation in the composite matrix's composition was a result of the poor quality of sintering rather than any deficiency in mixing.

Some other factors can also influence the powder mixing proficiency such as ceramic mixing balls, powder size, powder density, powder surface condition, which determines the surface friction in the mixing, and the powder type, which means alloyed or elemental powders [83]. Since this work is not a study on powder metallurgy, these possible influences were not further investigated in this work.

Sintering is the most critical step in powder metallurgy. The sintered material's mechanical properties are mainly formed in this stage. Before discussion of the sintering of the TiNi

matrix composite, the sintering of TiNi alloy is introduced here. Currently, two types of sintering techniques are often used. One is the conventional pressing and sintering technique [55-57, 84], and the other one is combustion sintering [85, 86]. The conventional sintering constitutes solid-state interdiffusion, which can generate intermetallic phases at the interface. The difficulties in conventional sintering lie in achieving high composition homogenization and composite density. Homogenization by solid-state diffusion during the sintering process requires a long time. Introduction of a liquid phase during the sintering cycle enhances the homogenization process. Since the existence of the liquid promotes kinetics of mass transport by causing the solid to dissolve, it consequently leads to a rapid homogenization of the composition [83]. Combustion sintering brings the initial compact of the mixed Ti and Ni powders to a high temperature, where the Ti and Ni powders violently react with each other to form the TiNi alloy. The advantage of this type of synthesis is with respect to the energy and time saving, but this technique presents problems in dimensional control of the samples [85]. In this work, the conventional sintering process was employed to fabricate TiNi-based composite.

During the sintering of the TiNi-based composite, the presence of a large amount of second phase particles has two effects. The first is the maintenance of the sample dimension at high temperature. The melting points of Ni and Ti are 1453°C and 1668°C respectively [15]. At 1500°C, the Ni powders were melted, and Ti powders were also very soft. The total volume fraction of the Ti and Ni powders was 48% of the entire green sample, which means a large portion of the sample had become liquid under vacuum conditions. However, the samples were still cylindrical after the sintering except that there was some shrinkage at the top of the

samples. This happened because the second phase particles formed a three dimensional network, which kept the overall shape of the compact even at high temperatures. However, the solidification of liquid Ni-containing phases still produced shrinkage to some extent. The second effect of the high content hard particles in the composite is that they blocked the diffusion of Ti and Ni atoms and thus made the sintering need a higher energy to alloy the Ti and Ni powders. Accordingly, even at 1500°C, the sintering process took 6 hours to achieve its optimum state, as shown in Fig. 2-17. The sintering of 6 hours of the composite was quite long compared with the pure TiNi alloys, which were usually sintered at 1300°C for 1 or 2 hours, as reported in the literature [55-57, 84].

Another important point is that the raw powders may have oxide scales and, at such a vacuum level 1.33×10^{-2} Pa (10^{-4} torr) and high temperature (1500°C), oxidation could also occur during the sintering process, which may hinder the sintering and stress-induced martensitic transformation in the TiNi alloy. However, oxides were not detected by XRD and EDX, and the sintered composite possessed a reasonably good pseudoelasticity, as demonstrated in the indentation testing. Therefore, the oxides, if any existed, were not sufficient to cause significant deterioration in pseudoelasticity and thus the wear performance of the material.

Since the 52vol%TiC/TiNi composite exhibited the highest wear resistance, attention was then paid to this composition. In order to identify the optimal sintering parameters, the 52vol%TiC/TiNi specimens were sintered at 1300°C, 1500°C, 1600°C, 1700°C and 1800°C for 6 hours respectively. Different sintering periods of time were also chosen. For instance,

some 52vol%TiC/TiNi specimens were sintered at 1300°C for 6, 12 and 18 hours, and at 1500°C for 6 and 14 hours, respectively. Fig. 2-17 illustrates the wear performance of the specimens sintered at different temperatures for 6 hours. 1500°C appeared to be the best sintering temperature among those tested. As for the sintering time, the wear resistance of the 52vol%TiC/TiNi was improved by prolonging the sintering time at 1300°C, while for those specimens sintered at 1500°C, the wear resistance was not markedly influenced when the sintering period was longer than 6 hours. This is understandable based on the fact that the sintering temperature affects atomic diffusion. Higher temperature corresponds to a higher mobility for atomic diffusion. Short time is therefore needed to finish the diffusion at high temperature, while at a lower temperature, diffusion takes a longer time.

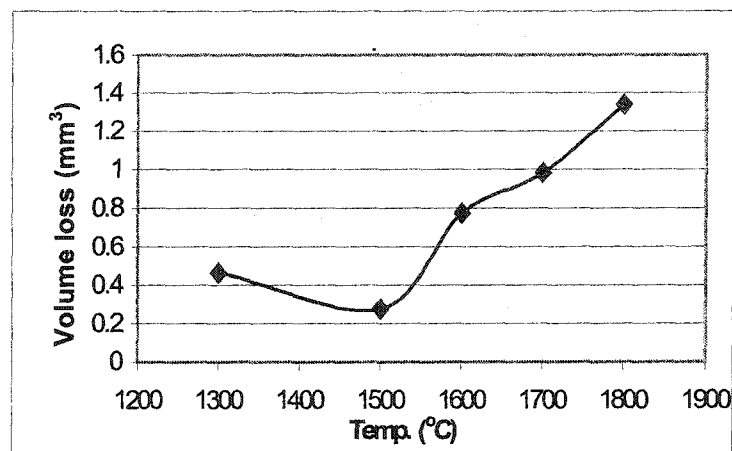


Fig. 2-17. Wear losses of samples sintered at different temperatures for 6 hours.

2. 2. 6. Wear mechanism of the TiNi-based composite

Knowledge of the wear mechanism helps to discern the cause of a material's wear. The wear mechanism of the TiNi based composite was examined in comparison with that of TiNi alloy. The wear characteristics of Ti-50at%Ni and Ti-51at%Ni alloys were studied by a

sliding wear against a Cr-steel under a load ranging from 9.8 N ~ 58.8 N (1 to 6 kg force) [42]. Four wear mechanisms were observed on the worn surface during the sliding wear, as shown in Fig. 2-18 to Fig. 2-21 respectively. In Fig. 2-18, besides the cutting tracks left on the worn surface, some fragments are clearly present. The fragments are adhesion damage. When the TiNi alloy (200 HV ~ 320 HV) adheres to the Cr-steel disc (720 HV), the TiNi protrusions are fractured and transferred to the disc because TiNi alloy is relatively soft. Therefore, adhesive wear is responsible for the wear of the TiNi alloy. In Fig. 2-19, abrasive cutting is the major source for the TiNi alloy's wear. Fig. 2-20 displays surface fatigue of the TiNi alloy. In the repeated loading and unloading cycles, many cracks form in the surface or subsurface and finally result in the breakup of the surface into large fragments, leaving chips on the worn surface. The last wear mechanism of the TiNi alloy is shown in Fig. 2-21. The TiNi alloy is soft, when it is subject to an external load, a large amount of plastic deformation occurs and forms many wavy tracks on the worn surface, which is called brinelling. Usually, the brinelling increases the friction coefficient, like in the case of the as-received TiNi alloy in Fig. 2-9, but has little contribution to the weight loss, as the material is not removed from the surface. The above four mechanisms, adhesive wear, abrasive wear, surface fatigue wear and brinelling wear, all contribute to the damage of the TiNi alloy.

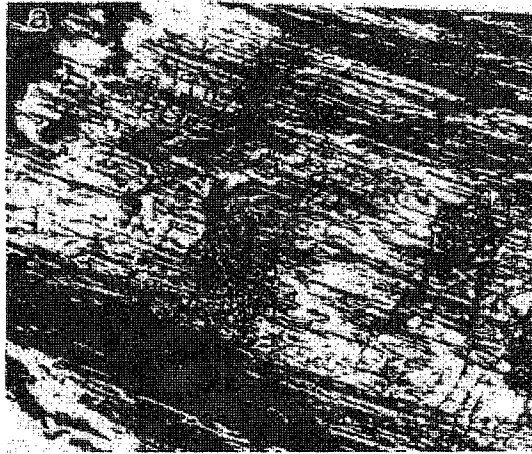


Fig. 2-18. The adhesive wear morphology of TiNi alloy [Ref. 42].



Fig. 2-19. The abrasive wear morphology of TiNi alloy [Ref. 42].

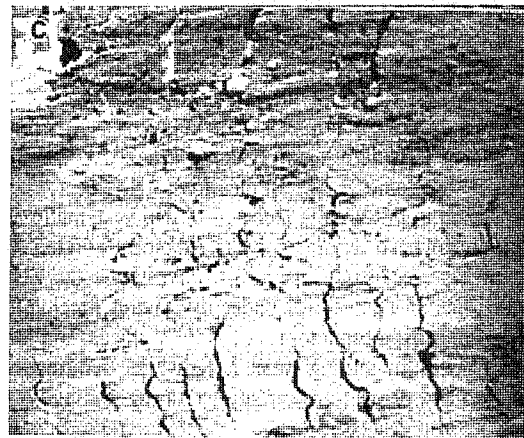


Fig. 2-20. The surface fatigue wear morphology of TiNi alloy [Ref. 42].

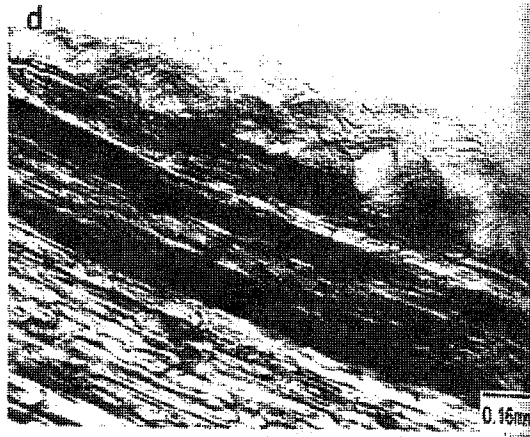


Fig. 2-21. The brinelling wear morphology of TiNi alloy [Ref. 42].

Fig. 2-11 and Fig. 2-12 show the worn surfaces of a 52vol%TiN/TiNi sample under 0.05 kN and 0.167 kN loads respectively. At low load, the major damage caused to the composite is micromachining. The wear features of the TiNi matrix composite are quite similar to those for abrasive wear of the TiNi alloy. At high load, the damage to the TiNi base composite is mainly caused by the breaking and/or tearing out of the hard TiN particles, which leaves pits on the worn surface.

Therefore, in the TiNi matrix composite case, the wear happening on the TiNi matrix is mainly abrasive. The other three mechanisms become minor. This is understandable. Adhesive wear only happens on the contact area between two wearing surfaces. In the composite, due to the presence of hard particle protrusions, the contact between the two surfaces actually takes place mainly between the hard particle and the wearing disc surface. Therefore, the TiNi matrix has less chance to contact the couple surface, or the adhesive force is not strong if it occurs. Thus adhesive wear is not detected after the test. The features of surface fatigue wear are not apparently present on the worn surface of the TiNi matrix

composite because of the following reasons. First, the pseudoelastic matrix can absorb impact energy, accommodate large deformation of the material, and thus is able to reduce crack initiation. Second, once there are some microcracks initiated in the matrix, the hard particles embedded in the matrix can impede the propagation. So the microcracks in the composite have a smaller chance to reach the surface and remove a piece of bulk material. For the brinelling, since the composite is much harder than the TiNi alloy, large amounts of plastic deformation without fracture is almost impossible. Therefore, the overall wear of the TiNi-based composite is mainly produced by abrasive wear on the matrix and the failure of the hard particles. In this case, the fraction of the hard particle and loading conditions are supposed to have a large influence on the material's wear resistance. Because of the high brittleness of the hard particle, it is easy for high impact loads to break the particles and then destroy the whole material. Thus a low fraction of the hard particle is preferable at high impact loading condition. In low impact loading conditions, due to the high hardness of the second particles, the material can resist the cutting of the external force. In such a case, a high fraction of the second phase particles is desirable.

2. 3. Conclusions

The mechanical properties and wear behavior of a newly developed wear-resistant material, TiNi-based composite, were investigated. The following conclusions can be drawn from the investigations.

- (1). TiNi-based composites having a high fraction of reinforcing particles (TiC, TiN) can be synthesized from elemental Ni and Ti powders and reinforcing particles using a

conventional pressing and sintering technique. The difficulties in the sintering of the above three constituents mainly lie in achieving good composition homogenization and a high density. Due to the presence of the second phase particles, the mass diffusion in the sintering process is retarded, and liquid phase sintering is necessary to introduce a higher diffusion speed of Ti and Ni atoms. Among the tested sintering parameters, the best sintering process was 1500°C for 6 hours when the fraction of the second hard particles reached 52 vol%. In the above sintered TiNi-composite, the matrix had a fluctuation in its composition, and this suggests that the sintering process could be improved. The major phase in the matrix was TiNi austenite β phase. The TiNi alloy in the composite possessed a medium pseudoelasticity compared with rolled TiNi alloys. The improvement in the matrix's composition is expected to further increase its pseudoelasticity.

(2). The tribological behavior of the new wear-resistant material, TiNi-based composite, was investigated. It was demonstrated that the wear resistance of the TiNi alloy was significantly enhanced by the hard particles. The wear resistance increased with an increase in the volume fraction of the reinforcing particles with the optimal fraction around 52 vol%. The wear performance of the TiNi-based composites was compared to that of the 304 stainless steel, TiNi alloy and WC/NiCrBSi overlay. It was shown that the wear resistance of the 52vol%TiC/TiNi composite was about three orders of magnitude higher than that of the 304 steel; and about one order of magnitude better than that of the TiNi alloy. Compared to high-performance WC/NiCrBSi hardfacing overlay, TiC/TiNi composites showed superior performance under low loads.

(3). Friction measurements showed that under oil-lubrication conditions, TiNi-based composite containing TiC or TiN had a friction coefficient between those of the heat-treated and as-received TiNi alloy specimens. It appeared that the pseudoelasticity had a considerable effect on the friction coefficient of the TiNi materials under the lubrication condition. The friction behavior of the TiNi-based composite was also influenced by the second phase particles.

(4). The wear mechanisms for the TiNi-based composites were studied in our test. Abrasive wear was mainly responsible for the wear of the composite's matrix, and the failure of the hard particles was also an important part of the composite's wear. Thus, in the composite design, the determination of the hardness and fraction of the hard dispersoid can be optimized with respect to the composite's service condition. In a service with a high impact, a low fraction of softer particles is preferable, while at low impact service conditions, particles of higher hardness and fraction are beneficial. The pseudoelasticity of the TiNi alloy matrix contributes to the good wear resistance of the composite. The combination of the pseudoelastic TiNi and the hard particles has clearly produced a large improvement in the wear resistance compared with the TiNi alloy, and any improvement in the matrix's pseudoelasticity is expected to enhance the material's wear resistance.

The great potential of this new wear-resistant material has been demonstrated by this preliminary study, and further research will be reported and discussed in the upcoming chapters. It should be noted that the TiNi matrix composite is still under development,

with space for further improvement. The possible approaches may include reducing voids, homogenizing the matrix composition, and improving the matrix pseudoelasticity.

Chapter 3. Influences of Porosity on Mechanical and Wear

Performance of TiNi-based Composites

In Chapter 2, the development of TiNi-based composite by powder metallurgy was reported. The structures, mechanical properties and wear behavior of these samples were investigated. The wear testing evinced that the wear resistance of the 52vol%TiC/TiNi composite was comparable to that of commonly used WC/NiCrBSi hardfacing overlay, although a large percentage of porosity was discovered in the sintered TiNi matrix composites. Since the porosity may strongly affect the mechanical properties and wear resistance of the composites, the influences of the pores on the sintered pseudoelastic TiNi-matrix tribo-composites were studied. In particular, changes in the density of pores and the corresponding variations in the matrix's pseudoelasticity and the wear resistance of the composites were inspected. It was found that the mechanical properties and wear resistance of the TiNi matrix composites were conspicuously affected by voids. The mechanical properties and wear resistance were elevated when the density of pores was abated by applying high compaction load or a lubricant such as wax during powder mixing and pressing. It was also interesting to observe that pores were self-sealed during the wearing process, which resulted in improved wear resistance during the ongoing wearing, especially under high loads. Results of these studies are presented in this chapter with discussions on the mechanisms involved.

3. 1. Experimental procedure

The influence of porosity on the mechanical properties and wear behavior of the TiNi matrix

composites were investigated with the 52vol%TiC/TiNi and 52vol%TiN/TiNi samples.

3.1.1. Powder mixing and compaction

Two methods were adopted to modify the porosity in the sintered TiNi composites. One was to introduce lubrication into the powder mixing and compaction, and the other was to press the mixed powders with a series of loads. Two groups of samples were used for evaluating the efficiencies of the two methods. The first group was 52vol%TiN/TiNi composites, mixed and compacted with or without wax respectively, to investigate the effects of lubrication during the mixing and compaction stage. Ti, Ni, and TiN powders having a mesh size of -325 ($< 45 \mu\text{m}$) were mixed in hexane, respectively, with and without dissolved paraffin wax (1.5 wt% of the total Ti, Ni and TiN powders), using a cemented WC ball mill for 2 hours. The detailed mixing process has been described in Section 2.1.2. The amount of the added hexane (from Caledon Laboratories Ltd., Georgetown, ON) was 0.8 ml per gram of powders. The granulated wax (from IGI International Waxes, Agincourt, ON) had an average size of $600 \mu\text{m}$ with a melting point of 55.6°C and dissolved into the hexane prior to powder mixing. After the mixing, the powders were then pressed into pin specimens under a pressure of 787 MPa (the corresponding compaction load was 22.222 kN, *i.e.* 5000 pounds) for 30 seconds, as illustrated in Fig. 2-2.

The second group of samples were 52vol%TiC/TiNi composites compacted under different loads for investigating the effects of compaction load on the mechanical properties and wear performance of the TiNi matrix composite. Ti, Ni and TiC powders having a mesh size of -325 were mixed in the same WC ball mill for 2 hours without addition of wax. The mixed

powders were then compacted with the same press and die for 30 seconds, under loads of 17.778 kN (4000 pounds), 22.222 kN (5000 pounds), 26.667 kN (6000 pounds) and 31.111 kN (7000 pounds), respectively.

3.1.2. Sintering of the composite

After compaction, both groups of compacts were desiccated in an oven at 50°C for 3 hours to vaporize the hexane. Then the waxed specimens were initially heated in the BREW vacuum sintering furnace at 350°C under a vacuum of about 1.33 Pa (10^{-2} torr) for 45 minutes to burn off the wax. These samples were subsequently sintered at 1500°C for 6 hours in vacuum of 6.7×10^{-2} Pa (5×10^{-4} torr). After sintering, the samples were furnace cooled to room temperature. The second group of samples were sintered at 1500°C for 6 hours in the same vacuum furnace. The dissimilarity in the sintering of these two groups of samples was that the samples in the second group were not held at 350°C to burn off the wax. Both groups of specimens were cylindrical samples with a length of 8 mm and a diameter of 6 mm.

3.1.3. Composition and phase structure analyses of the samples

The nominal composition of the composite's matrix was Ti-51at%Ni, and the matrix composition was determined with energy dispersive X-ray analysis in a JEOL 6301F SEM. The microstructures of the bulk materials and the worn surfaces were examined using both the JEOL 6301F SEM and an optical microscope. The bulk densities of the specimens were measured with a pycnometer. Alcohol was used as the measuring liquid, and the system was weighed using an OHAUS analytical balance to an accuracy of 0.1 mg. In order to

comprehend changes in the wear resistance, the sintered specimens were analyzed using a Rigaku Geigerflex powder X-ray diffractometer before and after the wear testing to determine whether or not there were phase changes, as described in Section 2.1.4.

3.1.4. Examination on mechanical properties and wear behavior of the TiNi composites

The hardness and pseudoelasticity of the composites' TiNi matrix were investigated by an indentation test using a Hysitron triboscope - a combination of an atomic force microscope and a nano-mechanical probe. From the loading-unloading curves, the hardness and the pseudoelasticity of the materials could be determined, as discussed in Section 2.2.3. The wear resistance of the specimens was evaluated using a pin-on-disc tribometer by measuring their weight loss. Two kinds of wear tests were conducted. The first type was direct examination of the weight loss of the samples after being worn under a series of loads, and the other was a measurement of the wear loss rate of the samples. The wear loss rate was defined as the weight loss of each sample per unit sliding distance (60 m) under a certain load. The wear loss was obtained by averaging 4 or 5 measurements. The disc of the tribometer was made of 304 stainless steel and was water cooled to reduce the temperature increase produced by frictional heat.

3. 2. Experimental results and discussion

3. 2. 1. Composition and microstructure of the TiNi composite

The microstructures of the composites were examined using an optical microscope and a SEM. The samples had a microstructure similar to that shown in Fig. 2 - 4. The TiC or TiN particles were uniformly distributed, and a fluctuation occurred in the matrix's composition.

A large number of pores were uncovered in the sintered samples, as shown in Fig. 3-1. Most of the voids had an irregular shape with sharp corners, and these voids varied in size.

The phase constitution of the composites was analyzed using X-ray diffraction. Fig. 3-2 presents a diffraction pattern of the TiN/TiNi composite, which demonstrates that no separated Ti and Ni powders existed in the composite, that is, the matrix was a TiNi alloy. The major phase in the matrix of the sintered composite was an ordered BCC β phase, with minor Ni_3Ti precipitates. The TiC/TiNi composite showed a similar XRD pattern.

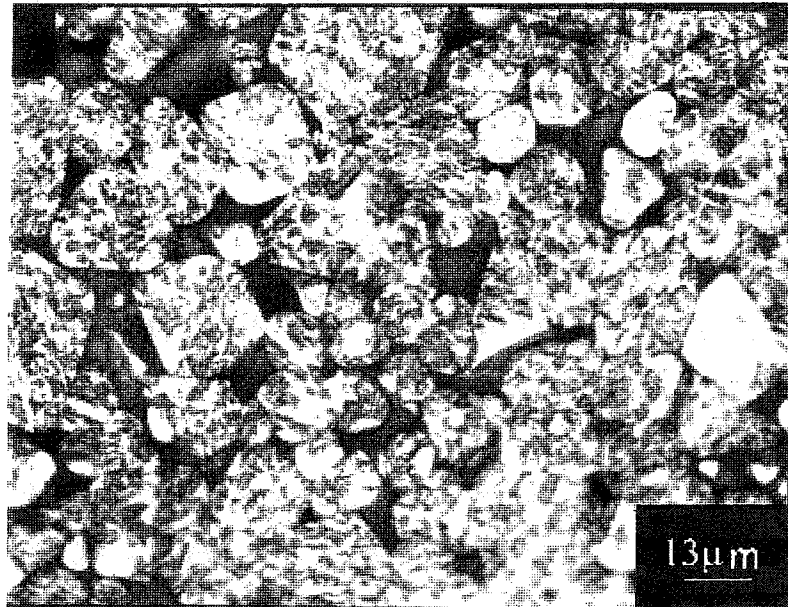


Fig. 3-1. The voids in the sintered composite.

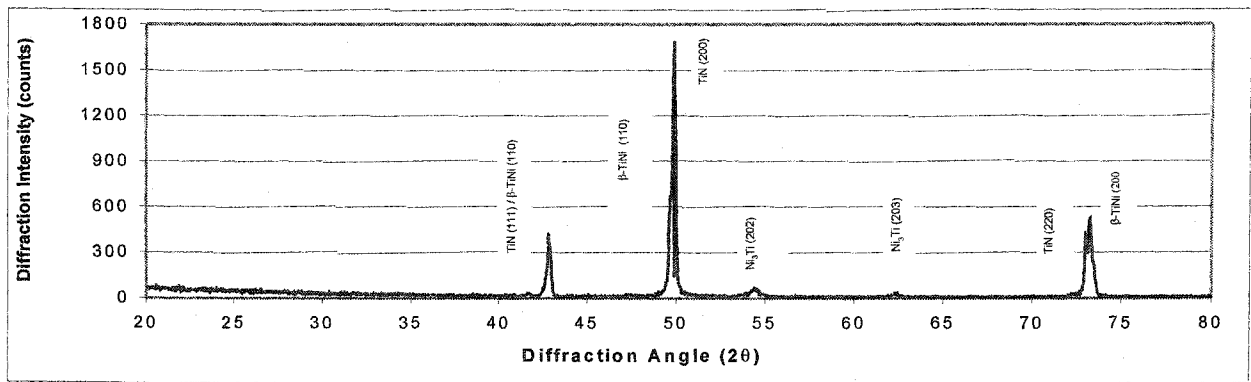


Fig. 3- 2. (Co-K α 1) X-ray diffraction pattern of a TiN/TiNi specimen.

3. 2. 2. Effects of the sealing of pores on the mechanical properties and wear behavior of the TiNi composite

In Chapter 2, it was observed that the wear losses of the TiC/TiNi and TiN/TiNi samples increased with the wearing load in the beginning. After the load reached about 0.17 kN, the wear losses of the samples commenced to decrease, as shown in Fig. 2-13. Usually, the wear loss of a material rises as the applied load is increased [7]. However, for the sintered TiNi composites, there existed a critical load corresponding to the maximum wear loss, above which the wear loss dropped as the load was continuously increased within the loading range of the wear test. Such a phenomenon differed from what is usually expected, *i.e.* under high loads, the TiNi alloy loses its pseudoelasticity due to enhanced plastic deformation, thus leading to an increase in the material's wear loss.

In order to better understand such a change in the wear behavior of the TiNi composite, a new specimen and a worn one were examined to discern possible variations in their density of pores, mechanical properties and the corresponding wear performance. Fig. 3-3 illustrates the volume losses of the new 52vol%TiC/TiNi and 52vol%TiN/TiNi specimens after sliding

over 600 meters under different loads. (The data in Fig. 3-3 was the average of 4 or 5 measurements with a variation of 20%.) As the applied load was increased, the volume losses of the composites were elevated until the load reached 0.17 kN and then the volume losses decreased. Under higher loads, the wear performances of the composites were considerably superior. This change was accompanied by changes in the surface morphology, as displayed in Fig. 3-4 and Fig. 3-5. It can be seen that after the material was worn at the low load, a lot of pits were left on the surface. These cavities were the original voids in the composite. However, after the material was worn at the high load, the surface became much denser. No pits were found on the surface, and the major damage was caused by the delamination of material. It appeared that the wearing pressure was quite high, and the pits were filled during the wearing process.

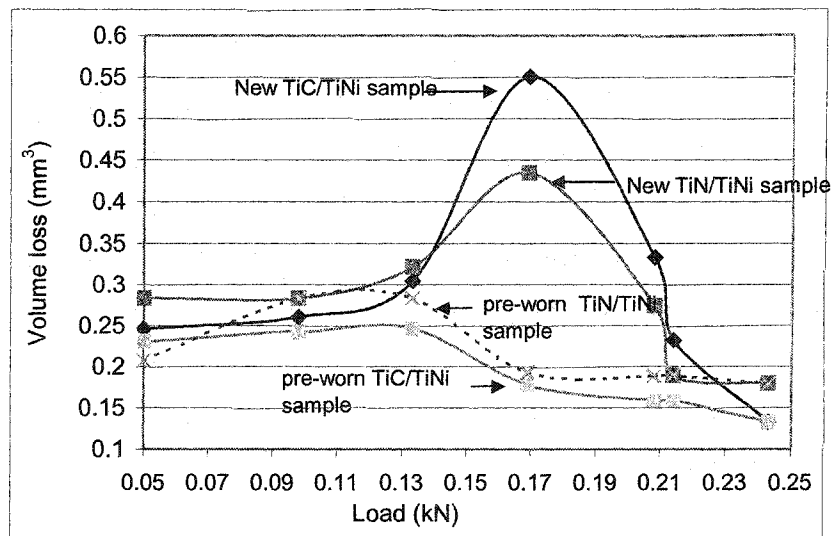


Fig. 3-3. The wear losses of samples at different loads.

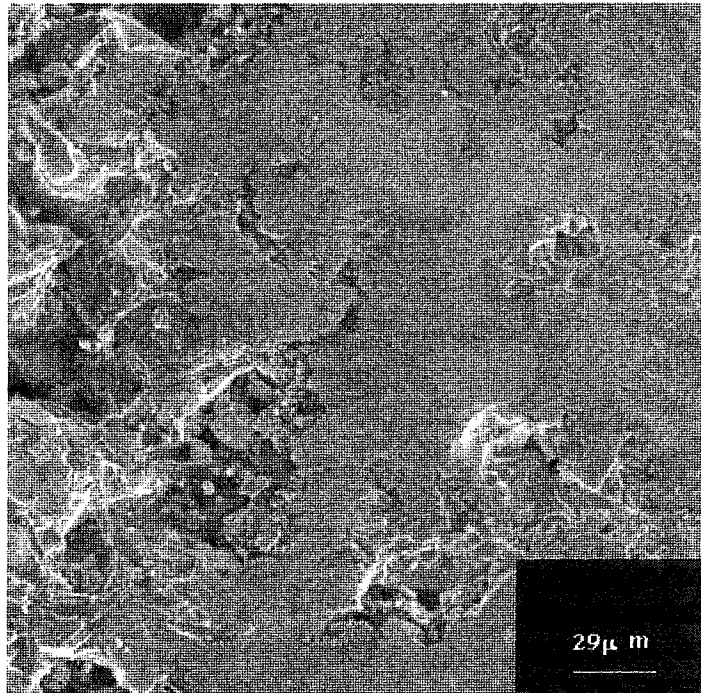


Fig. 3-4. Worn surface of TiN/TiNi under load of 0.05 kN.

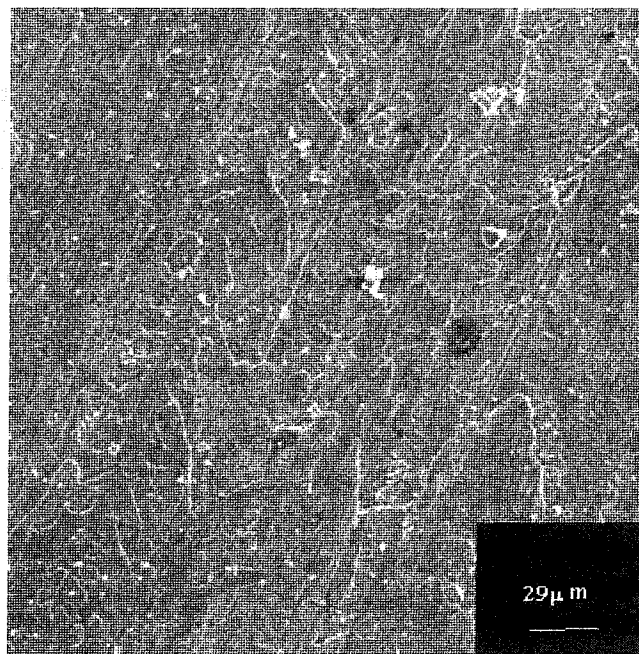


Fig. 3-5. Worn surface of TiN/TiNi under load of 0.243 kN.

In Fig. 3-3, volume losses of the specimens that experienced pre-wear under a load of 0.243

kN over 4800 meters are also presented. The pre-worn specimens showed similar wear behavior but their changes in the volume loss were much more gradual. In particular, the volume losses of the pre-worn specimens were significantly lower than those of the new samples under high loads around 0.17 kN. However, the difference in wear between the new and pre-worn specimens decreased as the load was continuously increased as Fig. 3-3 illustrates. This happened because of the self-sealing effect as discussed earlier. The new and pre-worn specimens were examined using XRD to check if there were phase changes caused by the pre-wear treatment. Fig. 3-6 illustrates a diffraction pattern of a pre-worn TiN/TiNi specimen. No detectable structural change inside the TiNi composite was found. During the pre-wearing process, transfer of material from the steel disc to the composite pin specimen was involved.

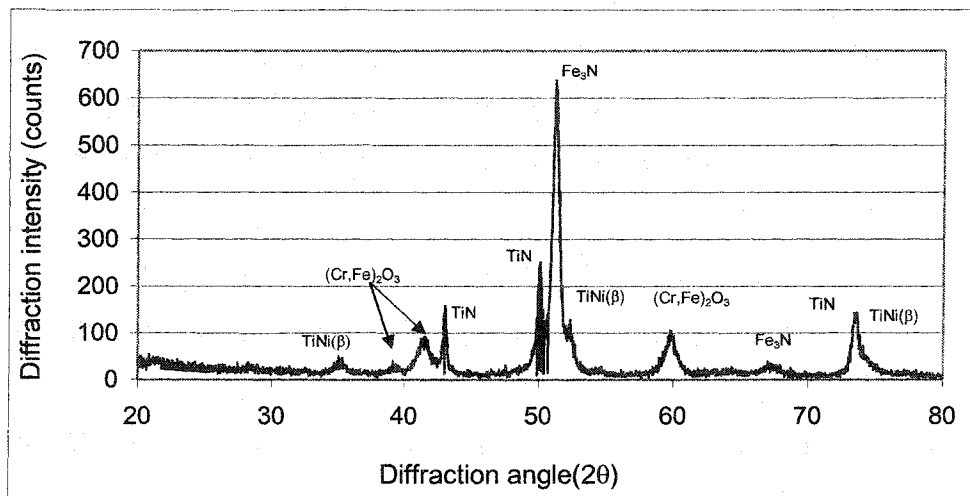


Fig. 3-6. (Co-K α 1) X-ray diffraction pattern of TiN/TiNi pre-worn at 0.243 kN.

As indicated, the XRD result did not find detectable structural changes in the TiNi composite during the pre-wearing treatment. However, the density of pores was greatly reduced. Fig. 3-7 and Fig. 3-8 are SEM micrographs of a new and a worn TiN/TiNi

specimen respectively, whose surfaces were lightly polished and etched before examination. Compared to the surface of a new specimen, the surface of the worn specimen was considerably denser with many fewer pores.

Since pores usually exist in the sintered composites, it is of importance to investigate the effects of pores on its wear behavior and the possible changes in porosity during wear, a dynamic surface process. As noticed, the density of pores on the surface decreased during wear, especially under high wearing loads. Such a decrease could be ascribed to the self-sealing of pores during the wear by the compaction effect of the contact force as well as the sealing of surface pores by the material transferred from the stainless steel disc. From the X-ray diffraction examination, $(\text{Cr,Fe})_2\text{O}_3$ and Fe_3N were detected on the worn surface of the TiNi composite. This means that the material of the stainless steel disc had been transferred to the composite specimen. The self-sealing and material transfer under high load could densify the surface layer of the specimen. It was also observed that the color of the worn surface under high loads turned to yellow. It is therefore expected that the interfacial temperature could be high under large wearing loads, which enhanced the compaction effect, similar to a hot pressing process. Indeed, during high-load wearing, the wear rate decreased considerably as the sliding distance increased, while such a decrease was negligible under lower loads due to the low compaction effect on the pores, as shown in Fig. 3-9.

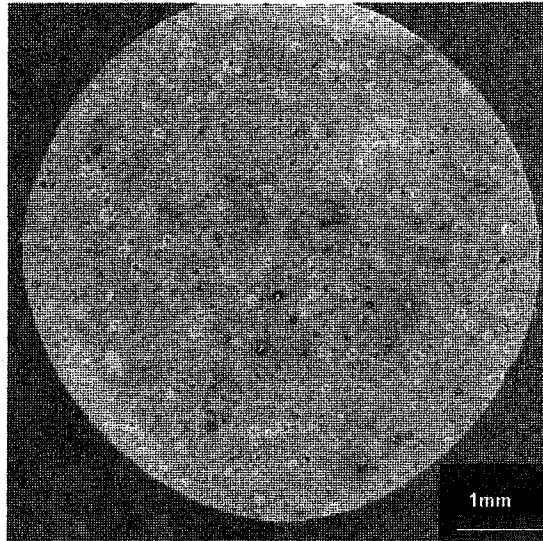


Fig. 3-7. The new unwaxed TiN/TiNi sample surface.

Improvement in the processing conditions for reduced porosity is an important step to optimize the material. Since wear is a dynamic surface process, the density of pores may vary during wear, and this could result in changes in the wear resistance. In fact, it was observed that the wear rate of the TiNi composites decreased as the sliding distance increased. Such a decrease in the wear rate was remarkable, especially under high loads. Fig. 3-9 illustrates the wear rate of unwaxed TiC/TiNi samples versus the sliding distance under 0.05 kN and 0.214 kN loads, respectively. Under the low load, the wear loss rate did not show significant changes, while under the higher load, a considerable decrease in the wear loss rate was observed. Clearly, the wear resistance of the composites was enhanced during wear.

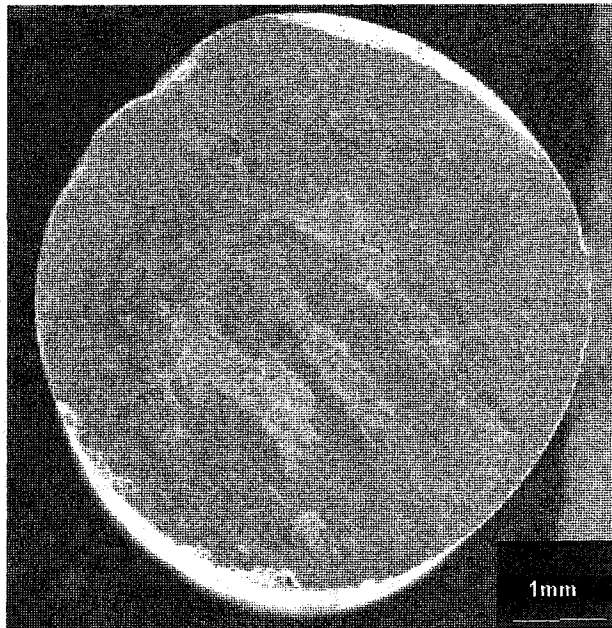


Fig. 3-8. The worn surface of pre-worn TiN/TiNi specimen.

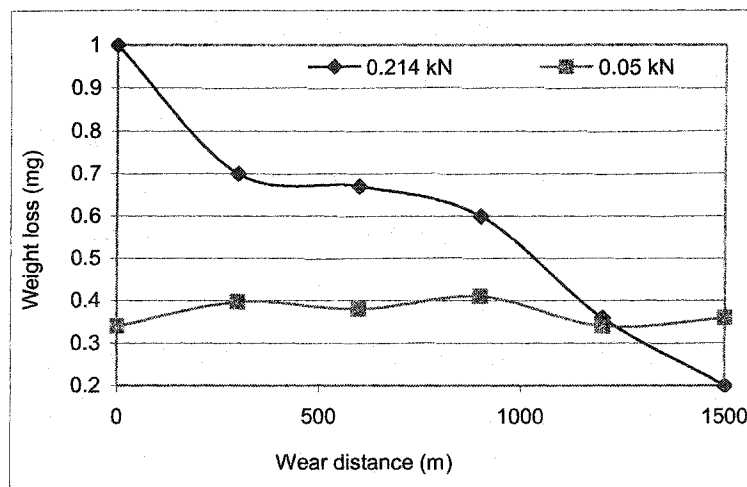


Fig. 3-9. The wear loss rate of unwaxed TiC/TiNi specimen.

As demonstrated by SEM and XRD, the pre-worn specimens had considerably fewer pores and no detectable second phases were induced. This implies that the improvement in the wear resistance of the pre-worn specimens could be largely attributed to the reduction in pores.

In summary, the decrease in the wear loss may be attributed to the compaction effect on pores. The higher the applied load, the more effective the compaction effect. Although higher wearing loads may increase the wear damage, the effect of load on the enhancement in the wear resistance of TiNi composite could be greater than that on the increase in wear damage, thus leading to a decrease in the wear loss, as Fig. 3-3 illustrates. The variation in wear loss as a function of load was significantly smaller for the pre-worn specimens (see Fig. 3-3). This is intelligible, as in the surface layer of the pre-worn specimens, the density of pores has already been reduced.

In order to better comprehend the effects of voids on the wear resistance, the hardness and pseudoelasticity of the TiNi matrix were investigated using a nano-mechanical probe. Fig. 3-10 illustrates typical load - depth curves of TiN/TiNi composites during nano-indentation. The tested specimens included a new specimen, a worn one under a load of 0.214 kN over a sliding distance of 1200 meters, and one with a double - wear treatment (*i.e.* twice the sliding distance under the same load). The penetration depth d is a measure of the hardness of the specimen. The η value reflects the degree of pseudoelasticity, as discussed in Chapter 2.

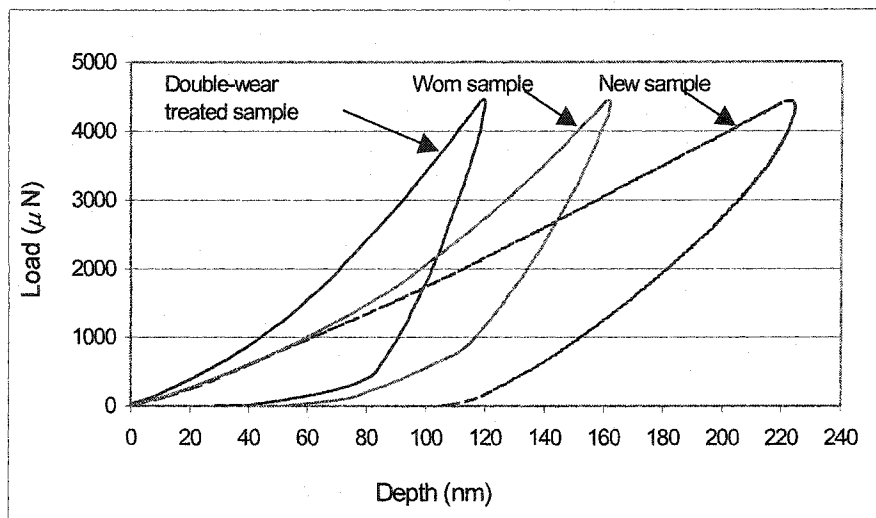


Fig. 3-10. The load-displacement curves during indentation under a 4500 μN load.

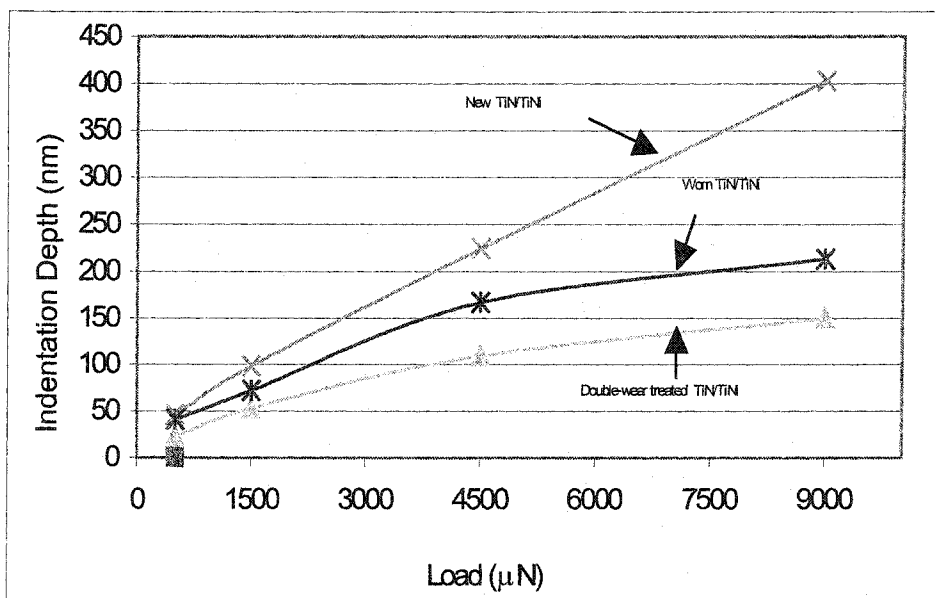


Fig. 3-11 The maximum depth versus the nano-indentation load.

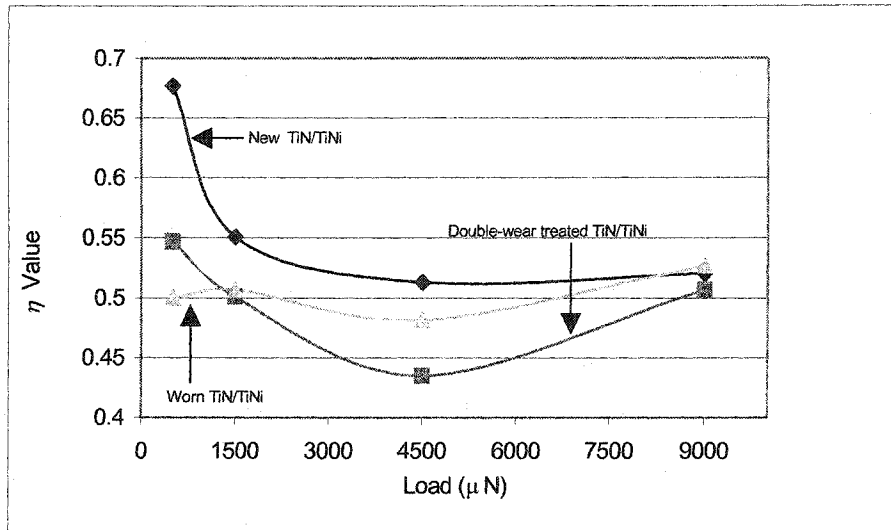


Fig. 3-12. η values of a new sample, a worn sample and a double-wear treated sample.

Fig. 3-11 presents d values of these samples versus the indentation loads, which provides the following information. Firstly, the new sample is the softest, the double-wear treated sample is the hardest, and the worn one has a medium hardness. The maximum difference in the penetration depths between the new and double-wear treated sample was about 250 nm at 9000 μN , which is over 1.5 times of the penetration depth on the double-wear treated sample at the same load. Moreover, the difference in depth between the new and worn samples was larger than that between the worn and double-wear treated samples at high loads. Secondly, the absolute values of the depth difference between these three samples increased as the wearing load increased. At the maximum load, the difference is about 200 times larger than that at the minimum load. Additionally, the increase in the penetration depth of the new sample was almost linear, while for the worn samples, the increase rate in indentation depth became smaller as the load was increased. Regarding the η ratio, the new sample had the highest η value, while the one with double-wear treatment had the lowest

η . However, under higher loads, η values of all samples became closer as Fig. 3-12 shows. The difference in the matrix's mechanical behavior between the three types of composites could be strongly affected by voids. The sample with double-wear treatment had fewer pores, and this diminished the stress concentration and thus the probability of material's fracture. The increased density of dislocations introduced during wear may also contribute to the enhanced hardness. On the other hand, the compacted structures of the worn (or pre-worn) samples with fewer voids and higher density of dislocations behaved less pseudoelastically. However, the difference in η between the new and worn/pre-worn samples decreased under high indentation loads, since during such an indentation process all samples were heavily deformed with the generation of high-density dislocations.

The nano-indentation test showed that the sample with double-wear treatment exhibited the highest hardness and a lower degree of pseudoelasticity. The wear resistance of the TiNi alloy does not entirely rely on its pseudoelasticity. Recent studies [87] demonstrate that the wear resistance of the TiNi alloy is dependent on the balance between its pseudoelasticity and hardness. Although the pseudoelasticity helps to accommodate large-scale deformation and absorb impact energy with less damage, the TiNi alloy still cannot effectively resist high-stress wear if its hardness is low. On the other hand, if the pseudoelastic TiNi alloy is too hard, its wear resistance is also low. Therefore, an appropriate combination of pseudoelasticity and hardness would result in the optimum wear resistance. In addition, the hardness becomes important during high-load sliding wear with larger frictional heating, since in this case the TiNi alloy may lose its pseudoelasticity, and the intrinsic wear resistance of the composite mainly depends on its hardness and work hardening capability.

The measured macrohardness of 52vol%TiN/TiNi ranges from 50 HRC to 59 HRC, and 52vol%TiC/TiNi from 58 HRC to 62 HRC. This high hardness certainly enhances the material's resistance to wear under high loads.

3. 2. 3. Influence of lubrication in powder mixing and compaction on the mechanical properties and wear behavior of TiNi-based composite

As shown, the sintered TiNi matrix composites contained many pores, which were detrimental to the wear resistance of the composites. One method to reduce the density of pores in this work was to use wax lubrication during the mixing and pressing of the specimen powders for lubrication purpose. Some 52vol%TiN/TiNi specimens were prepared with wax. Their density and the associated wear resistance were examined and compared to those of the unwaxed specimens.

Bulk densities of the waxed and unwaxed TiN/TiNi specimens were $5.03 \times 10^3 \text{ kg/m}^3$ and $4.80 \times 10^3 \text{ kg/m}^3$, respectively. Based on the TiN density of $5.22 \times 10^3 \text{ kg/m}^3$ [77] and theoretical density of TiNi of $6.45 \times 10^3 \text{ kg/m}^3$ [88], the density of the 52vol%TiN/TiNi composite was calculated to be $5.81 \times 10^3 \text{ kg/m}^3$, which implies that volume fractions of the pores in the waxed and unwaxed specimens were 13.4% and 17.4%, respectively. This density measurement is consistent with SEM surface image analysis of the pore fractions. Fig. 3-7 and Fig. 3-13 illustrate etched surfaces of the unwaxed and waxed specimens from the SEM with measured pore fractions equal to 16% and 11%, respectively. This difference in the pore density should be attributable to the wax, which acted as a lubricant to enhance the densification of powder specimens during the pressing

process before sintering. Such a difference in the porosity of the sintered composite is supposed to make the mechanical properties and wear resistance of the waxed specimens different from those of the unwaxed ones.

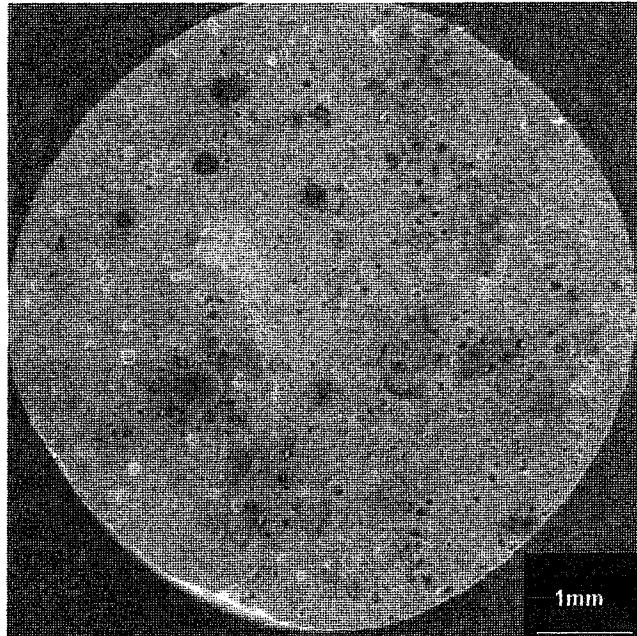


Fig. 3-13. The new waxed TiN/TiNi sample surface.

In fact, the influences of the porosity on the mechanical properties of the sintered materials have been extensively studied recently [89-95]. It has been found that the porosity, pore size, pore shape and inter-pore space have a strong influence on the material's mechanical properties. The major effect of the porosity is the increase in stress concentration and thus microcracking in the material. Another important effect is the reduction in the total load bearing area of the material. Holmes and Queeney have demonstrated that open surface porosity favors fatigue crack initiation [92]. Fleck and Smith found that the cracks propagate along pore-linked paths [93]. Hashin's calculations demonstrated that, with increasing porosity, the tensile and fatigue strength decrease because the pores act as receptors and transmitters of cracks [94]. H. Danninger *et. al.*

investigated the effects of pores on the mechanical properties of a Fe-Mo-C alloy [95]. Their findings are shown in Fig. 3-14 and Fig. 3-15. From the figures, it can be seen that the porosity is very harmful to the sintered material, reducing both the strength and elongation of the material. For instance, a 20% decrease in the alloy's density resulted in a 70% reduction in its strength and 90% reduction in the elongation. Since the material's strength is directly correlated to its hardness, it is expected that the porosity reduces both the hardness and ductility, which are critical parameters for the wear resistance of the material.

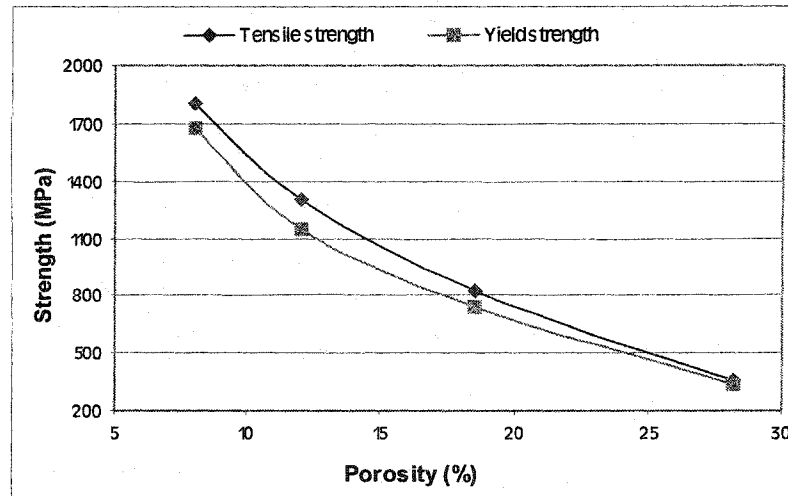


Fig. 3-14. The strength and the porosity of a Fe-Mo-C alloy [Ref. 95].

It is known that round pores are less deleterious than the sharp one [83]. The micrograph of the TiC/TiNi composite in Fig. 3-1 shows that the pores in this material are angular, which may reduce the material's wear resistance more severely.

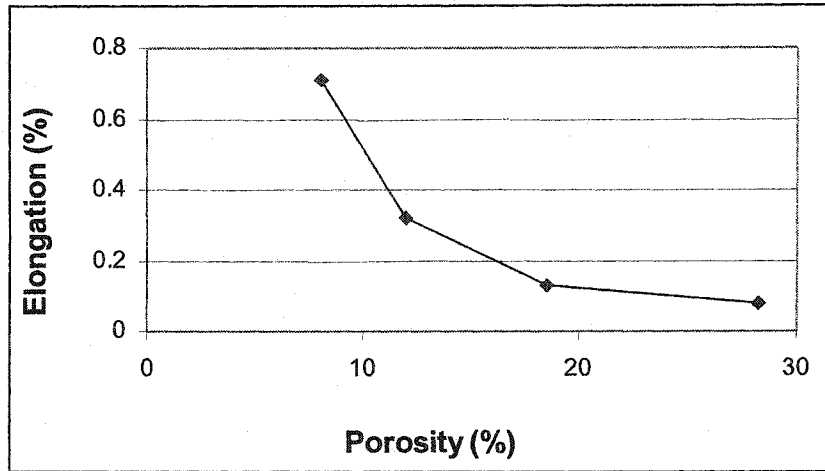


Fig. 3-15. The elongation and porosity of a Fe-Mo-C alloy [Ref. 95].

The results of the wear testing on the waxed and unwaxed TiN/TiNi samples are illustrated in Fig. 3-16. The volume losses of both the waxed and unwaxed specimens increased as the load was increased. However, when the load exceeded 0.17 kN, the volume losses began to decrease due to the effects of self-sealing. The wear resistance of waxed specimens was about 15% ~ 20% higher than that of the unwaxed specimens in the tested loading range. Comparing the density and wear loss of the waxed samples to those of the unwaxed samples clearly reflects the influences of porosity on the composite's wear resistance.

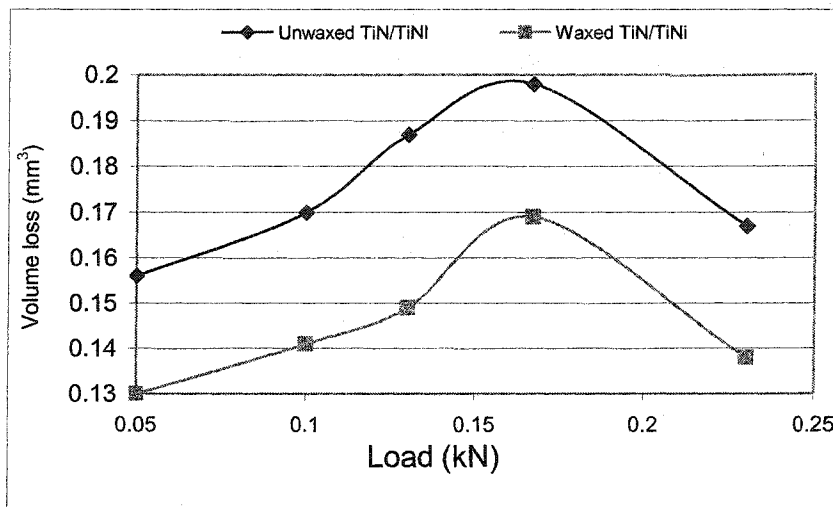


Fig. 3-16. The wear loss of the waxed and unwaxed TiN/TiNi specimens.

3. 2. 4. *Effects of compaction load on the mechanical properties and wear behavior of the TiNi composite*

Since the green density of the compact has a large influence on the final density of the sintered material, the material's bulk density should vary when the mixed powders were compacted under different loads. The 52vol%TiC/TiNi samples were compacted under 17.778 kN (4000 pounds), 22.222 kN (5000 pounds), 26.667 kN (6000 pounds) and 31.111 kN (7000 pounds), respectively. The densities of this group of samples were then measured with the pycnometer. It was observed that, as the compaction load was increased, the final bulk densities of these samples consequently increased. They are 4.31×10^3 , 4.73×10^3 , 4.92×10^3 , and 5.01×10^3 kg/m³ respectively.

The wear behavior of the 52vol%TiC/TiNi composite compacted under these different loads was investigated in a dry sliding test with a pin-on-disc tribometer. It was found that the wear loss of the material decreased with the increase in the compaction load, as shown in Fig. 3-17. At 17.778 kN (4000 pounds), the weight loss was about 1.63 mg, while at 31.111 kN (7000 pounds), the wear loss dropped to around 0.92 mg, a decrease of about 40%.

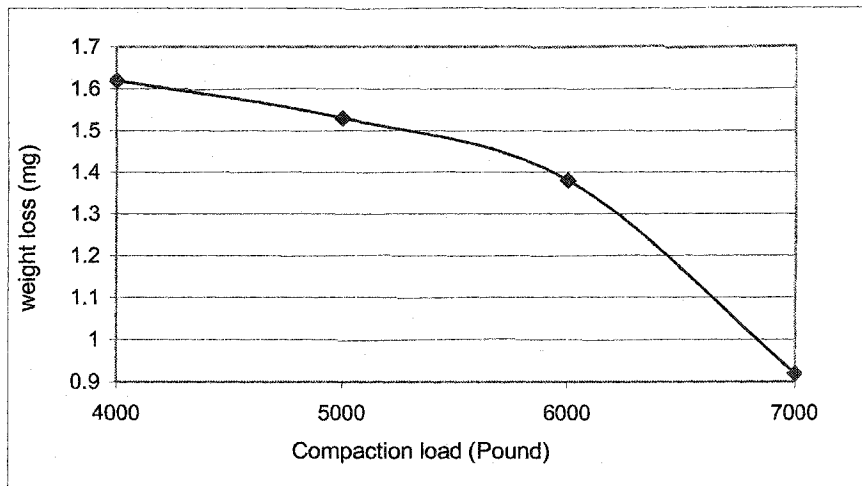


Fig. 3-17. The wear loss and compaction load of TiC/TiNi.

The mechanical properties of the second group of samples were examined by indentation tests under a series of loads. The maximum indentation depths at different testing loads were obtained, as shown in Fig. 3-18. All the samples had larger depths when the indentation load went up. At the same load, the sample compacted under 17.778 kN (4000 pounds) had the largest depth, and that compacted under 31.111 kN (7000 pounds) had the smallest depth. The difference in the indentation depth between the 17.778 kN (4000 pound) and 22.222 kN (5000 pound) compacted samples was generally larger than that between the 22.222 kN (5000 pound) and 31.111 kN (7000 pound) compacted samples. This shows that a greater compaction load produces a harder material, with a higher density. Another mechanical property, the η value, was calculated from the loading-unloading curves and presented in Fig. 3-19. Three conclusions can be drawn from Fig. 3-19. First, the hardest sample, namely, the sample compacted at 31.111 kN (7000 pounds) had the largest η value, while the softest sample, namely, the sample

compacted at 17.778 kN (4000 pounds) had the smallest η value. Under 4 mN, the difference in η value between the hardest and softest samples was 20%. Second, all the three η values decreased with the increase in the indentation load. Third, the η values became close to each other at a high indentation load. At 12 mN, the difference in η values between the hardest and softest samples dropped to 10%.

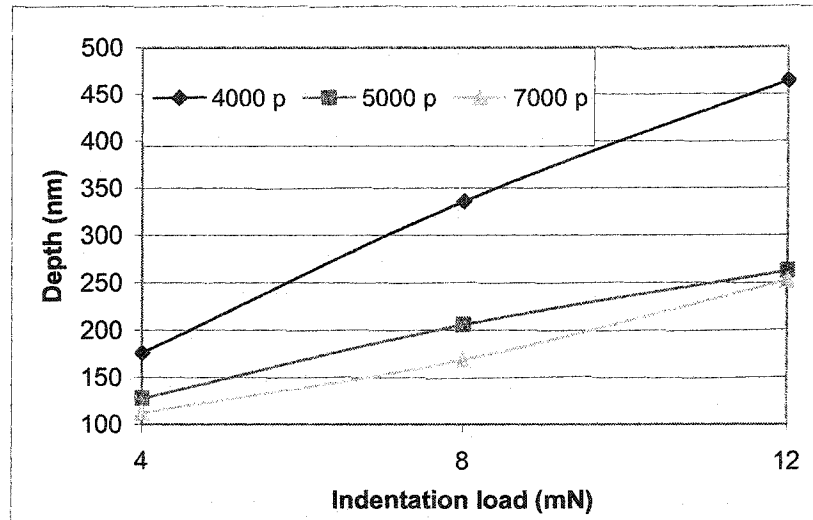


Fig. 3-18. Indentation depth of samples compacted at 4000, 5000 and 7000 pounds.

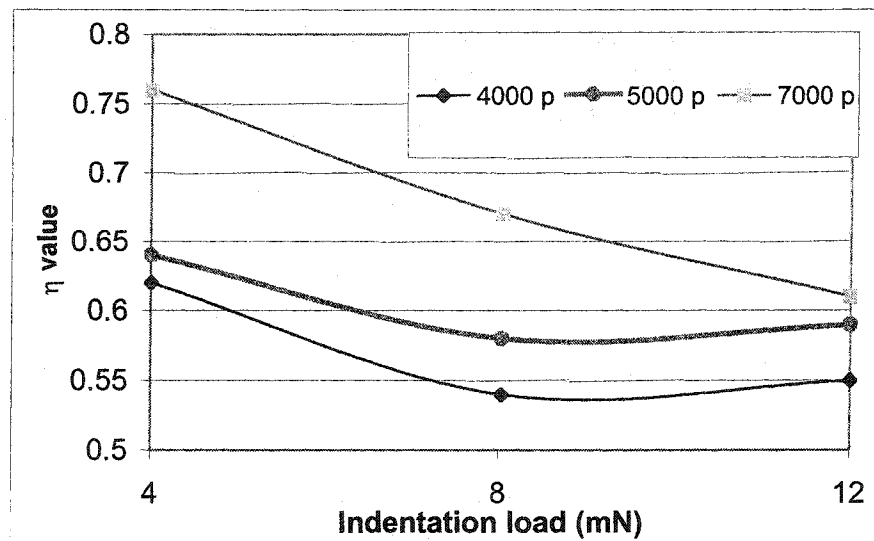


Fig. 3-19. The η value of the samples compacted under 4000, 5000 and 7000 pounds.

The effects of the porosity on the indentation depth d and the η value are understandable and may be explained as follows. When a load is applied on a body containing a pore, the total deformation of the material is affected by the solid matrix and the pore, as shown in Fig. 3-20. Under the load, both the solid body and the pore are deformed, producing the displacements of $\Delta\xi_1$ and $\Delta\xi_2$ respectively. So the total depth caused by the load is $\Delta\xi_1 + \Delta\xi_2$. However, if there is no pore, the deformation of the body is approximately equal to $\Delta\xi_1$. Accordingly, the pore increases the depth and softens the material. For the η value, as it is the ratio of the recoverable deformation energy over the total deformation energy, and the deformation energy is proportional to ξ^2 , the η value can be roughly expressed as $(\Delta\xi_r)^2/(\Delta\xi_t)^2$, where $\Delta\xi_r$ is the recoverable deformation, and $\Delta\xi_t$ is the total deformation. The deformation of the solid material is recoverable, while that of the pore is not. Therefore, the $\Delta\xi_r$ can be taken as $\Delta\xi_1$ illustrated in Fig. 3-20, because $\Delta\xi_1$ is the deformation of the pseudoelastic matrix. The $\Delta\xi_t$ can be taken as the sum of $\Delta\xi_1$ and $\Delta\xi_2$. Then the η value can be expressed as $(\Delta\xi_1)^2/(\Delta\xi_1 + \Delta\xi_2)^2$. When the load is removed from the body, the pseudoelastic matrix reverts to its original shape, and $\Delta\xi_1$ vanishes. However, because of the pore, $\Delta\xi_2$ remains after the removal of the load. Accordingly, in an ideally pseudoelastic material without pores, $\Delta\xi_2$ is 0, and

$$\eta = (\Delta\xi_1)^2 / (\Delta\xi_1)^2 \quad (3.1)$$

namely, η is equal to 1, if the load is not sufficiently large to produce plastic deformation. The η value of a body containing pores is $(\Delta\xi_1)^2/(\Delta\xi_1 + \Delta\xi_2)^2$ and thus always smaller than 1. This explains why the denser material shows a higher η value in our experiment. In addition, fewer voids and higher hardness may suppress plastic deformation, thus favoring β

⇔ M transformation and consequently the pseudoelasticity. Furthermore, pores increase the magnitude of stress or stress concentration. The collapse of pores could result in much larger displacement. Thus, $\Delta\xi_2$ could be much larger than $\Delta\xi_1$, and the influences of porosity on the mechanical properties of the material could be very strong.

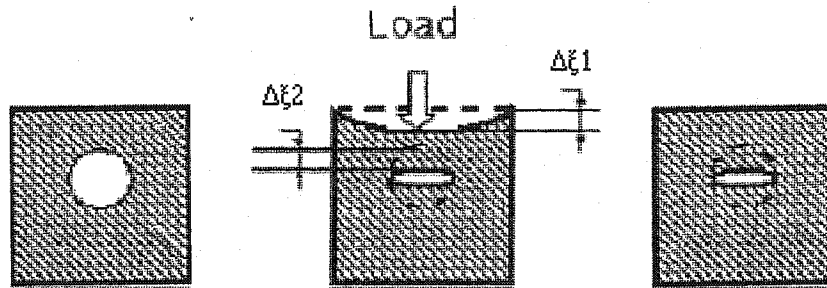


Fig. 3-20. The influence of porosity on the indentation depth and η value.

This mechanism for the effects of porosity on the indentation depth d and η value can be applied to explain the fact that, with an increase in the indentation load, the indentation depth d value increased while the η value decreased, as shown in Fig. 3-11/18 and Fig. 3-12/19. The higher the porosity of the material, the larger is the $\Delta\xi_2$ deformation. $\Delta\xi_2$ also increases as the load is increased. Thus both the porosity and indentation load increase the indentation depth. The decrease in η value with an increase in the indentation load may be attributed to the deformation of pores and solid material in the composite. At the outset, the load is very low, any solid material deforms elastically no matter how pseudoelastic it is. The pore is also not markedly distorted. In this case, all the materials show a high η value. However, as the load increases, the shape of the pore starts to change, and the solid material also begins to deform plastically when its elastic limit is reached. Since the material is not fully pseudoelastic, plastic deformation remains after the load is removed. This results in the

decrease in the η values. However, when the load reaches a level that is high enough to compact the pores in the surface area, the deformation of pores in all the materials could be similar since these materials have similar porosity and size of pores. The solid materials also contribute to the η value to a similar extent as they were processed in the same way and have the same degree of pseudoelasticity. Accordingly, at high loads, most of the surface pores are compacted, and the η values of all the composites originate from the deformation of solid materials and thus become closer.

3.2.5. Porosity and processing of the TiNi-based composite

The pores are formed at different stages of the composite's processing. When the green powders are compacted, porosity is produced, because the space between the particles can not be fully filled. In the case of Ti-51at%Ni alloy processed from elemental Ti and Ni powders, the typical value of the porosity in the green compact is from 20 vol % to 40 vol % [96]. For the TiNi-based composite processed in our work, the compact has a green density of about 70% when compacted at 22.222 kN (5000 pounds). Interparticle friction is the first factor that produces the porosity in the green compact. The presence of second hard particles is another factor that reduces compaction efficiency. The hard TiC or TiN particles have a volume fraction of 52%. During the compaction, these hard particles build up a three dimensional network. Because of high hardness and Young's modulus, the hard particle network resists the pressing force, and accordingly, a high porosity is formed in the green compact. The wear testing has clearly shown the improvement in the wear resistance due to the increase in the material's density caused by the lubrication or high load in compaction. The investigation indicated that an increase in the composite's density by 5% due to the wax

lubrication produced an increase in the wear resistance by about 20%. The compaction load of 31.111 kN (7000 pounds) also corresponded to a weight loss that was only about 60% of the weight loss of the sample pressed at 17.778 kN (4000 pounds). During compaction, the powders are pressed together first and then slide against one another to fill the space among them. However, interparticle friction prevents the sliding between powders and thus reduces the compaction efficiency. The lubricant lowers the interparticle friction and thus facilitates the powder sliding. As a result, the final density of the material is increased. The high compaction load overcomes the interparticle friction and the resistance to compaction of the second phase particles, thus increasing the green density of compact.

Porosity may develop during the sintering as well. Liquid phase sintering would be the most important process for the formation of the porosity in the sintered TiNi matrix composite. The actual sintering was conducted at 1500°C, at which temperature, all the Ni particles were melted. So there was a high fraction of liquid in the TiNi-based composite when it was sintered. During the cooling of the sample, the liquid solidified, and shrinkage normally happened to the sample. However, in the TiNi-based composite, the secondary hard phase particles occupied more than half the volume of the sample. These particles formed a network, impeding the contraction of the liquid, and thus retaining a high porosity. This porosity from the obstructed contraction of the solidifying liquid Ni is more overt as the sintering temperature increases. For the purpose of the composition homogeneity, a higher temperature is imperative to speed up the diffusion of Ti and Ni atoms, while it creates porosity. Therefore, all these essential sintering features of the TiNi-based composite make high porosity typical with this material, which is harmful to the material's mechanical

properties and wear resistance. How to solve this contradiction becomes very important to developing a good TiNi-based wear resistant material.

3. 3. Conclusions

Since pores typically exist in sintered composites, it is important to investigate the effects of porosity on the wear resistance of the composites and variations in porosity during wear. In this work, the influences of pores on the wear resistance of sintered TiC/TiNi and TiN/TiNi tribo-composites were investigated. It was demonstrated that pores in the composites were detrimental to the composites' wear resistance. A decrease in the density of voids improved the wear resistance of the composite. The following conclusions are drawn from this investigation.

(1). The existence of porosity is a typical problem in the sintered TiNi-based composite. In the compaction stage, the interparticle friction between the particles and the high hardness of the second phase particle network greatly reduce the compaction efficiency and leave a high-density of pores in the green compact. In the sintering stage, the high temperature liquid phase sintering and the presence of the second phase particles are very influential to the formation of porosity, since a lot of pores are formed during the hindered shrinking of the solidifying Ni liquid.

(2). The porosity in the sintered TiNi-based composite is very harmful to its mechanical properties and wear resistance. The porosity reduces the load bearing area of the composite and also acts as stress concentration raiser. These adverse effects greatly degrade the

mechanical properties and wear resistance of the material.

(3). The porosity in the sintered TiNi-based composite is variable. During the processing, high load compaction or lubrication reduces the porosity in the green compact and thus improves the bulk density of the final sintered product. Correspondently, the mechanical properties and wear resistance of the material are enhanced. During the wearing process, if the load is high enough, the porosity in the worn surface area is reduced. Such a reduction occurs because under high load the pores are compacted by the load or sealed by the material transferred from the wearing couple disc. This is especially true at high temperatures.

Chapter 4. Improvement in Wear Resistance of TiNi-based Composite by Hot Isostatic Pressing

In Chapter 3, the influences of pores on the sintered TiNi matrix composite were discussed. A high density of pores exist in the sintered TiNi-based composite, dramatically reducing the hardness and pseudoelasticity of the composite and thus its wear resistance. It has also been found that the porosity at the surface is variable during the wearing process. At high loads, the pores can be sealed by the compaction of the wearing force or the materials picked up from the wear couple material. This decrease in the porosity enhances the hardness, pseudoelasticity and wear resistance of the worn surface. Thus, an attempt was subsequently made to densify the sintered TiNi-based composite using hot isostatic pressing (HIP), since HIP creates a high-temperature and high-pressure condition, a process similar to that happened to the worn surface during the high load wearing process. This chapter reports and discusses an investigation of the effects of the HIP treatment on the reduction of pores in the sintered TiC/TiNi and TiN/TiNi composites and the resultant changes in their microstructure, mechanical properties, and wear resistance.

4. 1. Experimental procedure

In this work, hot isostatic pressing (HIP) was applied to the 52vol%TiC/TiNi and 52vol%TiN/TiNi specimens after they were sintered at 1500°C in high vacuum. The microstructures, mechanical properties and wear behavior of these specimens were determined to evaluate the effects of HIP on the material's properties. The experimental

procedure is described as follows, with some detailed information having been reported in the relevant sections of previous chapters, not being repeated here.

4. 1. 1. Powder mixing and compaction

The 52vol%TiC/TiNi and 52vol%TiN/TiNi composites were initially fabricated using a vacuum sintering process. The Ti, Ni and either TiC or TiN powders having a mesh size of -325 ($< 45 \mu\text{m}$) were mixed in hexane with dissolved wax (1.5 wt%), using a cemented WC ball mill for 24 hours, much longer than the previous one of 2 hours. The mixed powders were dried at 50°C in an oven for 3 hours to vaporize the hexane and then pressed into pin specimens under a pressure of 787 MPa held for 30 seconds.

4. 1. 2. The sintering of the composite

The above powder compacts were then placed in the BREW vacuum furnace. These specimens were first heated at 350°C in vacuum of 1.33 Pa (10^{-2} torr) for 45 minutes to bake off the wax and then sintered at 1500° C in vacuum of 6.7×10^{-2} Pa (5.0×10^{-4} torr) for 6 hours. The other sintering parameters were the same as those in the previous work. The cylindrical specimens were 8 mm long with a diameter of 6 mm.

4. 1. 3. The Hot Isostatic Pressing (HIP) of the composite

After the vacuum sintering, some of the specimens were treated by HIP with an Autoclave Engineers QIH-15 furnace. The HIP furnace had a maximum operating temperature of 2000°C and pressure of 30 ksi. The pin specimens were set in a cylindrical graphite container. Between the specimens and the container bottom was a stabilized ZrO₂ plate

(about 5 mm thick) to prevent possible reactions between the specimens and graphite. This setup is illustrated in Fig. 4-1. The container was then placed into the furnace chamber for the processing.

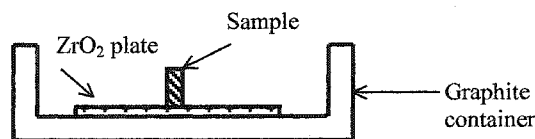


Fig. 4-1. The setup of the samples in HIP process.

The furnace was first evacuated to vacuum around 1.33 Pa (10^{-2} torr) with a mechanical pump, and Ar gas (with a purity of <1 ppm O₂, <1 ppm hydrocarbon, and ~4 ppm H₂O) was subsequently pumped into the chamber to 8.28 MPa (1200 psi), followed by the heating of the furnace at a rate of about 16°C/min. The samples were pressed at 1300°C under a pressure of 30 ksi (207 MPa) in Ar for 2 hours. The HIP pressure was obtained and maintained by a mechanical pump. After the hot pressing treatment, the samples were furnace cooled to 350°C at a rate of about 5°C/min and then air cooled to room temperature. The entire HIP procedure is shown in Fig. 4-2.

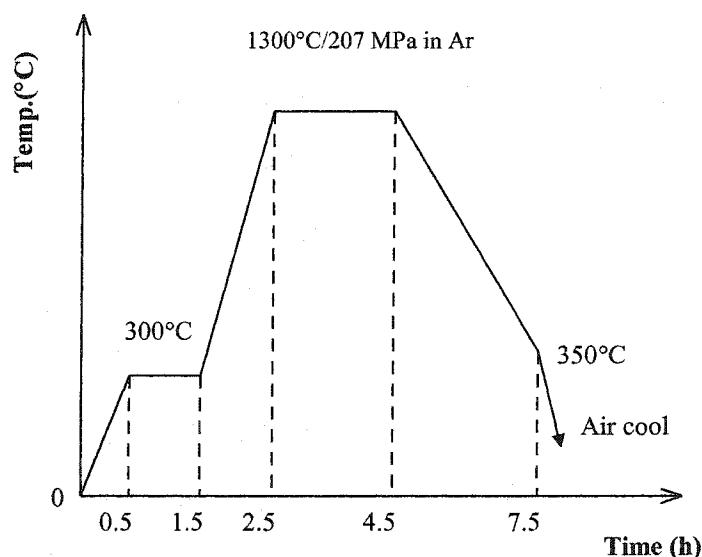


Fig. 4-2. The HIP procedure.

4.1.4. The composition and microstructure examination of the composite

The nominal composition of the composite's matrix was Ti-51at%Ni, and the composites contained 52 vol% of either TiC or TiN particles. The microstructures of the composites were examined using SEM and optical microscopy. The sintered specimens were analyzed using x-ray diffraction before and after the HIP treatment to determine whether or not there were phase changes during the HIP process. The bulk density of the specimens was measured using a pycnometer.

4.1.5. The mechanical properties and wear resistance test of the composite

The pseudoelasticity and hardness of the composite's TiNi matrix were investigated to assess the effects of HIP on the material's mechanical properties. The investigation was carried out by indentation tests using a Hysitron triboscope. The wear resistance of the specimens was evaluated using a pin-on-disc tribometer by measuring their volume losses after sliding over 600 meters on a 304 stainless steel disc at a speed of 60 m/min under different loads. The top end of the HIPped samples was used in the wear testing. The volume loss was obtained by averaging 4 or 5 measurements. The wear disc of the tribometer was fitted underneath with an attached copper tube, which circulated cooling water to reduce the temperature rise caused by frictional heating.

4. 2. Experimental results and discussion

4.2.1. The HIP densification mechanisms

Before the results of the study are presented and discussed, the densification mechanisms of the pores during the sintering and HIP process are introduced first for a better understanding

of what has happened to the samples. Material diffusion from the grain boundary and creep at high temperatures and high pressures are the two major mechanisms that are responsible for the densification of the sintered materials [83, 97].

4.2.1.1. The diffusion HIP densification mechanism

The driving force to achieve the densification of the sintered materials is associated with the reduction in surface area and, hence, surface energy of the pores. The surface area of fine powders is very large. A cupful of the powders with a particle size of 1 μm has a surface area of approximately 103 m^2 [97]. Grain boundaries and dislocations are also regions of disorder and, therefore, are zones of high energy relative to the perfect crystal. All these systems try to achieve their minimum energy configuration, which is the crystalline material. Furthermore, during HIP treatment, the process of grain growth often commences before the process of pore elimination is completed.

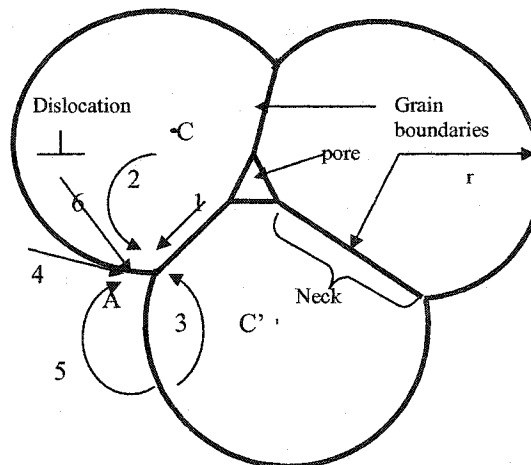


Fig. 4 - 3. Paths for mass transport during neck growth in sintering [Ref. 97].

Fig. 4 - 3 summarizes the diffusion mechanisms for removal of pores (including vapor transport) during sintering. Mass can be transported to fill pore A from a grain boundary

between two particles or from dislocations within the particle [97]. These transport paths are marked with 1, 2, and 6, which bring the centers of the particles (C and C') closer together. They, therefore, result in densification. However, paths 3, 4 and 5 do not cause densification because they only transport the mass from one place on the pore surface to another place. The net result of these diffusions is a change in the pore shape. When the pore is filled at point A, the neck between the two particles grows. In the paths in Fig. 4-3, apart from path 5, which involves vapor transport, the other paths all involve diffusion via the pore surface, the grain boundary or the lattice.

Assuming there is no gas in the pore to resist densification, the closure of an isolated spherical pore is ruled by the equation

$$P=2\gamma/r \quad (4.1)$$

where P is the pressure acting to close the pore, γ is the specific energy of the pore internal surface, and r is the radius of curvature of the pore surface [83, 97]. Two important points can be derived from this equation. First, the driving force for the removal of small pores is greater than that for the removal of larger ones. It, therefore, tends to be the larger pores that remain toward the end of the diffusion process. Second, in the irregularly shaped pores, mass will be transported to the concave regions of small radius of curvature from those areas where the surface is more rounded or convex. Thus, the irregularly shaped pores tend to spheroidize.

4.2.1.2. The creep HIP densification mechanism

The plastic flow of a material usually occurs along with the rearrangement of particles

during the sintering and HIP process. The occurrence of plastic flow in crystal materials is a transport of relatively large numbers of atoms by dislocation slip, and this generally requires high stress [83, 97].

The external gas pressure developed during the HIP cycle is achieved partially by the mechanical compressor and partially by the heating of the gas in the closed space. The HIP temperature is usually greater than 0.7 of the hipped material's melting point. This relatively high temperature during the HIP process is necessary to lower the yield strength and to raise the diffusivity of the material sufficiently for pore closure to occur in a reasonable time. HIP can remove both macro- and micro-porosity provided the internal porosity is isolated from the outside and there is a low pressure of gas in the porosity.

The HIP conditions are usually chosen so that the gas pressure is greater than the reduced yield point of the material at that temperature. Plastic flow can then occur on a microscopic scale. Under HIP conditions, considerable particle shear takes place and also creep processes. The solution precipitation and rearrangement of grains enhanced by pressure can also occur in the HIP process if the solidus temperature is exceeded. During the final stage of HIP densification, when only isolated pores are left, the surfaces of the pores are not simply pushed together to form a planar crack. Bonding between the surfaces occurs because atoms diffuse in both directions across the interface. At this stage, the pores are very small, usually less than 1 μm , and a hold time of 1 hour or longer is usually adequate to complete the closure [97].

Since wear is a surface process, surface-connecting porosity is a critical defect to the wear resistance of a material. Unfortunately, such porosity can not be removed by HIP, because the HIP gas can move into the pore and balance the external pressure. Some pretreatments must be performed before the HIP process. Coating and encapsulation are two common methods used to isolate the porosity from the surface. After these treatments, the open pores become closed, and the HIP gas can then forge these pores to close them, as illustrated in Fig. 4 - 4, not as effective though if gas is trapped. The open porosity usually corresponds to a density lower than 90% [98, 99].

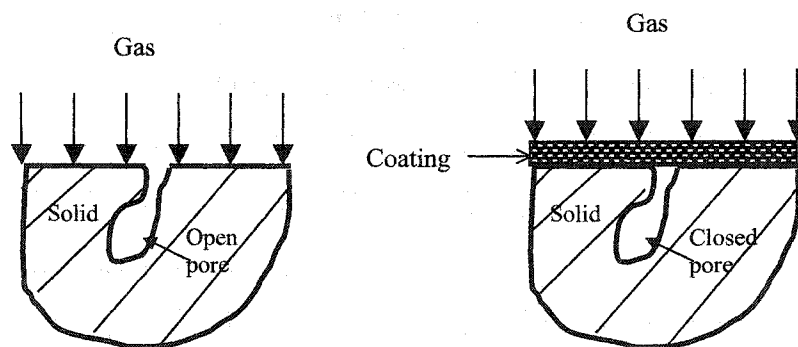


Fig. 4-4. The closure treatment of the open pores before HIP.

4.2.2. Effects of HIP on the structure of the sintered TiNi matrix composite

For comparison, the structures of specimens with and without experiencing HIP treatment were investigated. The SEM metallograph of a 52vol%TiC/TiNi specimen shows its microstructure characteristics after the vacuum sintering without HIP, as in Fig. 2-4. The TiC particles were distributed uniformly in the TiNi matrix. The phase constitution in such a composite was analyzed using X-ray diffraction. It revealed a phase constitution that was the same as that presented in Fig. 3-2. The TiNi, TiN and Ni₃Ti were still the primary phases present in the composite after the high vacuum sintering. The composition of the TiNi

matrix after the vacuum sintering was analyzed using EDX, and the results showed that the matrix still had a composition in the range of Ti-54at%Ni with some fluctuations. Porosity was present in the vacuum sintered specimens without HIP, especially in the central region of the specimen, as shown in Fig. 3-1. The pores formed a network in the composite and reduced its mechanical properties as well as wear resistance.

The structures of the hipped samples were examined by SEM and optical microscopy. Fig. 4 - 5 provides a SEM structure image of the hipped 52vol%TiC/TiNi. Fig. 4 - 6 illustrates an optical microscopy image of this sample. Compared with Fig. 3 - 1, these figures indicate that HIP is an effective approach to reduce the porosity. Most of the pores in the matrix were removed with only a few left at boundaries between the TiNi matrix and TiC particles. However, no significant improvement in the composition homogenization of the composite's matrix was observed. Fig. 4 - 7 shows a SEM image of the matrix. The matrix still displayed contrast, as illustrated in Fig. 2 - 5. The composition of the white location *A* was Ti-74at%Ni.

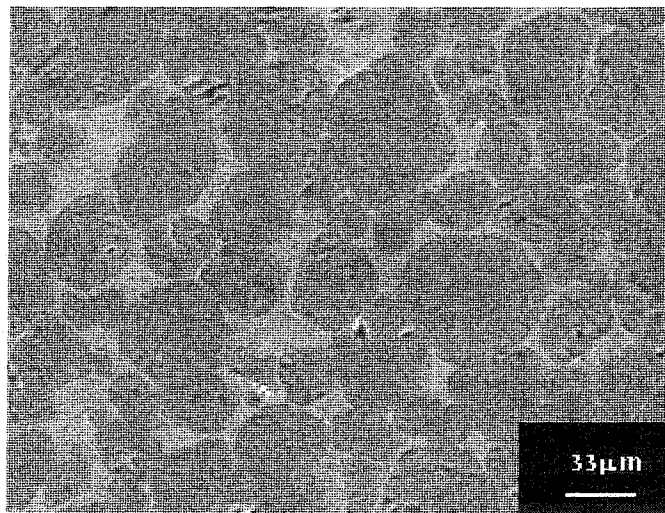


Fig. 4-5. The SEM image of the 1300°C hipped 52vol%TiC/TiNi.

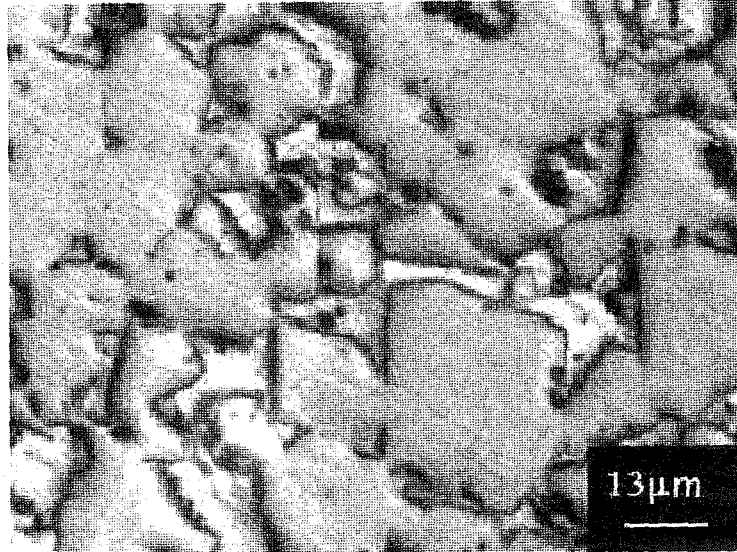


Fig. 4-6. The pore structure of 52vol%TiC/TiNi after HIP at 1300°C.

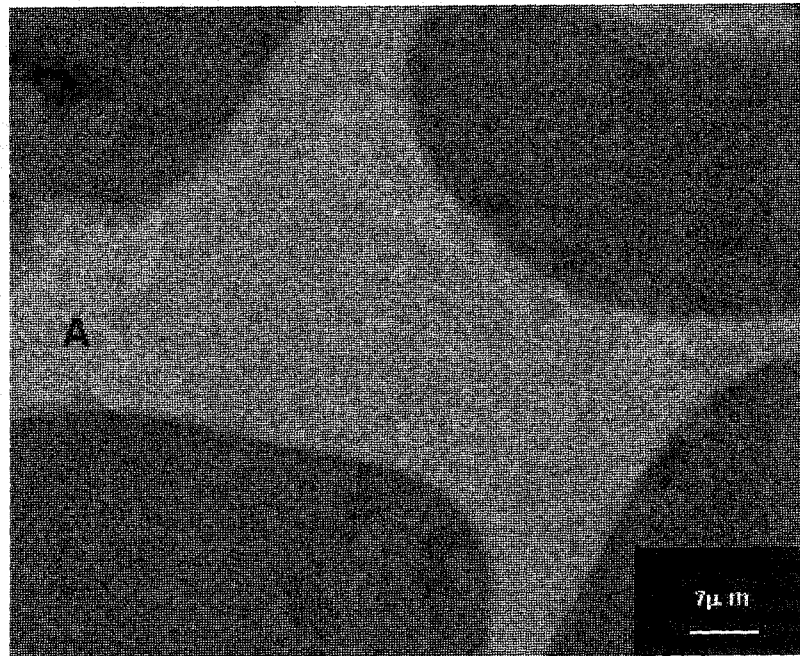


Fig. 4-7. The matrix of HIPed 52vol%TiC/TiNi.

The XRD did not detect any structural change caused by HIP. Fig. 4 - 8 is an X-ray diffraction pattern of the HIPed 52vol%TiN/TiNi sample. Compared with the unhipped samples, there was no substantial difference in the phase constitution in the HIPed samples.

This is understandable. The primary effects of HIP on a material's microstructure are the removal of porosity and grain growth. These changes involve diffusion and, therefore, are enhanced at elevated temperatures.

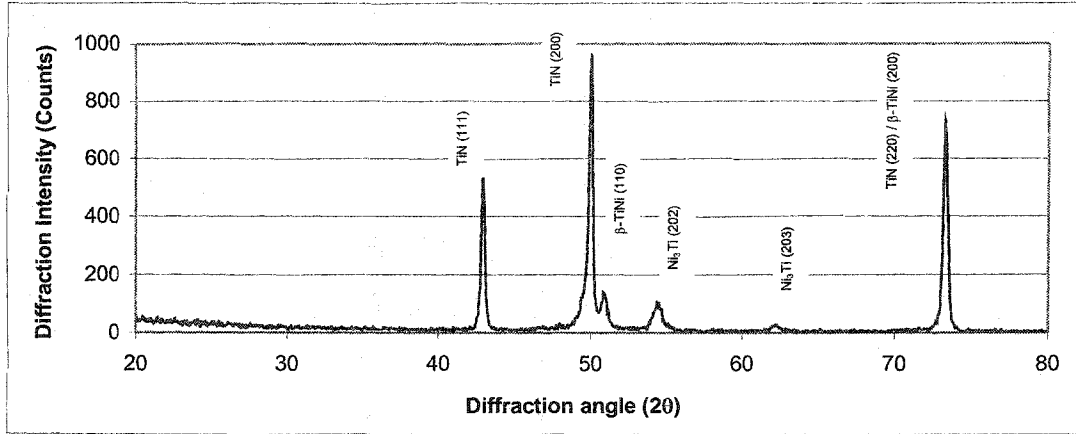


Fig. 4-8. (Co-K α 1) X-ray diffraction pattern of TiN/TiNi after 1300°C HIP.

The densities of the 52vol%TiN/TiNi specimens before and after the HIP treatment were measured. The sample without the HIP treatment had a density of $5.2 \times 10^3 \text{ kg/m}^3$, while the hipped sample had a density of $5.9 \times 10^3 \text{ kg/m}^3$. Clearly, a significant densification of the specimens was accomplished by the HIP process. After the 1300°C HIP treatment, the density is increased by about 14%. Compared with the porosity of 13.4% in the waxed samples described in Chapter 3, the samples processed in this stage of work had a porosity of 10% before the HIP treatment. The difference in the processing of these two groups of samples was that the mixing time of the powders for preparing the present samples was 24 hours, which was much longer than the previous mixing time (2 hours). This prolonged mixing time can help to coat the powders with the dissolved wax more uniformly and thus enhance the compaction of the powders, leaving less porosity in the green compact and the final sintered samples.

Macroscopically, the hipped samples maintained the same shape as the unhipped samples. Bulk distortion was not observed. This fact is due to the isostatic feature of HIP pressure. The isostatic pressure in HIP arises from Ar atoms colliding with the surface of the TiN(C)/TiNi composite. Each gas atom applies an individual compaction. The Ar atoms move at a very fast velocity, and a large number of collision events happen per unit area per unit time. These tiny atomic compactions take place on all external surfaces of the composite reliably and consistently, independent of the shape. On the average, the number of gas atoms moving through a unit area and their velocities are the same in all directions. Thus, for each surface of the composite, the press is the same and normal to the surface. It is just this isostatic nature of the press that allows the original shape of the composite to be kept during the HIP processing.

In the composite material, the role of the reinforcing phase is to constrain the deformation of the surrounding matrix, making it stronger and more creep resistant. However, it also constrains the displacements that lead to the densification. A study with a 1100 Al and a Pb-5% Sb alloy found that the inclusion phase offers little constraint to the matrix's deformation at a volume fraction less than 20%, but the constraint rapidly increases at a larger fraction of the second phase. Two mechanisms are responsible for the constraint. First, the matrix must be deformed more within the composite because of the excluded volume associated with the cracking of the particles and inclusions with different sizes. Second, above a certain fraction, the second phase particles form a continuous network that supports a portion of the applied stress and thus, partially shields the deformable phase from the total applied pressure. This is why the maximum HIP pressure of the furnace was

employed for the HIP treatment of the 52vol%TiN/TiNi and 52vol%TiC/TiNi composite, in which over half volume was occupied by the hard TiN or TiC particles. In terms of the HIP temperature and time, two factors were considered to determine the value of these two parameters. The first was densification, while the other was grain growth during the HIP process. In order to facilitate the HIP process, a HIP temperature greater than 0.7 of the melting point of the hipped material is often selected to reduce its yield strength. The melting point of TiNi alloy is around 1310°C. According to the empirical rule, a temperature greater than 917°C would be workable for HIP TiNi alloy. However, due to the large fraction of the TiN and TiC particles, 1300°C was used in our trial so that the matrix was greatly softened while not melted. At such a high temperature, both the diffusion and plastic flow of material were significantly enhanced, and thus the HIP process is accelerated. However, the high HIP temperature may also have a harmful effect on the material's structure, that is, it could lead to excessive growth of the grains and thus reduce the material's final mechanical properties, especially toughness.

The grains grow through the migration of the grain boundaries. Second phase particles can help to pin the grain boundaries. But at the high HIP temperature and pressure, the diffusion of the elements in the second phase particles is also enhanced, and precipitates may coarsen or dissolve and thus allow grain boundaries to migrate. In the current experiment, the HIP time was selected as 2 hours. However, according to the effects of HIP temperature, pressure and time on the hipped material's structures, it can be seen that a series of HIP treatments and studies are needed to determine the optimum HIP parameters in pressing any material. Thus, the HIP treatment in our current study requires more studies to avoid the

negative influence of HIP treatment on the composite's structures and properties, although it has significantly densified the material.

4.2.3. Effects of HIP on the mechanical behavior of the TiNi composites

As demonstrated, HIP did not change the phase constitution of the sintered TiNi matrix composite, and the reduction of porosity was the main effect of HIP on its structure. In order to better comprehend the effects of HIP on the wear resistance, the influences of HIP on the hardness and pseudoelasticity of the TiNi matrix were investigated using a nano-mechanical probe. Fig. 4 - 9 illustrates typical load - depth curves of a 52vol%TiN/TiNi composite during nano-indentation prior to and following the HIP treatment. The indentation test indicated that the specimen after the HIP was significantly harder. Fig. 4-10 presents the penetration depth d values of these specimens versus the indentation loads. The data confirms the densification of the specimens after HIP. Regarding the η ratio, the HIP process increased the η value at all loads, as illustrated in Fig. 4 -11. This increase in η value is certainly conducive to an improvement in the material's wear resistance. The differences in the d and η values of the hipped and unhipped samples may result from the densification, as discussed in Section 3.2.4.

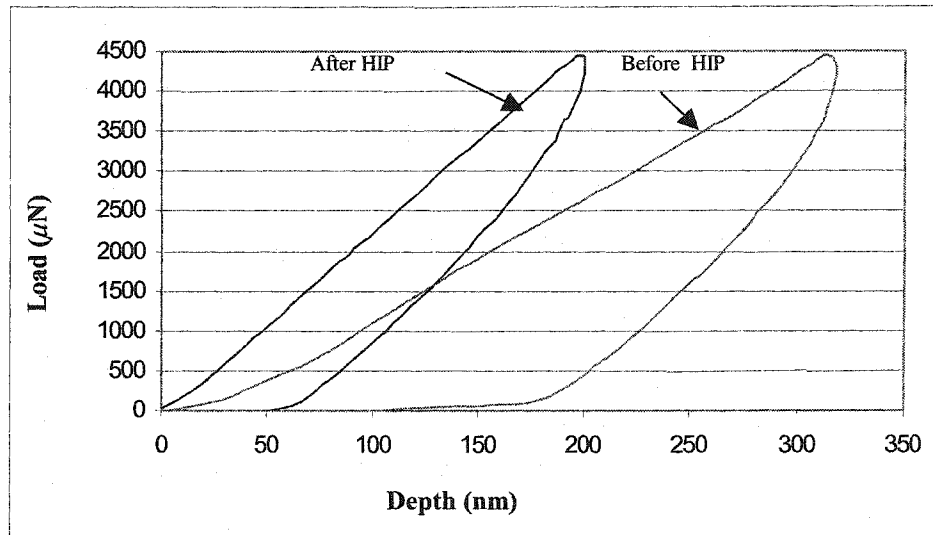


Fig. 4-9. The Load-displacement curves of one indentation under 4500 μN .

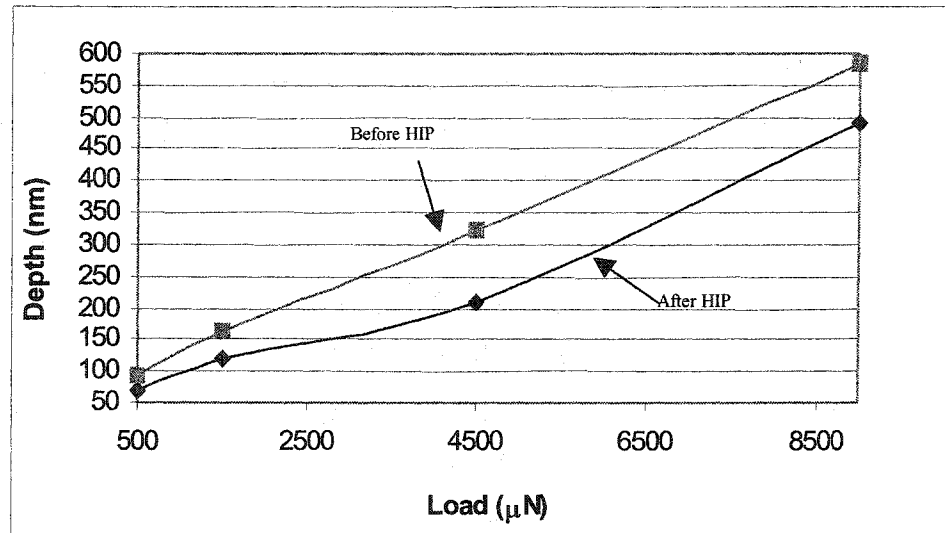


Fig. 4-10. The average maximum depth versus the nano-indentation load.

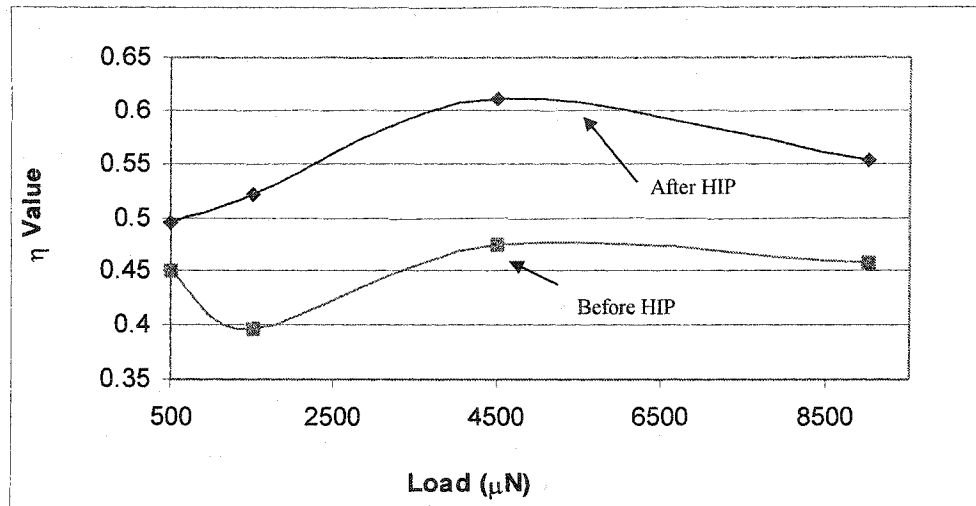


Fig. 4-11. η values of TiN/TiNi specimen before and after HIP.

In addition to the performed indentation tests, some other experiments were also reported regarding the improvement in the mechanical properties of bulk materials by HIP treatment. Fig. 4-12 shows a typical improvement in the yield strength, ultimate tensile strength and elongation to failure of a cast Ni-Al bronze alloy by HIP treatment [97]. Along with the increase in the strengths, the elongation of the material also jumped to 21.7% after HIP from 10% of the cast state. This amelioration in both the material's strength and toughness is expected to produce an increase in its wear resistance.

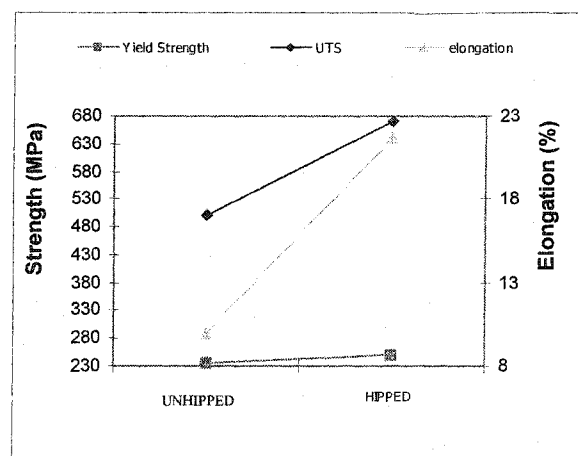


Fig. 4 -12. HIP and mechanical properties of a Ni-Al alloy [Ref. 97].

4. 2. 3. Effects of HIP on the wear behavior

An improved wear resistance can be anticipated after the HIP treatment, as both the strength and toughness of the material are increased. Since the density of pores was greatly reduced by the HIP process, the wear resistance of a HIP treated composite would be improved. The wear resistance of TiNi-based composites before and after the HIP treatment were evaluated using a pin-on-disc wear tester, and the results of the test are shown in Fig. 4-13. (The data in Fig. 4-13 was the average of 5 measurements with a variation of 20%.) It can be seen that there are two major differences between specimens with and without HIP treatment. Firstly, the specimens experiencing HIP showed higher wear resistance, especially under the highest wearing load, where the difference in the wear losses of the HIP treated and non-HIP treated TiC/TiNi samples was more than 50%. The specimens were densified by HIP, so that cracking became relatively difficult, thus resulting in improved wear resistance. Secondly, the specimens exhibited different responses to the wearing load. For the specimens without HIP, there was a decrease in wear loss between 0.14 kN and 0.17 kN, as Fig. 4-13 illustrates. This drop in wear loss was attributed to the self-sealing of pores or sealing by the materials picked up from the stainless steel disc under high wearing loads. Details have been reported in Section 3. 2. 2. When HIP was conducted, the specimens were almost fully densified before the wear testing. Therefore, no similar drop in the wear loss was observed, and the increase in wear was markedly lower than those of the specimens without HIP. At the highest load, HIP reduced the wear loss of TiN/TiNi by 40% ~ 50%. In addition, generally, it can be seen that TiN/TiNi had higher wear resistance than TiC/TiNi. This could be ascribed to the higher toughness of the TiN particles, which made TiN/TiNi perform better especially under higher loads, as discussed in Section 2. 2. 4. 2.

It should be pointed out that there was a data scattering of 20% in the wear loss of the materials. This is common in wear test, but could affect the examination of the wear losses of the tested materials at low load stage. However, the averages shown in Fig. 4-13 still demonstrate the wear loss trend of the materials versus the load, and at high load stage, the data scatter is smaller than the wear loss difference. Furthermore, the wear loss data are compatible with the examination on the mechanical properties of the composite. All these validate Fig. 4-13.

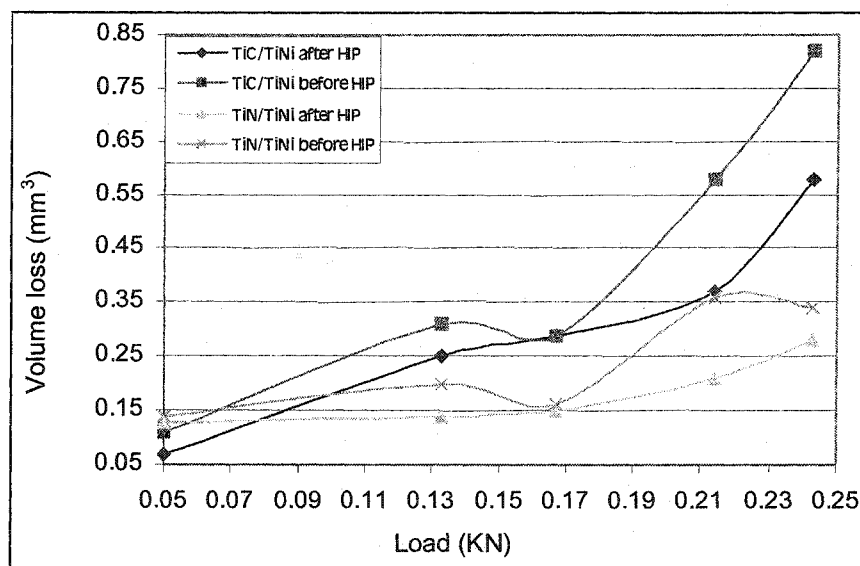


Fig. 4-13. Wear loss of 52vol %TiC/TiNi and 52vol %TiN/TiNi before and after HIP.

The improved wear resistance may also be indicated from the worn surface. The worn surfaces of the specimens with and without HIP under both low and high loads were examined using SEM. Fig. 3-4 and Fig. 3-5 illustrate worn surfaces of a 52vol%TiN/TiNi specimen without HIP. The surfaces of the specimen had different morphologies when worn under low and high loads. At the low loads, a lot of pits were found on the worn surface, while under the high loads, no pits were displayed, with the major damage being the

delamination of material from the surface.

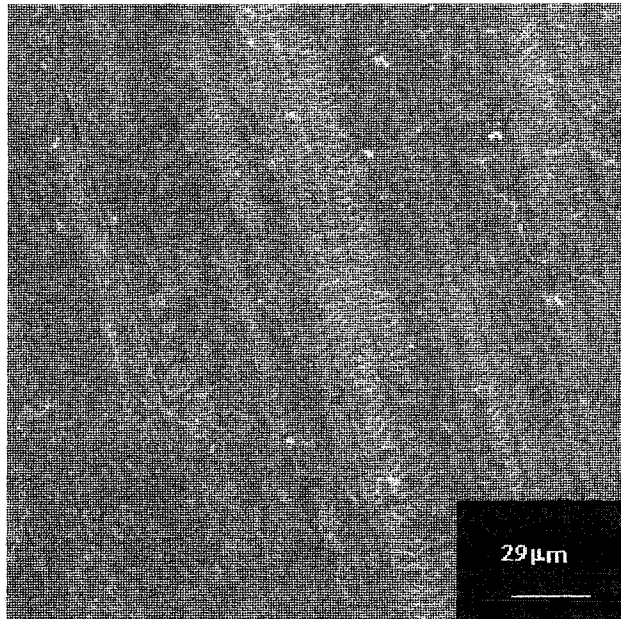


Fig. 4-14. Worn surface of HIPped 52vol%TiN/TiNi composite under 0.05 kN.

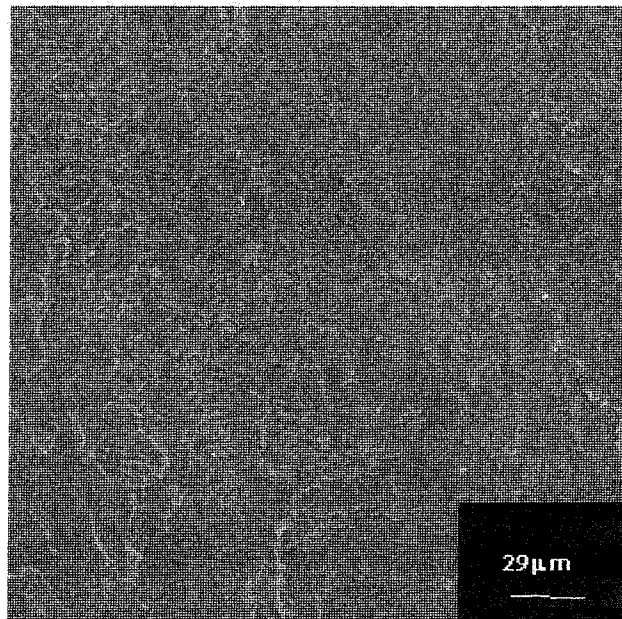


Fig. 4-15. Worn surface of HIPped 52vol%TiN/TiNi composite under 0.243 kN.

Fig. 4-14 and Fig. 4-15 show the surfaces worn under low and high load respectively of a specimen with HIP treatment. When worn at low load, both cutting and delamination tracks

of the material were present on the surface. When worn at high load, the delamination of the material was more overt than cutting. However, the morphological difference between the HIP processed specimens worn respectively under low and high loads was not as significant as that of the specimens without HIP. The specimens without HIP were not dense enough. A lot of pores remained in the material after pressing and vacuum sintering. Worn at low loads, the pores were not compacted. Worn at high loads, the self-healing of the surface pores improved the wear behavior of the specimens. The hipped samples had few pores inside and thus exhibited few pits on the worn surface no matter how high or low the wearing force was. However, a comparison between Fig. 3-5 and Fig. 4-15 indicates that the HIP process produced a higher densification on the material than the self-sealing of pores during the wearing process, as Fig. 3-5 shows more severe delamination of the material.

4. 3. Conclusions

The effects of hot isostatic pressing (HIP) on the wear and mechanical properties of the TiC/TiNi and TiN/TiNi composites were investigated. The following statements can be concluded from these investigations.

- (1). The HIP process is an effective way to densify the sintered TiNi-based composite. After the HIP process, most of the pores in the composite are removed.
- (2). The removal of the porosity greatly increases the hardness and pseudoelasticity of the material and thus its wear resistance.

Chapter 5. The Phase Transformation and Wear Behavior of TiNi-based Composite

In chapters 2 - 4, the studies on the mechanical properties and wear behavior of the sintered TiNi-based composite have been reported and discussed. The high wear resistance of the composite benefits from the pseudoelasticity of the composite's TiNi alloy matrix, which is in turn resulted from a reversible thermoelastic martensitic phase transformation. It is thus of importance to investigate the phase transformation behavior in the sintered TiNi matrix composite. This chapter provides and discusses the results of the examination on the composite's phase transformation behavior and the effects of temperature on its wear performance.

5. 1. Experimental procedure

The 1300°C hipped 52vol%TiN/TiNi samples described in Chapter 4 were used to study the phase transformation behavior and the effects of temperature on the wear performance of TiNi-based composite. The experimental procedure is as follows, and more details are offered in the relevant sections of previous chapters, if not specified here.

5. 1. 1. Sample preparation

The 52vol%TiN/TiNi composites were first fabricated using the vacuum sintering process. The powders were mixed and pressed with wax dissolved into hexane. The powder compacts were sintered at 1500°C for 6 hours in vacuum of 6.7×10^{-2} Pa (5×10^{-4} torr). The

sintered samples were then HIPped at 1300°C for 2 hours in high purity Ar. Such prepared samples were then ready for studies.

5.1.2. Microstructure analysis and mechanical property examination

The microstructure of the sample was examined using optical microscopy, SEM and XRD. The pseudoelasticity of the composite was evaluated by indentation tests. Compared with the previous indentations, the present ones were performed at a much higher load on a Fisher triboscope, which offered an indentation load up to 1 N. 304 stainless steel, pure Ti-51at%Ni alloy and 52vol% TiN/TiNi composite were compared in the indentation tests, and all the samples had a size of 6 mm in diameter and 5 mm in height.

5.1.3. Phase transformation characterization

Differential scanning calorimetry (DSC), X-ray diffraction (XRD) and transmission electron microscopy (TEM) were employed to characterize the phase transformation in the 52vol%TiN/TiNi composite.

5.1.3.1. DSC analysis

Differential scanning calorimetry was used to identify the phase transformation in our work. The 52vol%TiN/TiNi sample was sliced with a BUEHLER linear precision diamond saw at a very low speed (around 0.7 mm/min) to avoid excessive heating. The weight of the final DSC composite samples was in a range from 30 mg to 150 mg. The scan was conducted in a temperature range from – 50°C to 150°C with a Dupont 2200 calorimeter. During the scanning, the sample was heated to 150°C from room temperature, held for 3 minutes, and

subsequently cooled to -50°C and held there for 3 minutes. Finally, the sample was brought back to room temperature. The scanning rate was $5^{\circ}\text{C}/\text{min}$ in both heating and cooling. 10 mg of Ti-56wt%Ni (Ti-51at%Ni) prealloyed powders ($> 10\ \mu\text{m}$) (from Special Metals Corporation, New Hartford, NY) were also scanned under the same condition from -60°C to 120°C as a reference.

5.1.3.2. X-ray diffraction

The pure Ti-51at%Ni prealloyed powders (total weight of about 5 g) and bulk 52vol%TiN/TiNi were used to examine the temperature-induced phase transformation by X-ray diffraction performed with a Rigaku Geigerflex X-ray diffractometer. The Ti-51at%Ni alloy powder had its M_s and A_s points at about 30°C and 25°C respectively, as detected in DSC. Originally, the X-ray diffraction test is supposed to be conducted at a constant high or low temperature, but due to the availability of facility, the X-ray diffraction test was performed in the following way.

The TiNi alloy powders were fed into a plate aluminum holder having a size of 25 mm (length) \times 15 mm (width) \times 3 mm (thickness). Then the assembly of TiNi powders and aluminum holder was heated to 120°C . After the heating, the assembly was quickly moved to the sample chamber of X-ray diffractometer for scanning. After scanned at high temperatures, the assembly was taken out and cooled in dry ice (solid CO_2). Thereafter, it underwent the low temperature scanning. The whole analysis was composed of a heating \sim cooling \sim heating \sim cooling cycle. The obtained X-ray patterns were used as a reference to study the possible phase transformations in the TiNi-based composite.

A bulk 52vol%TiN/TiNi composite sample having a size of 6 mm in diameter and 4 mm in height was used in the XRD test. The surface of the composite sample was ground and polished before the test. The experimental procedure was the same as that for the TiNi alloy powder except that the bulk composite experienced a heating ~ cooling ~ heating cycle and was respectively cooled in dry ice and in liquid N₂ in each scanning cycle.

During the above diffraction analysis, the sample's temperature was changing. In order to avoid a large change in the sample's temperature and also attain an explicit XRD diffraction pattern, the scanning was performed at a scanning speed of about 8° per minute and 0.05° per step from 20 degrees to 80 degrees for the scanning angle 2θ . Such an XRD test took about 7 minutes in total.

5. 1. 3. 3. TEM analysis

The wear debris of 52vol%TiN/TiNi sample was analyzed by transmission electron microscopy to determine if the martensitic phase transformation was induced by wear. The 52vol%TiN/TiNi sample was worn against a 304 stainless steel disc on a pin-on-disc tribometer. Before wearing, the sample was heated to 120°C to obtain the full austenite phase. During the wearing, in order to collect enough wear debris in a reasonable period of time, a high wearing load (0.214 kN) was used. In order to keep the sample at a relatively low temperature, where martensite can be stress-induced and maintained, oil was placed on the stainless steel disc to lubricate the worn surfaces. The sliding speed was 30 m/min, relatively low so that the temperature did not rise significantly. The wear debris was collected from the stainless steel disc, cleaned in alcohol and then air-dried. Subsequently,

the wear debris was examined using selected area diffraction (SAD) with a JEOL 2010 TEM. During the TEM diffraction analysis, the composition of the debris particles was first analyzed by EDX. When an area having both Ti and Ni was identified on a debris particle, SAD was conducted around this area.

5. 1. 4. Wear of the composite with respect to the temperature

The effects of temperature on the wear resistance of the TiNi-based composite were investigated using a pin-on-disc tribometer. In order to control the temperature, a low wearing load, 0.023 kN, a low sliding speed, 18 m/min, and a short sliding distance, 60 m, were used for the testing. The frictional heat produced during the wear process was negligible, and the sample's temperature could be largely controlled. The sample's temperature ranged from about -15°C to 140°C . Solid CO_2 was applied to cool the sample and its holder to around -15°C . A heating gun, which can heat air over 300°C , was employed to heat the sample and the sample holder to 150°C and maintain it at that temperature during the sliding process. The temperature of the sample was monitored by a FLUKE 52 thermal couple attached to the sample near its bottom surface during the wear testing. In order to produce wear losses that were large enough for an accurate measurement, fresh SiC abrasive paper (320 grit) was used as the wearing couple material for each measurement. After the wear, the sample was cleaned in alcohol, air dried and then weighed by the OHAUS analytical balance to an accuracy of 0.1 mg to obtain the wear loss. The wear loss data shown in this chapter are an average of 4 measurements.

5. 2. Experimental results and discussion

5. 2. 1. Microstructure and composition of the 52vol%TiN/TiNi composite

The microstructure and composition of the composite was examined with optical microscopy, scanning electron microscopy (SEM) and XRD. The SEM image and the composite's phase constitution at room temperature are illustrated in Fig. 4-5 and Fig. 4-8 respectively.

5. 2. 2. The mechanical properties

The mechanical properties of the matrix material were evaluated by indentation testing. All the indentation tests reported in the previous chapters were carried out using a Hysitron triboscope under an indentation load up to 20 mN. Under a small indentation load, the elastic deformation of a material takes a large portion of its deformation. Such a large portion of elastic deformation reduces the credibility of the evaluation on pseudoelasticity by indentation, because under a low load, the material deforms elastically and thus results in a high η value (see Section 2. 2. 2 for definition). In order to more precisely evaluate the pseudoelasticity of the materials, a series of indentation tests were performed at much higher loads up to 1000 mN in the current examination. The indented materials included a 52vol%TiN/TiNi composite, pure Ti-51at%Ni alloy and a 304 stainless steel. The deformation energy recovery ratio, η value, and the maximum indentation depth curves are shown in Fig. 5-1, Fig. 5-2 and Fig. 5-3 respectively.

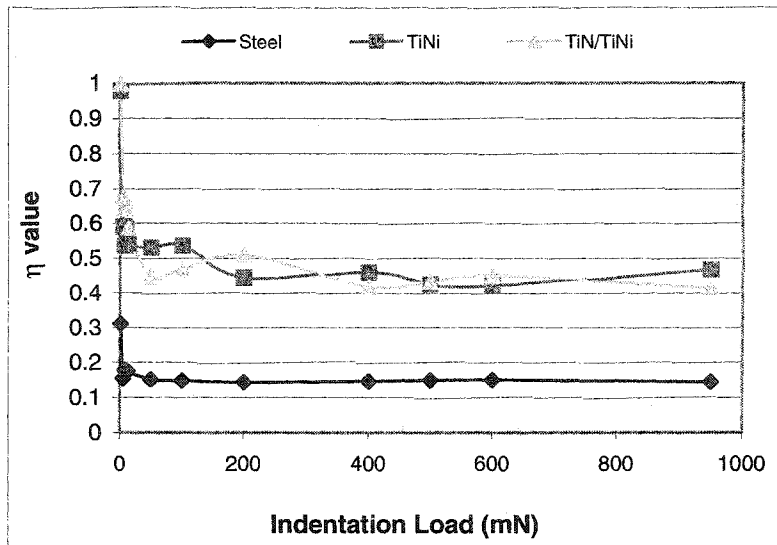


Fig. 5-1. The η value of the tested materials over the whole indentation load range.

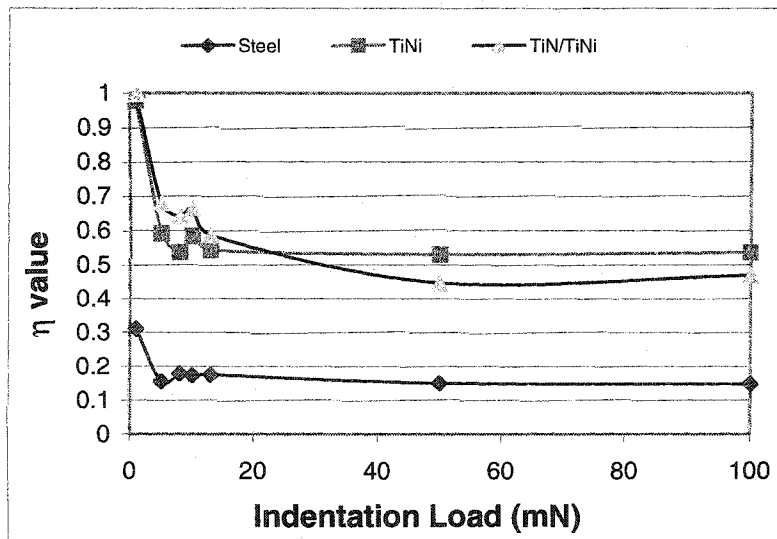


Fig. 5-2. The η value of the tested materials under low load range in Fig. 5-1.

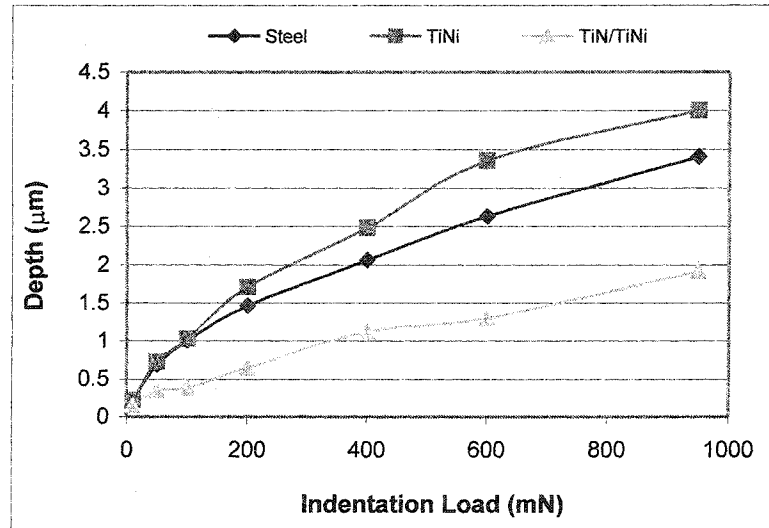


Fig. 5-3 The maximum depth of the materials in the indentation test.

Fig. 5-1 and Fig. 5-2 display the η value magnitudes, which agree with the previous results for these materials. The 52vol%TiN/TiNi had a η value comparable with that of the Ti-51at%Ni alloy, and the steel had a much lower η value in the load range. This trend held even at the smallest load, 1 mN, where the η value is supposed to be largely determined by the material's elasticity. The η value of the stainless steel was about 0.3, which was much lower than those of the TiNi alloy and the 52vol%TiN/TiNi composite. Compared to the pure Ti-51at%Ni alloy, the 52vol%TiN/TiNi composite may not have a comparable real pseudoelasticity. However, since the composite contained over 50 vol% of hard TiN particles, the yield strength of the material was much higher than that of the TiNi alloy. In this case, 52vol%TiN/TiNi had a larger elastic limit, which may thus increase the η value. Compared with the stainless steel, the 52vol%TiN/TiNi had both a higher elasticity and pseudoelasticity because of the presence of TiN particles and TiNi alloy. This enabled the 52vol%TiN/TiNi composite to exhibit a higher η value than the stainless steel. The

maximum indentation depths on the materials presented in Fig. 5-3 provide information on the hardness of these three materials. 52vol%TiN/TiNi was the hardest, and Ti-51at%Ni alloy was the softest, which was consistent with the materials' bulk hardness.

The three materials also showed the same trend of variation in terms of their η values versus the indentation loads. In the low load range, the η value was relatively high because of the material's elasticity. However, when the load reached about 20 mN, all the η values came to be stable with load, no matter how large or small the η value was. The stabilized η values further demonstrated the superior pseudoelasticity of the 52vol%TiN/TiNi composite, which was comparable with that of the pure Ti-51at%Ni alloy. The stabilization of the η value also justified the application of indentation test to reflect the material's capability of accommodating the strain caused by the external load. The stabilization of the η value versus the indentation load might result from the stabilization of the ratio of elastically strained volume to the total strained volume. Further studies on this issue need to be conducted in order to better understand the pseudoelasticity reflected by η values. Under light loads, the surface is mainly elastically deformed. As the load is increased, plastic deformation increases, so that the ratio of W_e/W_t decreases and eventually stabilizes.

5. 2. 3. *Phase transformation in Ti-Ni binary system*

To check whether or not the martensitic phase transformation in the sintered 52vol%TiN/TiNi is essential to the observed pseudoelasticity, studies were conducted to investigate possible phase transformations in the TiNi composite. The phase transformations in the pure TiNi alloy powder were used as a reference.

The martensitic phase transformation in TiNi alloy usually involves 3 phases. They are the parent austenite B₂ phase, the martensite M phase and the so-called pre-martensitic R phase. The structure of the parent austenite phase is illustrated in Fig. 5-4. It has an ordered BCC structure, with the cubic body center and eight cubic corners being occupied by the Ti or Ni atoms alternatively. The lattice parameter, a , of the TiNi austenite is 0.3014 nm [100, 101]. The structure of martensite phase is shown in Fig. 5-5. It is a monoclinic structure with $a=0.2889$ nm, $b=0.4120$ nm, $c=0.4622$ nm, and angle $\beta=96.80^\circ$. The monoclinicity of martensite is a result of coupling between a non-basal plane shear $\{001\}\langle 1\bar{1}0\rangle_{B_2}$ (the negative sign of the crystal orientation in the Miller's indices is put at the bottom instead of on the top of the number in this thesis) and the basal plane shear $\{110\}\langle 110\rangle_{B_2}$ [102].

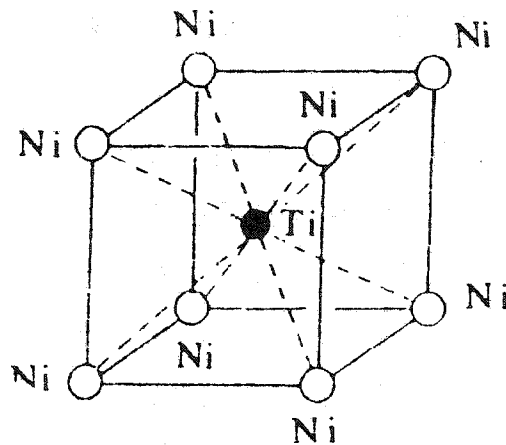


Fig. 5-4. The ordered BCC structure of the TiNi austenite [Ref. 101].

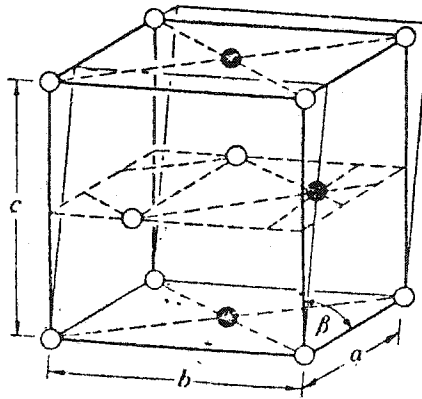


Fig. 5-5. The structure of TiNi alloy martensite phase [Ref. 102].

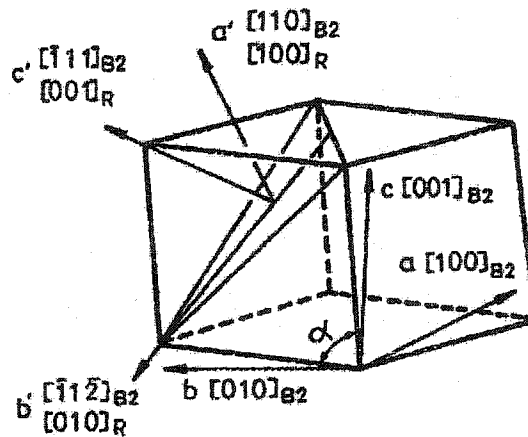


Fig. 5-6. The structure of TiNi alloy R phase [Ref. 101].

The structure of R phase is shown in Fig. 5-6. It has a rhombohedral crystal structure with dimensions of $a_R=0.738$ nm and $c_R=0.532$ nm. The R phase is formed by elongating any of the four $\langle 111 \rangle$ directions of the parent austenite structure. The rhombohedral angle α is smaller than 90° and decreases with decreasing temperature. As reported, the rhombohedral angle is in fact very close to 90° , therefore the austenite cubic indices are often used to analyze R phase for convenience in practice. The orientation relationship between the parent B_2 phase and R phase is $(111)_{B_2} // (0001)_R$ and $\langle 211 \rangle_{B_2} // \langle 2110 \rangle_R$ [101].

During the phase transformation, all the Ti-Ni binary alloys and TiNi-based multi-component alloys tend to transform into martensite, either directly from the parent austenite phase, or indirectly transform into R phase and then into martensite. In some cases when the intermediate R phase is stabilized by alloying addition, the subsequent $R \leftrightarrow M$ transformation may be suppressed [45].

X-ray diffraction (XRD), differential scanning calorimetry (DSC) and transmission electron microscopy (TEM) analysis are the most common methods used to explore the martensitic phase transformation, including the R phase transformation in the TiNi alloy. An x-ray diffraction pattern at high temperature (70°C) and low temperature (-20°C) are presented in Fig. 5-7 and Fig. 5-8 respectively [103]. The X-ray diffraction was conducted with $\text{Cu-K}\alpha$ radiation ($\lambda=0.154\text{ nm}$) on some TiNi powders ($44\text{ }\mu\text{m} \sim 70\text{ }\mu\text{m}$) at a temperature range from -20°C to 80°C . Fig. 5-7 shows the strongest detected peak of the TiNi high temperature austenite phase at 42° of the diffraction angle 2θ , and Fig. 5-8 is regarded to be the martensite XRD pattern. The martensite and austenite X-ray patterns appeared repeatedly during the cooling and heating cycles.

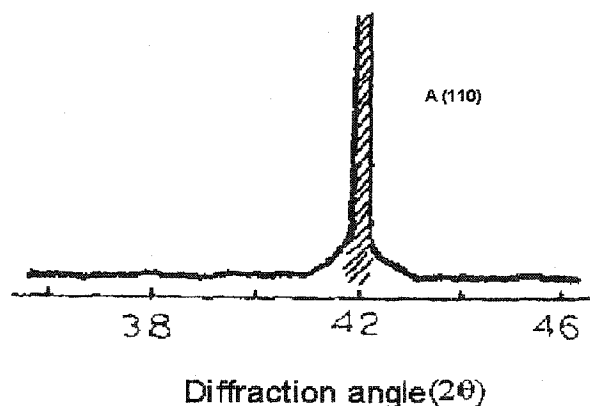


Fig. 5-7. The high temperature X-ray pattern of TiNi alloy [Ref. 103].

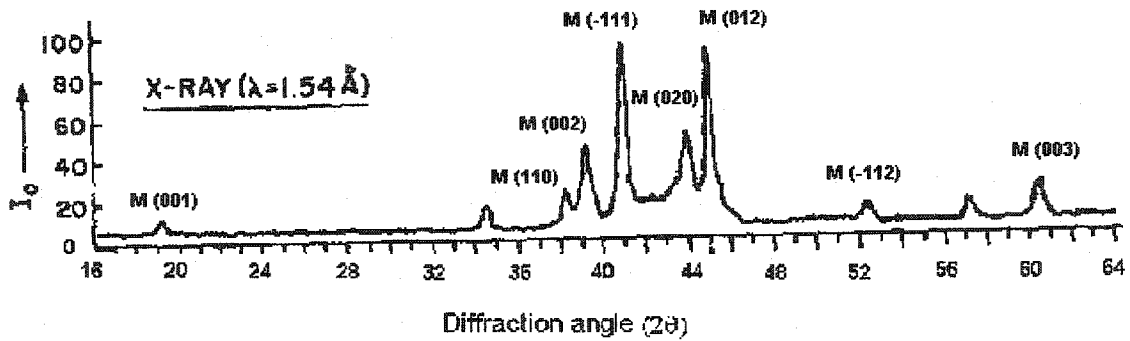


Fig. 5-8. The low temperature X-ray pattern of TiNi alloy [Ref. 103]

In many cases, R phase is present prior to the martensitic phase transformation in the Ti-Ni alloy system. Therefore, the R phase is often referred as a pre-martensite phase. The reported R-phase transformation is often detected through DSC and TEM. Fig. 5-9 provides an example of a DSC curve for both the martensitic and R-phase transformations in a Ti-50at%Ni alloy [104]. Upon cooling, the R phase formation occurred before the formation of martensite. The enthalpy (ΔH) of the $B_2 \leftrightarrow R$ phase transformation is relatively small (≈ 3.5 J/g), compared to that of the martensite phase transformation (10.2 J/g).

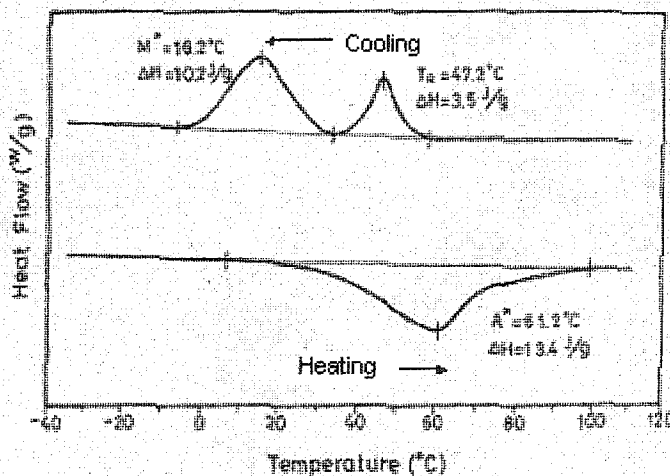
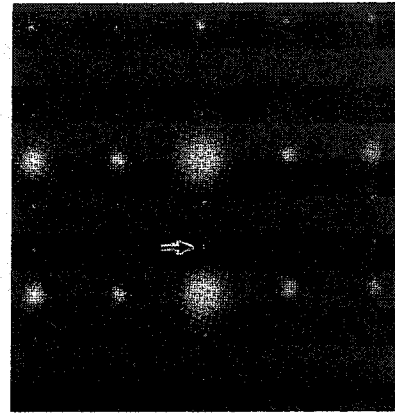


Fig. 5-9. DSC curve of the martensite and R phase transformation of TiNi alloy [Ref. 104].

In TEM diffraction patterns, the R phase results in the so-called 1/3 diffraction spots present in the austenite diffraction pattern. Sample TEM diffraction patterns of the austenite and R phase in a $\text{Ti}_{50}\text{Ni}_{47}\text{Fe}_3$ alloy are illustrated in Fig. 5-10 [105, 106]. In the figures, 1/3 (110) and 1/3 (111) reflection spots of the R phase can be observed, as indicated by the arrows.



A. 1/3 (110) reflection [Ref. 105]



B. 1/3 (111) reflection [Ref. 106]

Fig. 5-10. The 1/3 diffraction spots in TEM diffraction pattern of the R phase.

In our study, the Ti-51at%Ni powder was analyzed using DSC and XRD respectively to help determining if the martensitic phase transformation occurred in the TiNi matrix of our composite samples. A DSC plot of the Ti-51at%Ni powder is shown in Fig. 5-11. During the cooling cycle, the martensite phase transformation was triggered at about 30°C and was finished at about -10°C. During the heating cycle, the martensite phase transformed back to the austenite phase, starting at about 25°C and finishing at about 75°C.

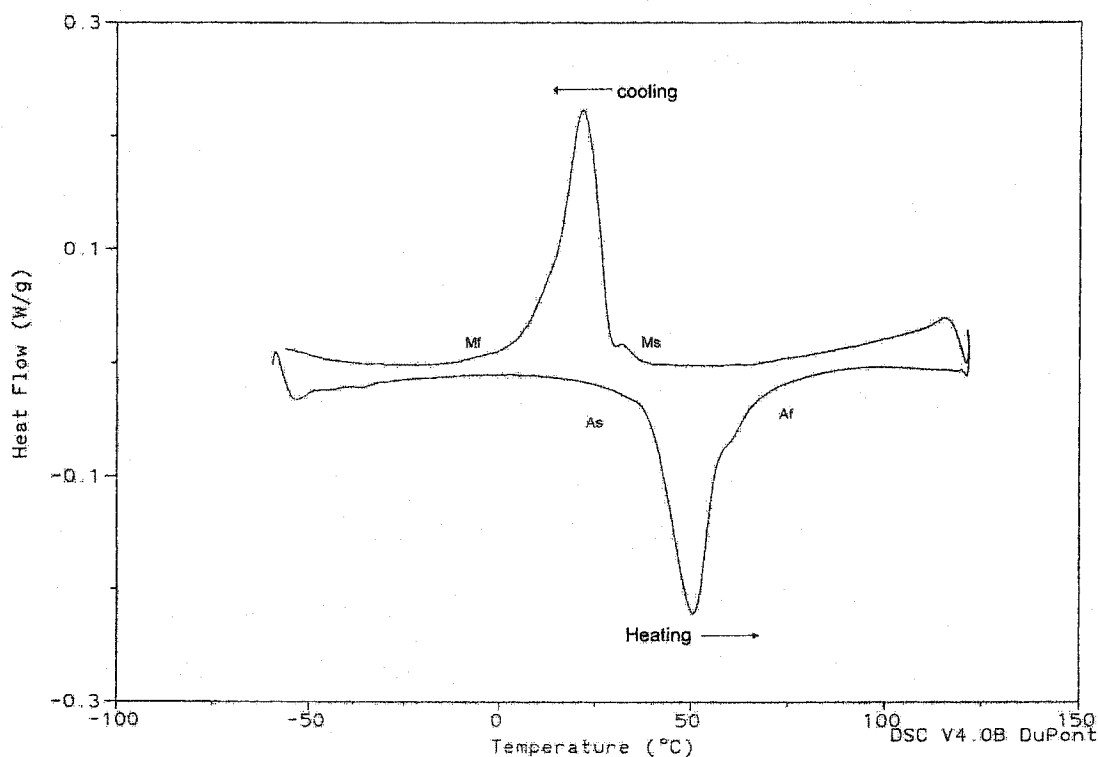


Fig. 5-11. The DSC curves of the prealloyed TiNi powder.

The TiNi powder was also examined by XRD at high and low temperatures. The radiation wavelength λ_{Co} was 0.1789 nm. The resulting high temperature and low temperature XRD patterns are given in Fig. 5-12 and Fig. 5-13 respectively. According to ASTM XRD diffraction file card 19-850 and 18-899, the reflections from (110), (200) and (100) crystal planes of the austenite β phase were present during the XRD diffraction at high temperature. So at high temperatures, the TiNi powder existed in the austenite β phase. Following ASTM XRD diffraction file card 27-344, the low temperature XRD pattern of the TiNi powder is indexed as shown in Fig. 5-13, and it indicates that the austenite phase transformed to martensite phase. However, the peaks *a*, *b*, *c*, *d*, and *e* in Fig. 5-13 have not been indexed. The corresponding crystal interplanar distance *d* values of these peaks are 0.3903 nm, 0.3671 nm, 0.3447 nm, 0.2864 nm and 0.2603 nm respectively. It was noticed that the

interplanar distance d values of peaks b , d , and e are just 3 times the d values of the (211), (310) and (222) crystal planes of the TiNi high temperature austenite phase. After calculation, peak a corresponds to a d value that is 3 times the (210) d value, and peak c is related to (220) plane of the austenite in the same way. Because of this factor 3 relationship between the interplanar distances of the parent austenite and transformed phase, the additional peaks are tentatively indexed as the intermediate R phase. Moreover, the appearance of the austenite (110) peak in the low temperature XRD pattern indicates that the temperature during the diffraction was not adequately low to completely transform the powder into martensite phase, and thus some austenite phase still remained in the TiNi powder. The coexistence of the austenite and martensite phases also implies the formation of R phase during the XRD analysis.

The TiNi powders also underwent some heating and cooling cycles, and the corresponding XRD patterns are shown in Fig. 5-14. The martensite phase, along with the R phase, repeatedly appeared at low temperatures and transformed back to the austenite phase, when the temperature was raised, which confirms the reversibility of these phase transformations in the TiNi alloy.

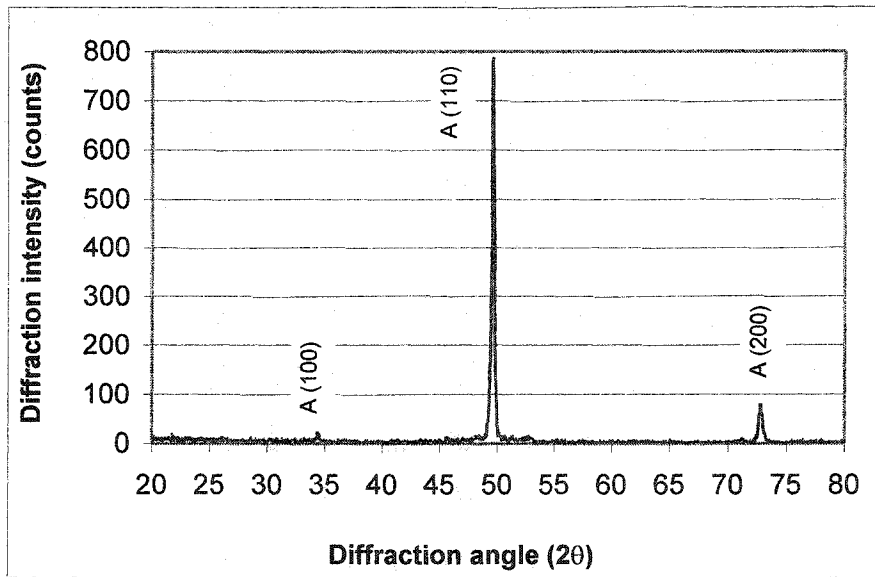


Fig. 5-12. XRD pattern of the TiNi alloy at high temperature.

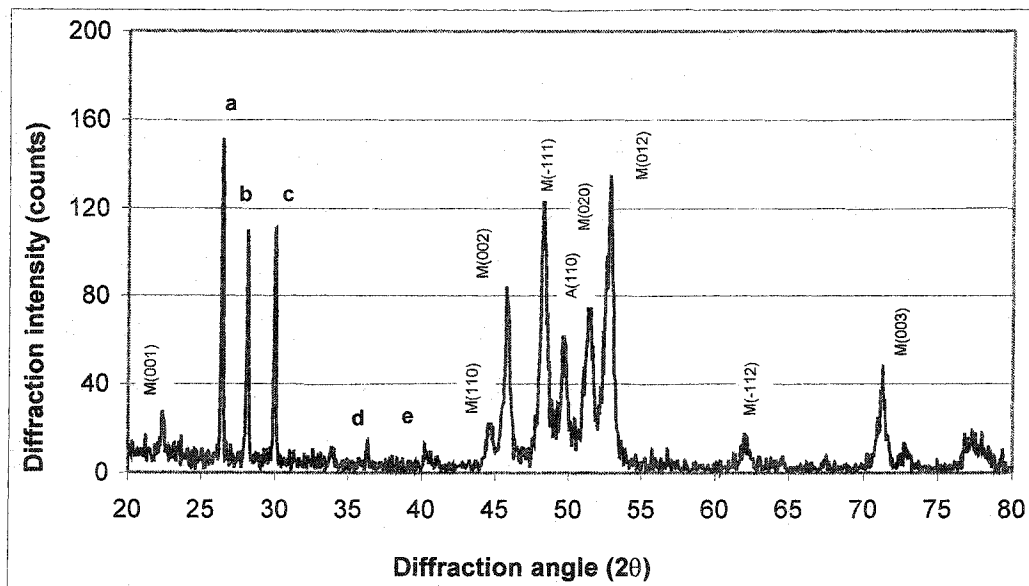


Fig. 5-13. XRD pattern of the TiNi alloy at low temperature.

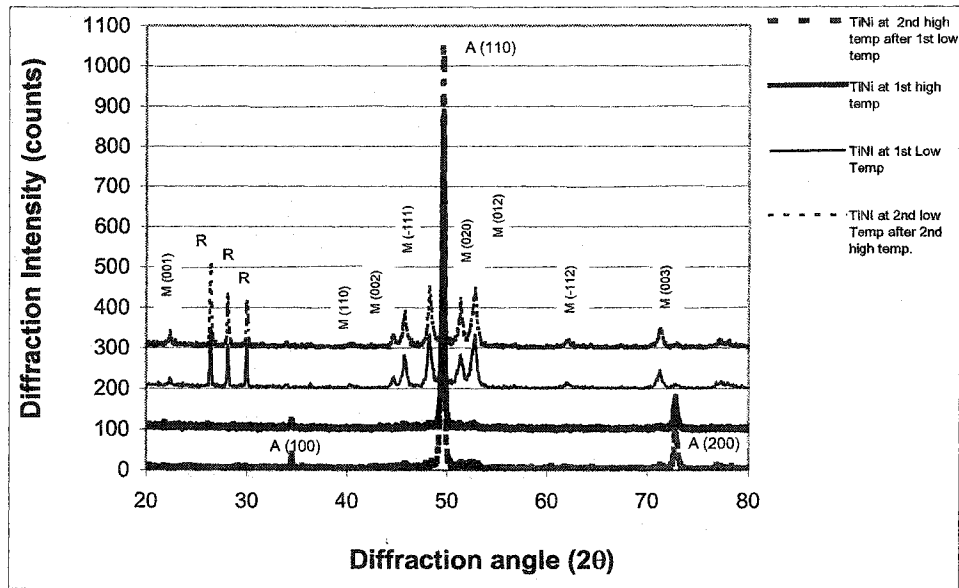


Fig. 5-14. The XRD patterns of TiNi alloy during heating and cooling cycles.

5.2.4. The phase transformations in 52vol%TiN/TiNi composite

The 52vol%TiN/TiNi composite was examined to check if the martensitic phase transformation occurred in the TiNi matrix when the temperature was changed. This analysis was intended to confirm that there was a martensite phase transformation induced by stress during the wear process. Since 52vol%TiN/TiNi has more complicated microstructures, the phase transformations of this composite were studied in comparison with those of the pure TiNi alloy powder. DSC was first employed for the analysis under a scanning speed of 5°C/min. Several 52vol%TiN/TiNi samples of weights from 30 mg to 150 mg were analyzed using DSC. Fig. 5-15 illustrates a typical DSC curve, from a sample with a weight of 65.43 mg. No apparent phase transformation peaks were observed. However, the DSC curve displayed curvature as temperature decreased during the cooling process.

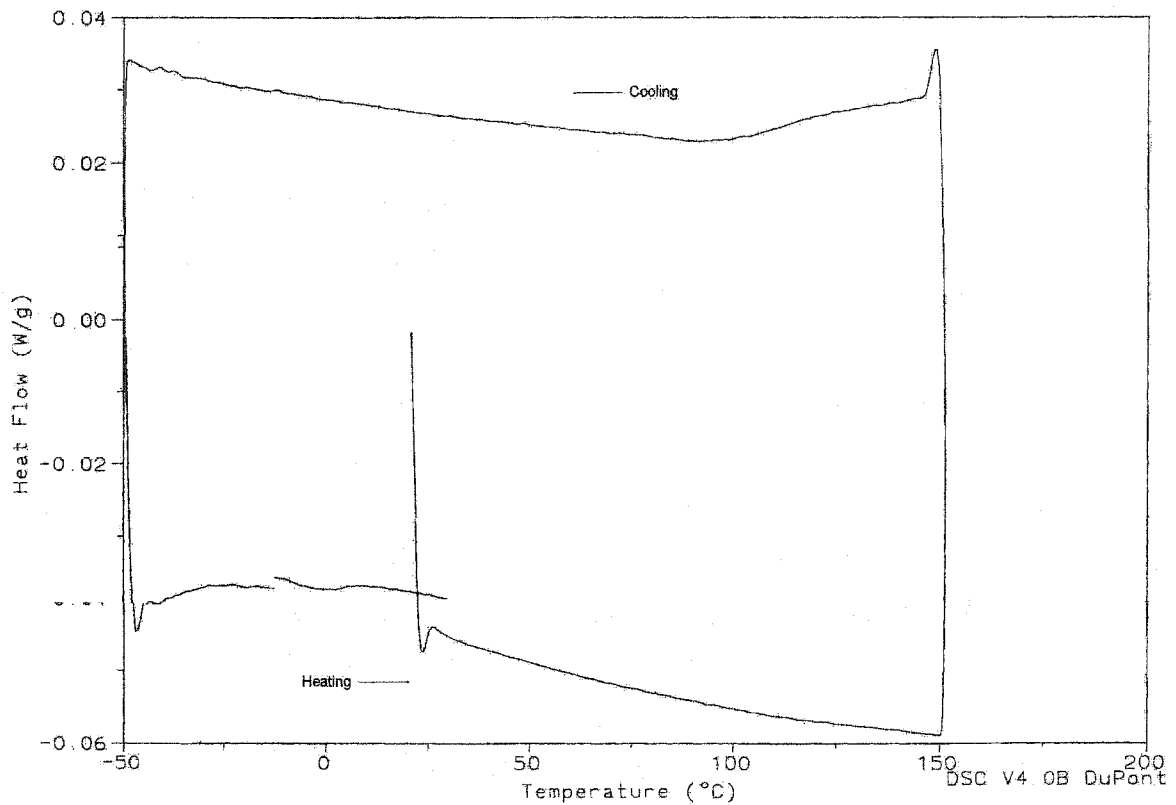


Fig. 5-15. The DSC curve of TiN/TiNi composite.

The absence of transformation peaks could be attributed to the following reasons. First, the sample was a composite with only 48 vol% of the matrix being TiNi alloy, which could reduce the peak height. Second, the matrix had a large composition fluctuation, leading to variation in M_s and/or T_R points at the different regions in the matrix. At a certain temperature, only the region of the matrix whose M_s and/or T_R coincided with the scanning temperature would experience phase transformation, and thus at that particular temperature, only a relatively small volume fraction of the bulk material that experienced phase transformation released or absorbed heat. This heat could be easily shielded by the surrounding areas. When the temperature decreased, the originally concentrated peak was leveled out, and thus only a gradually increased DSC curve was observed, as Fig. 5-15

illustrates. This is especially true, if only R-phase transformation was involved in the 52vol%TiN/TiNi, as demonstrated later. The R phase transformation has an enthalpy smaller than that of martensite phase transformation. The corresponding DSC curve is more likely to have a shape similar to that shown in Fig. 5-15.

XRD was also employed to examine the phase transformations in the 52vol%TiN/TiNi composite. The 52vol%TiN/TiNi sample experienced a heating ~ cooling ~ reheating cycle. The 52vol%TiN/TiNi composite was initially cooled by solid CO₂. The corresponding XRD pattern is shown in Fig. 5-16. Compared with the room temperature XRD pattern of this composite shown in Fig. 3-2 and Fig. 4-8, no other phases were detected in such a solid CO₂ cooled composite except TiN, austenite TiNi and TiNi₃. In order to further decrease the sample's temperature, liquid N₂ was then used to cool the composite sample so that the low temperature phases may exist during the XRD analysis. The corresponding pattern is shown in Fig. 5-17. In Fig. 5-17, some of the R phase peaks in Fig. 5-13 are present. Therefore, the temperature of the sample cooled in solid CO₂ was not low enough during the scanning, as both R-phase and martensitic phase transformations happen at low temperatures. However, the XRD analysis did not detect martensite phase. This happened possibly because the martensitic phase transformation could take place at a lower temperature in the 52vol%TiN/TiNi composite, in which both the material's composition and the second phase particles influenced the R-phase and martensitic phase transformations. The 52vol%TiN/TiNi composite also experienced XRD examination through a heating ~ cooling ~ heating cycle, as illustrated in Fig. 5-18, which shows the reversibility of the R-phase transformation in the TiNi matrix of the composite. Since the R-phase transformation is also

thermally elastic, its existence contributed to the pseudoelasticity in the matrix of the 52vol%TiN/TiNi composite and thus its wear resistance. The XRD analysis confirmed the existence of the reversible R-phase transformation in the TiNi matrix composite.

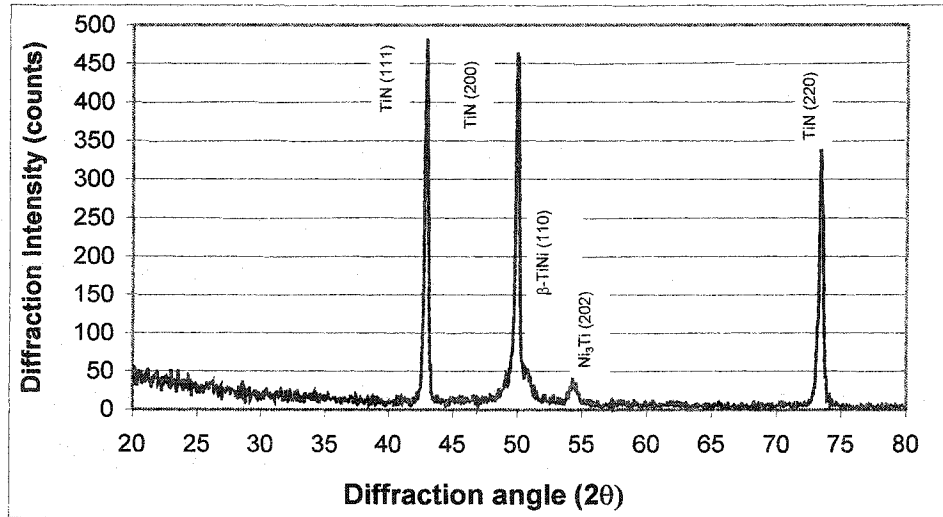


Fig. 5-16. Low temperature XRD pattern of TiN/TiNi cooled with solid CO₂.

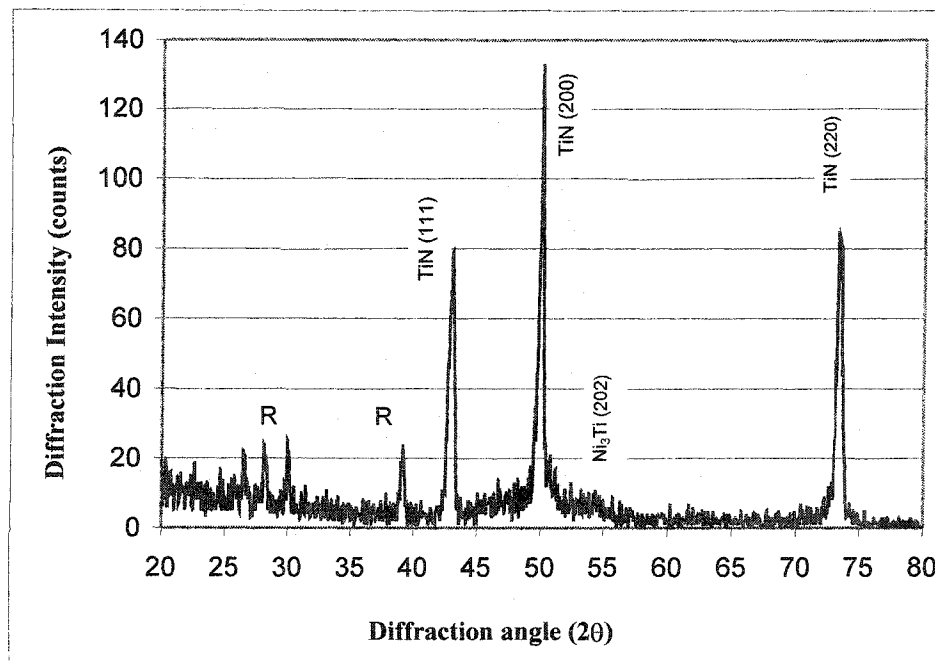


Fig. 5-17. Low temperature XRD pattern of TiN/TiNi cooled with liquid N₂.

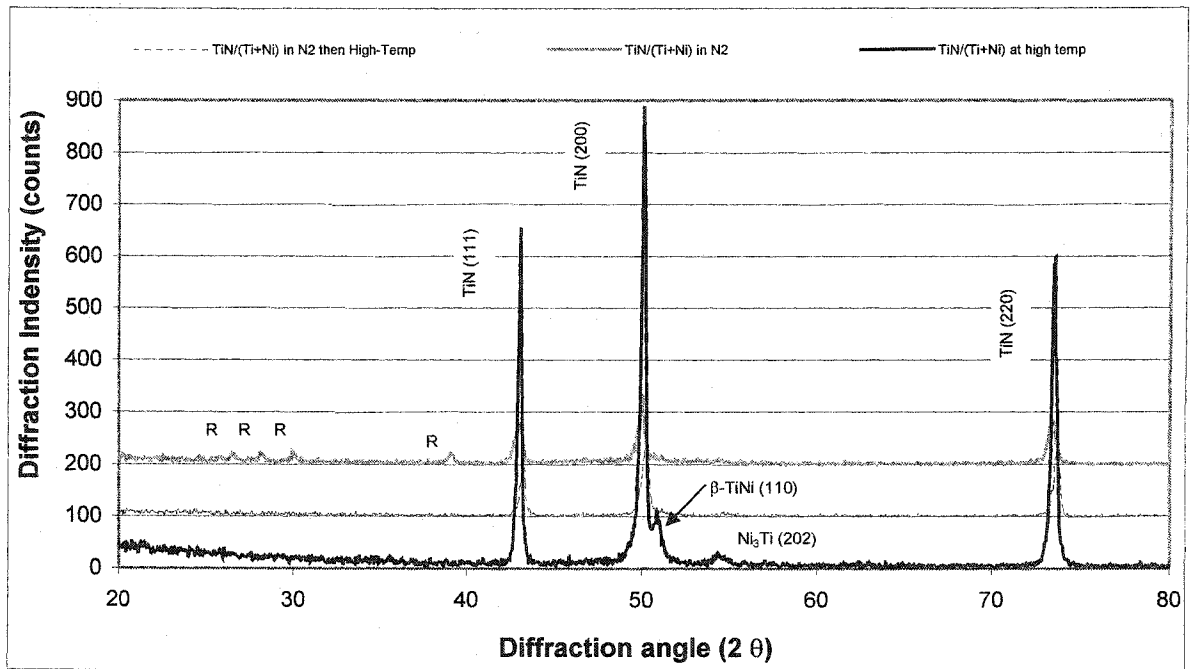


Fig. 5-18. High and low temperature XRD patterns of TiN/TiNi cooled with liquid N₂.

In order to determine whether or not the R-phase transformation was involved during the wearing of TiNi matrix composite, the wear debris of the 52vol%TiN/TiNi composite collected during the sliding wear test was analyzed using TEM. A TEM image of the wear debris is displayed in Fig. 5-19. The composition of an area is shown in Fig. 5-20. In addition to Ti and Ni, there were some other elements detected in the selected area. Cu and C may come from the sample holding grid, while Fe may come from the stainless steel disc, and Co and Si from the lubrication oil or contamination.



Fig. 5-19. The TEM image of the wear debris.

A TEM diffraction pattern of a selected area (SAD) of the 52vol%TiN/TiNi wear debris is shown in Fig. 5-21. The diffraction zone axis was parallel to $[3\bar{1}1]$ of the austenite B_2 phase. Along with the diffraction spots of parent austenite phase, the so-called $1/3$ diffraction spots of the R phase were also present in the diffraction, as indicated by the arrow in Fig. 5-21. The TEM result is consistent with XRD analysis for the 52vol%TiN/TiNi composite. The $B_2 \leftrightarrow R$ phase transformation in the TiNi alloys also contributes to pseudoelasticity. The observed pseudoelasticity of the 52vol%TiN/TiNi may mainly originate from $B_2 \leftrightarrow R$ phase transformation induced by stress during the indentation or wear process, as the martensitic phase transformation was not detected.

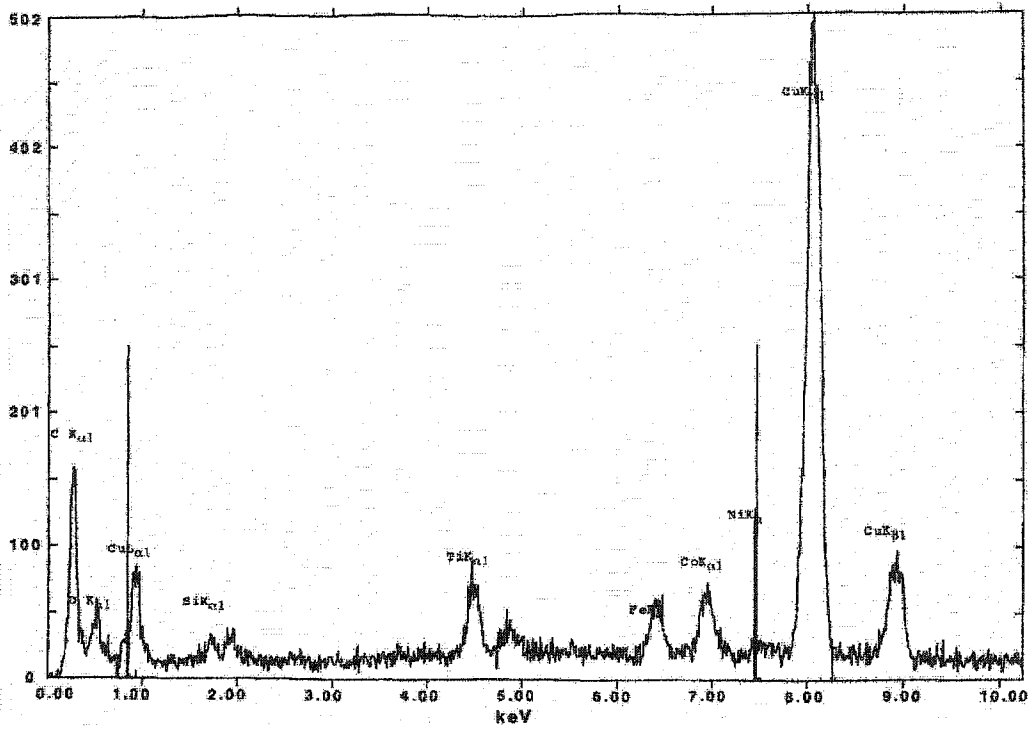


Fig. 5-20. The composition of a selected area for TEM examination.

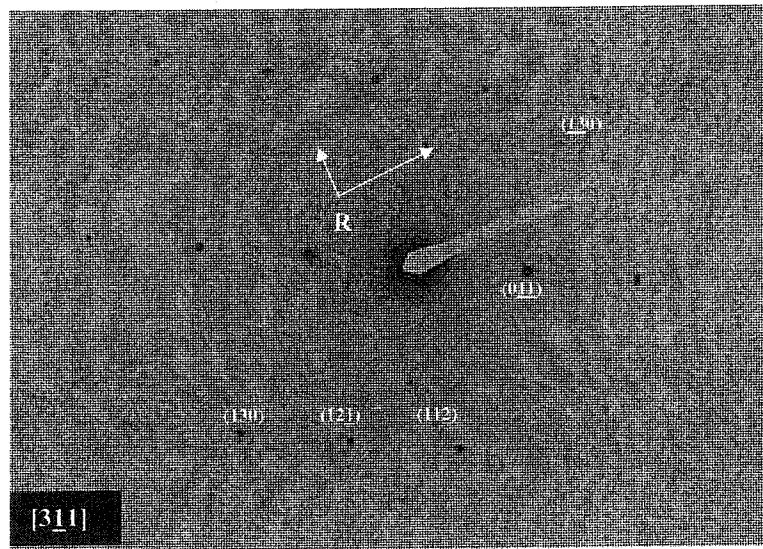


Fig. 5-21. The TEM diffraction pattern of the wear debris.

Several factors can affect the martensitic phase transformation in the TiN/TiNi composite. The composition of the matrix is the major one. It is well known that increasing Ni content reduces the start temperature, M_s point, of the martensitic phase transformation. An increase of 0.1% in the Ni content can decrease the M_s by about 10°C [51]. In the 52vol%TiN/TiNi composite, the average Ni content was 54 at%, a significant deviation from the designed 51 at%. This could largely suppress the martensite phase transformation. Although the fluctuation in the composition of the matrix could allow martensitic phase transformation to occur in some regions, the amount of the martensite phase could be too small to be detected. The TiN particles in the composite would also influence the martensite phase transformation. Since the martensite phase has a larger specific volume, its occurrence results in compressive stress inside the matrix. The presence of a large number of rigid particles would increase the stress and thus decrease the M_s point. Therefore, the martensite phase transformation in the 52vol%TiN/TiNi was further suppressed. When the composite had a low M_s temperature, the martensitic phase transformation would not occur and contribute to the pseudoelasticity of the material during the indentation and wear process at ambient temperature.

During wear, the R-phase transformation took place due to its higher transformation temperature. The defects introduced during the wearing may also influence the phase transformation behavior of the composite to some extent. Fig. 5-22 shows the R-phase and martensitic phase transformation temperatures (R^* and M^*) of a TiNi alloy versus the annealing time for various annealing temperatures after cold drawing [107]. At the same degree of cold work, as annealing time was increased, R^* slowly decreased while

M_s^* quickly increased. This showed that the defects induced by the cold drawing depressed the martensitic phase transformation but promoted the R-phase transformation. During the annealing, these defects were continuously removed, and the internal residual stress also decreased. Therefore, the effects of plastic deformation on the phase transformation temperature decreased with increasing annealing time. Accordingly, the defects in the material can further suppress the martensitic phase transformation but may favor the R phase transformation.

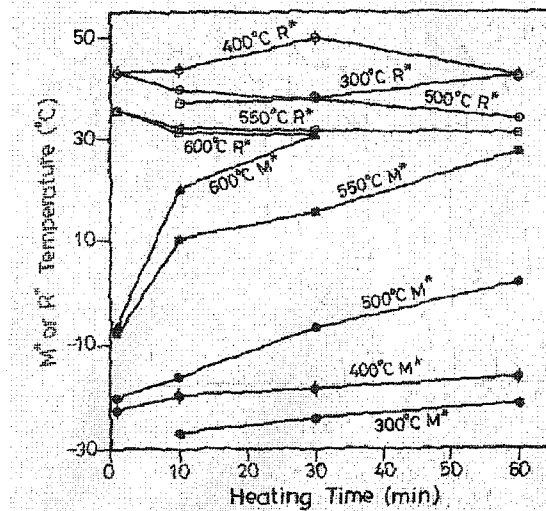


Fig. 5-22. R^* and M^* versus annealing time [Ref. 107].

In our study, the appearance of R-phase transformation could be affected by the production of dislocations in the 52vol%TiN/TiNi composite. During the XRD analysis, due to the heating and cooling of the composite, the TiNi alloy matrix and TiN hard particles expanded and contracted incoherently, producing a stress between these two phases. This stress could be large enough to introduce dislocations, which would be favorable to the R-phase transformation. From the TEM diffraction analysis, since the wear debris experienced large deformation, a large dislocation density was produced inside the composite, and thus the R-

phase transformation was promoted. However, compared to the composition, the defects inside the composite may have only minor effects on its phase transformation.

5. 2. 5. Wear behavior and the phase transformation of the TiNi-based composite

In order to investigate the correlation between the wear performance and phase transformation behavior of the TiNi-based composite, wear tests of the 52vol%TiN/TiNi composite were conducted in a temperature range from -15°C to 140°C . The weight losses of the 52vol%TiN/TiNi samples are shown in Fig. 5-23. It can be seen that the weight loss of 52vol%TiN/TiNi decreased with an increase in temperature at the beginning and then increased after reaching its minimum. The minimum weight loss occurred at about 80°C . The occurrence of minimum wear of 52vol%TiN/TiNi composite resulted from its pseudoelasticity. A similar phenomenon was observed during an erosion test of a pseudoelastic TiNi alloy [108]. It was demonstrated that the minimum erosion loss happened at a temperature about $20^{\circ}\text{C} \sim 30^{\circ}\text{C}$ above the M_s point of the TiNi alloy.

In our studies, the temperature range in which the pseudoelasticity of the 52vol%TiN/TiNi influenced its wear loss was relatively wide. For instance, the minimum wear loss corresponded to 80°C , and the material's pseudoelasticity improved its wear resistance by about 40%, as shown by the straight line *AB* in Fig. 5-23. It was estimated that the wear loss was increased by 5%, 7% and 10% when the temperature changed from 80°C by 10°C , 20°C and 30°C respectively. Therefore, the pseudoelasticity may have a beneficial effect on the wear resistance of the 52vol%TiN/TiNi over a relatively wide range of temperature.

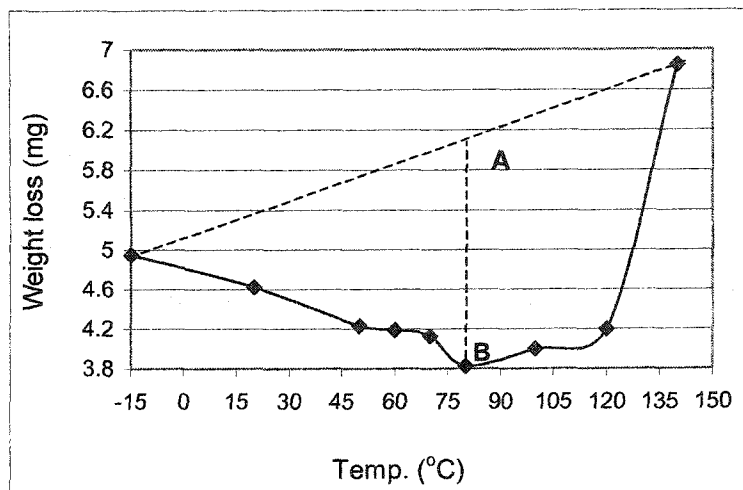


Fig. 5-23. The weight loss versus temperature of TiN/TiNi.

Since only the R-phase transformation was detected in the 52vol%TiN/TiNi, a further improvement in its wear resistance can be expected if martensitic phase transformation is induced. The R-phase and martensitic phase transformations and their effects on the TiNi alloy's mechanical properties have been studied by tensile tests [109]. The loading ~ unloading curves of the TiNi alloy corresponding to its R-phase and martensitic phase transformations are listed in Fig. 5-24 and Fig. 5-25 respectively. During the loading process, the "yielding" due to the R-phase transformation occurred at a stress around 180 MPa. The same "yielding" of the TiNi alloy corresponding to the martensitic phase transformation happened about 580 MPa. Before the "yielding", namely, before the start of the phase transformation, all the deformation of the material is austenite elastic strain, which is totally recoverable. Accordingly, a higher "yielding" strength enables the material to withstand a larger load and thus improves its wear resistance.

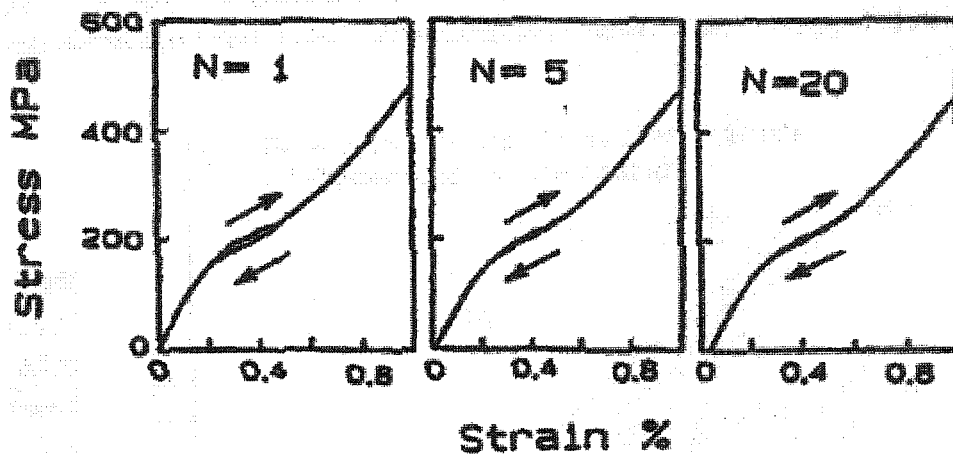


Fig. 5-24. The pseudoelasticity due to R-phase transformation [Ref. 109].

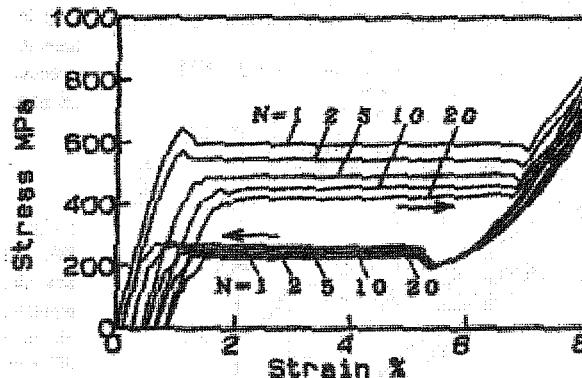


Fig. 5-25. The pseudoelasticity due to martensitic phase transformation [Ref. 109].

The R-phase transformation and martensitic phase transformation also show different effects on the pseudoelasticity of the TiNi alloy. Fig. 5-24 and Fig. 5-25 also illustrate the stress ~ strain curves of the TiNi alloy under loading ~ unloading cycles (up to 20 cycles).

The nonlinear recoverable strain induced by the R-phase transformation in the loading process was up to 1% in Fig. 5-24. The width of the hysteresis loop was very small, and

the difference in stress between the loading and unloading curves was smaller than 20 MPa. The stress ~ strain curves varied little from 1 to 20 loading ~ unloading cycles. However, the stress ~ strain curves due to the martensite phase transformation displayed significant differences. First, the nonlinear recoverable strain amounted to 8%. At the same time, the yield stress and the reverse transformation stress decreased with an increase in the number of loading and unloading cycles. Both the stresses decreased significantly in the early cycles and only slightly afterwards. The residual strain which appeared after unloading increased significantly in the early cycles and only slightly increased after these cycles. These features imply some significant differences in the pseudoelasticity caused by R-phase transformation and martensitic phase transformation. First, the maximum strains that these two phase transformations can accommodate are different. R-phase transformation can only recover a strain of 1%, and martensitic phase transformation can recover a strain up to 8%. Obviously, a larger recoverable strain can produce a greater pseudoelasticity and thus higher wear resistance of the composite. However, the hysteresis in the R-phase transformation is much smaller than that in the martensitic phase transformation. This means that the pseudoelasticity from R-phase transformation may not deteriorate much during wear or under repeated load, compared with that from martensitic phase transformation. On the other hand, since the hysteresis loop represents the energy that the material can absorb due to the reversible phase transformation, the larger hysteresis loop in the stress ~ strain curves of the martensitic phase transformation means that the TiNi alloy can absorb a larger energy if martensitic phase transformation occurs. Actually, due to its martensitic phase transformation, TiNi alloy has a very good damping capability, which is certainly beneficial to its wear

resistance, especially in an impact loading condition. Furthermore, the larger recoverable strain and higher “yield” strength may make martensitic phase transformation contribute more to the pseudoelasticity. It is therefore expected that the composite could be improved if martensitic phase transformation can occur inside the composite by controlling the composition of its matrix.

Another issue associated with the larger hysteresis loop of the martensitic phase transformation is the stabilization of martensite phase. A portion of the absorbed energy is stored in the material to produce heat or lattice defects, which may stabilize the martensite phase and destroy pseudoelasticity by pinning the martensite boundary. Therefore, the TiNi matrix composite may need regular treatment to revive the reversible phase transformation, as the TiNi alloy can be restored to their original thermoelastic state, when the stabilized martensite phase is heated to a temperature above A_s and A_f , and the origins of the stabilization are annealed out.

5. 3. Conclusions

From the above experimental results and discussions, the following conclusions can be drawn.

- (1). The recoverable phase transformation in the current sintered TiNi-based composite has been identified to be mainly the R-phase transformation.
- (2). The martensitic phase transformation could be suppressed in the present composite probably due to the Ni-rich composition and presence of large amount of the TiN second

phase particles, which may constrain the martensitic phase transformation. The large stress due to the external load during the wear process or the thermal cycles in the experiment produces a large dislocation density, which may also suppress the martensitic phase transformation but promote the R-phase transformation.

(3). The R-phase transformation is also thermal elastic and contributes to the pseudoelasticity of the TiN/TiNi. The correlation between the pseudoelasticity and wear behavior of the TiN/TiNi has been investigated. The pseudoelasticity markedly contributes to the high wear resistance of the TiN/TiNi composite.

(4). Since the martensitic phase transformation can accommodate a larger strain and absorb a larger impact energy, a further improvement is expected if the martensitic phase transformation can be induced in the composite.

Chapter 6. Summary and Future Work

The previous chapters have reported the studies on the processing, microstructure, mechanical properties, phase transformation behavior and wear performance of the TiNi-based composite. The completed work has revealed the high potential of the TiNi-based composite in wear applications. In the preliminary studies, the wear resistance of this material has been found to be much higher than that of 304 stainless steel and TiNi alloy and comparable to that of the commercial tribo-material WC/NiCrBSi. The good wear resistance of the composite is mainly attributed to the high hardness of the reinforcing particles and especially the pseudoelasticity of the TiNi matrix. However, neither of these two beneficial factors in the composite has been completely investigated. Accordingly, considerable future work can be conducted to further improve this material for realistic applications in industry. The first section of this chapter summarizes the foregoing work about this composite, while the second discusses the possible improvement of the TiNi-based composite and finalizes the thesis.

6. 1. Summary of the thesis

A new type of wear-resistant material has been developed using a vacuum sintering process. The processing, structures, mechanical properties and wear behavior of this TiNi-based composite have been investigated. Summaries are made as follows.

- (1). The TiNi-based composite having a high fraction of a second phase hard particle (TiC or TiN) was synthesized using a conventional pressing and sintering technique from elemental Ni/Ti powders and the reinforcing particles. The major difficulties in the

sintering of the Ti, Ni and TiC or TiN three constituents were to achieve good composition homogenization and a high bulk density of the material. Due to the presence of the second phase particles, mass diffusion during the sintering was retarded, and thus liquid phase sintering was necessary to accelerate the diffusion process. Among the tested sintering parameters, the best sintering process was 1500°C for 6 hours when the fraction of the second hard particles reached 52 vol%. In the above sintered TiNi-composite, the matrix had a fluctuation in composition, and the sintering process needed to be improved. The major phase in the matrix was TiNi alloy with some TiNi₃ precipitates. Compared with rolled TiNi alloys, the TiNi alloy matrix in the composite possessed a medium pseudoelasticity. Improvement in the matrix's composition would be expected to further increase the pseudoelasticity of the matrix.

(2). Porosity was a typical problem for the sintered TiNi-based composite. During the compaction stage, the interparticle friction of the powders and the high hardness of the second phase particle network could greatly reduce the compaction efficiency, resulting in a high porosity in the green compact. During the sintering stage, the liquid phase sintering and the second phase particle network also produced a high porosity. The porosity in the sintered TiNi-based composite reduced the mechanical properties and wear resistance of the composite.

(3). Under the oil-lubricated condition, TiNi-based composite containing TiC or TiN had a friction coefficient between those of the heat-treated and as-received TiNi alloy specimens. Pseudoelasticity and second phase particles had a considerable effect on the friction coefficient of the TiNi materials under the lubricated condition. The wear resistance of the

TiNi alloy was significantly enhanced by the hard particles. The wear resistance increased with an increase in the volume fraction of the reinforcing particles, and the optimal fraction was around 52 vol%. The wear resistance of 52vol%TiC/TiNi composite was about three orders of magnitude higher than that of the 304 steel; and about one order of magnitude better than that of the TiNi alloy. Compared to high-performance WC/NiCrBSi hardfacing overlay, 52vol%TiC/TiNi composite showed superior performance under low loads. The abrasion of TiNi matrix and the failure of hard particles were the major cause of the wear of the composite.

(4). The porosity in the sintered TiNi-based composite was variable. During the material's processing, lubrication or high load compaction reduced the porosity in the green compact and thus improved the bulk density of the final sintered product. Consequently, the mechanical properties and wear resistance of the material were enhanced. During the wear process, if the load was high enough, the porosity in the worn surface area was reduced. This reduction resulted from the compaction of pores at high load and/or sealing of the pores by the material transferred from the wearing couple disc. The HIP process was an effective way to densify the sintered TiNi-based composite. After the HIP process, most of the pores in the composite were removed. The removal of the porosity greatly increased the hardness and pseudoelasticity of the material and thus its wear resistance.

(5). The pseudoelasticity of the TiNi alloy matrix contributed to the wear resistance of the composite. The combination of the pseudoelastic TiNi and the hard particles had clearly led to a large improvement in the wear resistance compared with the TiNi alloy. The

recoverable phase transformation in the TiNi-based composite had been identified to be the intermediate R-phase transformation. The R-phase transformation was thermal elastic and contributed to the pseudoelasticity of the TiN/TiNi.

6. 2. Possible future work

Since both the matrix and hard second phase particles are critical to the wear performance of the TiNi matrix composite, the possible improvement of this material needs further studies on its matrix and second phase particles in the following aspects.

6. 2. 1. Control of the matrix composition and optimization of the composite processing

The pseudoelasticity of TiNi alloy is dramatically dependent on the alloy's composition. The composition that produces the largest pseudoelasticity is between Ti-50at%Ni and Ti-51at%Ni. EDX has shown that the current composite has a fluctuation in its matrix composition. So the control and homogenization of the matrix's composition needs further study. In the sintering process, the Ti and Ni atoms diffuse into each other to form the TiNi alloy. A study about the sintering of a eutectic Ti-Ni alloy has found that some Ti-Ni intermetallics are always produced during the sintering process of TiNi alloy [110]. Therefore, from the perspective of composition homogenization, vacuum casting may be a better process as the Ti and Ni atoms can completely diffuse into each other. However, the homogenization of the second phase particles may be more difficult due to gravity segregation. In this case, agitation must be introduced in the casting process to distribute the second phase particles uniformly. Therefore, the vacuum stir casting becomes an alternative method for the processing of the TiNi matrix composite, like that used to

fabricate aluminum matrix composites [111-114]. In addition to the composition homogenization of the composite, vacuum stir casting offers another benefit: high density of the cast composite.

6. 2. 2. Heat treatment

During the sintering process, various Ti-Ni intermetallics, such as $Ti_{11}Ni_{14}$, Ti_2Ni and $TiNi_3$, can precipitate from the austenite β phase.

Precipitate strengthening is the first effect of these Ti-Ni intermetallics on the TiNi alloy. The wear behavior of the Ti-50.3at%Ni and Ti-51.5at%Ni alloys aged at 500°C for different times were studied [115], and the wear test results are shown in Fig. 6-1. The mechanism found responsible for the wear resistance difference is that some $Ti_{11}Ni_{14}$ precipitated from the Ti-51.5at%Ni alloy austenite phase. When the TiNi alloy was aged for 1.5 hours, the $Ti_{11}Ni_{14}$ precipitates were fine and coherent with the matrix and thus strengthened the matrix. When aged for 24.5 hours, the precipitates increased in size and became incoherent with the matrix. This caused deterioration of the strength of the over aged Ti-51.5at% TiNi alloy and thus reduced the wear resistance of the TiNi alloy.

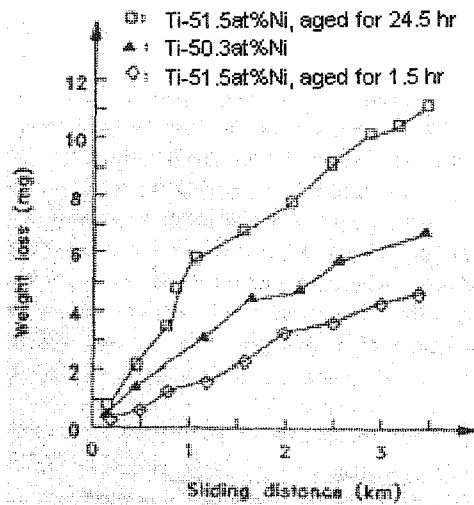


Fig. 6-1. The wear losses of the aged TiNi alloys [Ref. 115].

This finding of the strengthening of the TiNi alloy by $Ti_{11}Ni_{14}$ precipitation could be introduced to the TiNi-based composite even though the second phase hard particles have functioned to strengthen the matrix. Since the precipitates are produced from the TiNi alloy itself, they can be controlled to be finer and more coherent with the matrix than the artificially added hard particles. The strengthening of the TiNi matrix can markedly enhance the overall wear resistance of TiNi-based composite. This has been demonstrated by recent work on TiC/TiNi composite with additional nano TiN particles [116].

The second effect of the precipitates is that they can strongly affect the TiNi alloy's phase transformation behavior. The effect of Ti_3Ni_4 precipitates on the R-phase transformation has been studied [117-119]. The Ti_3Ni_4 precipitates have two large influences on the TiNi alloy. First they lower the proportion of Ni in the matrix. This decrease in the matrix Ni concentration raises the martensitic phase transformation temperature. Second, the Ti_3Ni_4 precipitates introduce a stress field in the matrix, which can affect the R-phase and

martensitic phase transformations. This finding about the effects of the precipitate size on the reversible phase transformation temperature could be applied to adjust the M_s and T_R points of the TiNi matrix composite.

6.2.3. Amorphization

As pseudoelasticity is a very important beneficial factor to the wear performance of the TiNi-based composite, any technique that can enhance the pseudoelasticity is expected to improve the wear resistance of this composite. Recent studies have found that neutron irradiation is another way to effectively increase the pseudoelasticity of the TiNi alloy [120-122]. Ti-50.0at%Ni, Ti-50.5at%Ni and Ti-51.0at%Ni alloys were exposed to neutron irradiation at 1.2×10^{23} n/m² and then a strain up to 5%. After the stress was removed, all the 5% strain was recovered. The recoverable strain was closely dependent on the neutron irradiation intensity. Some stress and strain curves in loading ~ unloading cycles are shown in Fig. 6-2 [120]. They indicate that the recoverable strain was proportional to the neutron irradiation exposure, and this effect was independent on the TiNi alloy's composition. All three compositions of TiNi exhibited the same recovery. Another advantage of this strain recovery was that the strain-stress curve was almost linear without a large strain hysteresis. This means that during the strain recovery, very little energy is stored inside the TiNi alloy, and thus the alloy structure can be maintained during many stress-strain cycles. Thus, such an irradiated material is expected to have a longer service lifetime.

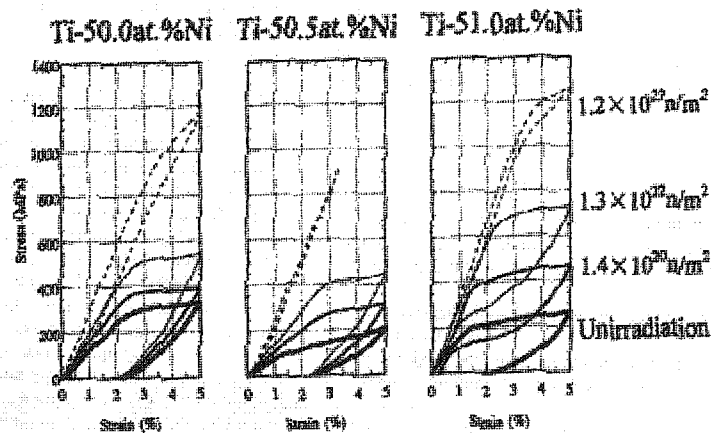


Fig. 6-2. The stress-strain curves under different irradiation intensities [Ref. 120].

The mechanism for this improvement of the pseudoelasticity was found to be the amorphization of the structure. The amorphous TiNi alloy is highly elastic. All the deformation that the above TiNi alloys experienced after the irradiation is elastic with little hysteresis. This pseudoelasticity has a different cause from the previously described one, for which the reversible austenite and martensite phase transformation is responsible. However, despite this difference, the pseudoelasticity caused by amorphization may also improve the wear resistance of a material. A correlation between the crystalline and amorphous TiNi alloys is that the amorphous TiNi alloy can be transformed into a crystalline alloy upon heating to a certain high temperature. All these findings could provide a path for the further improvement of the TiNi wear-resistant composite.

Following the above findings, it is logical and interesting to treat the TiNi-based composite by neutron irradiation. After high intensity neutron irradiation, if the TiNi matrix in the surface of the composite were transformed into an amorphous structure, and

the composite worked in a low load condition, the large elasticity of the amorphous matrix would be expected to sustain the external load. When the load reaches a certain level, where working can heat the composite to a high temperature and activate the amorphous to crystal structure transformation, the pseudoelasticity induced by martensitic phase transformation in the crystal matrix may be expected to take the place of the elasticity of the amorphous TiNi matrix in service. Thus this combination of these two mechanisms may produce a higher wear resistance of the TiNi-based composite. Some unknown points are present in the case of the sintered TiNi-composite. The first is the amorphization of the TiNi matrix in the composite. Even with some findings of the successful amorphization of the pure TiNi alloys, it still needs to be confirmed by experiment that the amorphization will happen in the TiNi-based composite, and compared with that in the pure TiNi alloy case, the amorphization must have its own characteristics if it can really occur. The second factor that needs further study is the design of matrix's composition so that the amorphization of the matrix can occur, and the pseudoelasticity induced by the martensitic phase transformation can be maintained at a high temperature where the crystal structure can be transformed from the amorphous state. Some other studies [123-125] have found that pure TiNi alloy, modified by adding a small amount of ternary element such as Au, Pd, Zr and Cr can keep the reversible martensitic phase transformation and the corresponding pseudoelasticity to temperatures as high as 610°C. This offers a possibility for the development of the above-mentioned amorphous TiNi-based wear-resistant composite. Thirdly, whether or not the amorphization is beneficial to TiNi matrix composite also needs further study, even if the first two issues are satisfied. In the case of a composite, the secondary hard particles and

their interfaces with the composite matrix may be influenced by the matrix's amorphization in the composite, and thus the final property of the amorphous matrix composite is still unknown.

6. 2. 4. Investigation of the interface between the matrix and second phase particles

TiC and TiN hard particles were used in the current studies. However, other hard particles such as SiC, Al₂O₃, and B₄C might be suitable or even better for the TiNi matrix composite. Whether or not the combination of hard particles and matrix is appropriate is largely dependent on the interface between the TiNi matrix and the hard particles. TiN and TiC were chosen as the reinforcing particles under an assumption that these two particles may have a stronger interface with the TiNi matrix than other particles as they both contain Ti atoms. However, this hypothesis needs further examination. Thus, a series of interface investigation and the corresponding wear tests are needed to obtain a deeper understanding of TiNi matrix composite.

Publications:

- [1]. Development of a new wear-resistant material: TiC/TiNi Composite; H. Z. Ye, R. Liu, D. Y. Li, and R. Eadie; Scripta Materialia, Volume 41, No. 10, pp 1039-1045, 1999.
- [2]. Wear and friction of a new wear-resistant material: TiNi-based composites; H. Z. Ye, R. Liu, D. Y. Li, and R. L. Eadie; Composites Science and Technology, Volume 61/7, pp 987-994, 2001.
- [3]. Improvement of wear behavior of TiNi-based composites by hot isostatic pressing; H. Z. Ye, D. Y. Li, and R. L. Eadie; Mater. Sci. & Eng. A, (in press).
- [4]. Influences of porosity on mechanical and wear performance of pseudoelastic TiNi-matrix composites; H. Z. Ye, D. Y. Li, and R. Eadie; Journal of Materials Engineering and Performance, pp 178-185, Volume 10, No.2 April 2001.

References:

- [1]. Glossary of terms and definition in the field of friction, wear and lubrication-tribology; Research group on wear of engineering materials; OECD publications, Paris, 1969.
- [2]. Economics of wear and corrosion in the mining industry; V.S. Sastri, M. Elboujdaini; CIM bulletin, Volume 90, July, 1997, pp63-65.
- [3]. Friction, wear, lubrication: a textbook in tribology; Kenneth C Ludema; CRC Press, 1996.
- [4]. Surface and engineering, for corrosion and wear resistance; J. R. Davis; ASM International, 2001.

- [5]. Wear characteristics of metals; Eyre, T. S., Tribology International; 10, (1976), pp. 203-212.
- [6]. Tribophysics; Nam P. Suh; Massachusetts Institute of Technology, Prentice-hall, Inc., Englewood Cliffs, New Jersey 07632, 1986.
- [7]. Friction, lubrication and wear technology; Volume 18, ASM Handbook; ASM International, 1992.
- [8]. A study of abrasive wear under three-body conditions; Rabinowicz, E., L. A. Dunn, P. G. Russell; Wear, Volume 4, 1961, pp345.
- [9]. Friction and wear of materials, 2nd edition; Ernest Rabinowicz; A Wiley-Interscience Publication, 1995.
- [10]. Friction, lubrication and wear technology; Volume 18, ASM Handbook; ASM International, 1992, pp236.
- [11]. Electronic structure and properties of transition metal compounds: introduction to the theory; Isaac B. Bersuker; New York, Wiley, C1996.
- [12]. Contact and rubbing of flat surfaces; Archard, J. F.; J. Appl. Phys., 24 (1953), 981.
- [13]. Subsurface stress field of a dry line contact; Mihailidis, A., Bakolas, V., Drivakos, N.; Wear, Volume 249 n 7 July 2001, pp 546-556.
- [14]. Friction, lubrication and wear technology; Volume 18, ASM Handbook; ASM International, 1992, p244.
- [15]. Materials science and engineering: an Introduction, 4th Edition; William D. Callister, Jr.; John Wiley & Sons Inc. 1997.
- [16]. Fatigue and fracture; ASM Handbook, Volume 19; 1996, pp316.

- [17]. Surface and engineering, for corrosion and wear resistance; edited by J. R. Davis; ASM International, 2001, pp57.
- [18]. Friction, lubrication and wear technology; Volume 18, ASM Handbook; ASM International, 1992, pp699.
- [19]. Cast irons, ASM specialty handbook; edited by J. R. Davis; 1996, pp244.
- [20]. Friction, lubrication and wear technology; Volume 18, ASM Handbook; ASM International, 1992, pp71, 75.
- [21]. Metals handbook, Volume 1, 10th edition, Properties and selection: irons, steels, and high-performance alloys; ASM International, 1990.
- [22]. Friction, lubrication and wear technology; Volume 18, ASM Handbook; ASM International, 1992, pp698.
- [23]. Friction, lubrication and wear technology; Volume 18, ASM Handbook; ASM International, 1992, pp697.
- [24]. Friction, lubrication and wear technology; Volume 18, ASM Handbook; ASM International, 1992, pp698.
- [25]. Surface wear, analysis, treatment, and prevention; R. Chattopadhyay; ASM International, 2001.
- [26]. Friction, lubrication and wear technology; Volume 18, ASM Handbook; ASM International, 1992, pp760.
- [27]. Surface wear, analysis, treatment, and prevention; R. Chattopadhyay; ASM International, 2001, pp221.
- [28]. Surface wear, analysis, treatment, and prevention; R. Chattopadhyay; ASM International, 2001, pp210.

- [29]. Metals handbook, Volume 1, 10th edition, Properties and selection: irons, steels, and high-performance alloys; ASM International, 1990, pp97.
- [30]. Friction, lubrication and wear technology; Volume 18, ASM Handbook; ASM International, 1992, pp761.
- [31]. On the importance of work hardening in the design of wear-resistant materials; A. Ball; Wear, 91 (1983) 201.
- [32]. Cavitation erosion of NiTi explosively welded to steel; R. H. Richman, A. S. Rao, D. Kung; Wear 181-183 (1995) 80.
- [33]. A new type of wear-resistant material: pseudo-elastic TiNi alloy; D. Y. Li; Wear, 221 (1998) 116.
- [34]. Wear-resistance of TiNi intermetallics with TiN coating; H. C. Lin, H. M. Liao, J. L. He, K. M. Lin, K. C. Chen; Surface and Coatings Technology, 92 (1997) 178.
- [35]. Explosive welding of a near equiatomic nickel-titanium alloy to low-carbon steel; C. A. Zimmerly, T. Inal, R. H. Richman; Mater. Sci. and Eng. A188 (1994) 251.
- [36]. Cavitation erosion of two NiTi alloys; R. H. Richman, A. S. Rao, D. E. Hodgson; Wear 157 (1992) 401.
- [37]. Wear resistance of Ni--Ti alloy; J. Jin, H. Wang; Acta Metall. Sinica 24 (1988) A66.
- [38]. Dry sliding wear mechanisms in a Ti₅₀Ni₄₇Fe₃ intermetallic alloy; J. Singh, A. T. Alpas; Wear, 302 (1995).
- [39]. Water jet erosion behavior of Ti-Ni binary alloys; Y. Shida, Y. Sugimoto; Wear, 146 (1991) 219.
- [40]. Wear behavior of a TiNi alloy; Y. N. Liang, S. Z. Li, Y. B. Jin, W. Jin, S. Li; Wear 198 (1996) 236.

- [41]. Metals handbook, Volume 2, 10th edition, Properties and selection, nonferrous alloys and special-purpose materials; ASM international, 1990, pp 899.
- [42]. Wear characteristics of TiNi shape memory alloys; H. C. Lin, J. L. He, K. C. Chen, H. M. Liao, K. M. Lin; Metallurgical and Materials Transactions A (USA), Volume 28A, no. 9, pp. 1871-1877A, Sept. 1997.
- [43]. Woldman's engineering alloys; ASM International, 9th edition, 2000.
- [44]. Alloy digest source book: stainless steels; Edited by J. R. Davis; ASM International, 2000.
- [45]. Understanding the martensitic transformations in TiNi-based alloys by elastic constants measurement; X. Ren, N. Miura, K. Taniwaki, K. Otsuka, T. Suzuki, K. Tanaka, Yu. I. Chumlyakov, M. Asai; Materials Science and Engineering A 273-275 (1999) 190 - 194.
- [46]. Wire drawing conducted in the R phase of TiNi shape memory alloys; S. K. Wu, H. C. Lin, Y. C. Yen, J. C. Chen; Materials Letters 46 (2000) 175-180.
- [47]. Premartensitic phase of $Ti_{50}Ni_{47}Fe_3$; M. B. Salamon, M. E. Meichle, C. M. Wayman; Physical Review B, Volume 31, Number 11, 1985, pp7306 - 7315.
- [48]. X-ray investigation of the premartensitic phase in $Ni_{46.8}Ti_{50}Fe_{3.2}$; S. M. Shapiro, Y. Fujii, and Y. Yamda; Physical Review B, Volume 30, Number 8, 1984, pp4314 - 4321.
- [49]. Experimental studies on tribological properties of pseudoelastic TiNi alloy with comparison to stainless steel 304; R. Liu and D.Y. Li; Metall. Mater. Trans. A, 31A (2000) 2773.
- [50]. Tribological behavior of a Titanium--Nickel alloy; P. Clayton; Wear 162-164 (1993) 202.

- [51]. Effect of Ni content and aging on transformation temperature and hysteresis in TiNi alloys; Z. He; Transactions of Metal Heat Treatment (China) (China), Volume 20, Suppl., pp. 424-428, Oct. 1999.
- [52]. The effect of alloying by 3d, 4d, 5d transition metal elements of martensite transformation temperature in compound TiNi; Kolomytsev; VI, Scr. Metall. Mater., Volume 31, no. 10, pp. 1415-1420, 15 Nov. 1994.
- [53]. Two-step martensitic transformations in TiNi (10% Cu) shape memory alloys; Moberly, W. J., Duerig, T. W., Proft, J. L., Sinclair, R.; Materials Research Society (USA), pp. 55-60, 1992.
- [54]. Phase transformation in ternary TiNiX alloys; K.R. Edmonds, C. M. Hwang; Scripta Metallurgica, Volume 20, PP733-737, 1986.
- [55]. Shape memory and mechanical properties in powder metallurgy TiNi alloys; Miura, S; Kato, H; Koyari, T; Isonishi, K; Tokizane, M; Mechanical Behavior of Materials, VI. Volume 3, Kyoto, Japan, 29 July-2 Aug. 1991, Pergamon Press plc (UK), pp. 223-230, 1992.
- [56]. Stress-strain behavior and shape memory effect in powder metallurgy TiNi alloys; Kato, H; Koyari, T; Tokizane, M; Miura, S; Acta Metallurgica et Materialia (UK), Volume 42, no. 4, pp. 1351-1358, Apr. 1994.
- [57]. Processing of TiNi from elemental powders by hot isostatic pressing; McNeese, MD; Lagoudas, DC; Pollock, TC; Materials Science and Engineering A (Switzerland), Volume 280, no. 2, pp. 334-348, 31 Mar. 2000.
- [58]. U.S. Patent, 3, 012, 882.
- [59]. U.S. Patent, 3, 450, 372.

- [60]. Nitinol heat engines for low-grade thermal energy conversion; W. S. Ginell, Jr. J. L. McNichols, J. S. Cory; *Mech. Eng.* 101, (5), 1979, 28.
- [61]. Characteristic of the human heart, Design requirement for replacement; P. N. Sawyer; *Trans. Am. Soc. Artif. Int. Organs*, 17, 1971, 470.
- [62]. Shape memory alloys: medical applications; Sekiguchi, Y; Dohi, T; Funakubo, H, J.; *Met. Finish. Soc. Jpn.*, Volume 35, no. 8, pp. 383-391, Aug. 1984.
- [63]. Control of fatigue crack propagation in the TiNi shape memory fiber reinforced smart composite; Shimamoto, A, Furuya, Y, Abe, H, A.A. Balkema; *Experimental Mechanics: Advances in Design, Testing and Analysis. II (Netherlands)*, pp. 1085-1090, Aug. 1998.
- [64]. Enhancement of mechanical properties of TiNi fiber composites by shape memory effect; Furuya, Y, Shimamoto, A, Taya, M; *Minerals, Metals and Materials Society/AIME (USA)*, pp. 65-74, 1997.
- [65]. The effects of thermal cycling on the reverse martensitic transformation of prestrained TiNi alloy fibers embedded in Al matrix; Cui, L. S., Zheng, Y. J., Zhu, D., Yang, D. Z.; *Journal of Materials Science Letters (USA)*, Volume 19, no. 3, pp. 1115-1117, 1 July 2000.
- [66]. Thermomechanical behavior of TiNi shape memory alloy fiber reinforced 6061 aluminum matrix composite; Hamada, K, Taya, M, Inoue, K, Lee, J. H., Mizuuchi, K.; *Metallurgical and Materials Transactions A (USA)*, Volume 29A, no. 3A, pp. 1127-1135A, Mar. 1998.

- [67]. Fabrication and characterization of Al/TiNi shape memory composites; Han, C, Choi, I, Cho, K, Park, I; Metals and Materials (South Korea), Volume 6, no. 2, pp. 169-175, Apr. 2000.
- [68]. The constrained phase transformation of prestrained TiNi fibers embedded in metal matrix smart composite; Zheng, Y, Cui, L, Zhu, D, Yang, D, Materials Letters (Netherlands), Volume 43, no. 3, pp. 91-96, Apr. 2000.
- [69]. Structure, phase composition and character of fracture of sintered TiC-NiTi composite materials; T. M. Poletika, S. N. Kulkov, V. E. Panin; Poroshkovaya Metallurgiya, No 7 (247), PP 54-59, July, 1983.
- [70]. Influence of the phase composition of TiC-NiTi composite materials on the character of failure and mechanical properties; S. N. Kulkov, T. M. Poletika; Poroshkovaya Metallurgiya, No. 8 (260), PP 88-92, August, 1984.
- [71]. Effects on composite composition and structure from compound loading during hot pressing; S. N. Kulkov, A.G. Melnikov; Poroshkovaya Metallurgiya, No. 5 (341), PP 1-4, 1991.
- [72]. Martensitic transformation of NiTi and NiTi-TiC composites; D. Mari, D.C. Dunand; Journal De Physique, Volume 5, December, 1995.
- [73]. NiTi and NiTi-TiC composites: part 1. Transformation and thermal cycling behavior; D. Mari and D.C. Dunand; Metallurgical and Materials Transactions A, Volume 26A, November 1995.
- [74]. NiTi and NiTi-TiC composites: Part 2. Compressive mechanical properties; K. L. Fukami-Ushiro, D. Mari, D. C. Dunand; Metallurgical and Materials Transactions A, Volume 27A, January 1996.

- [75]. NiTi and NiTi-TiC composites: Part 3. Shape-memory recovery; K. L. Fukami-Ushiro, D. C. Dunand; Metallurgical and Materials Transactions A, Volume 27A, January 1996.
- [76]. NiTi and NiTi-TiC composites: Part 4. Neutron diffraction study of twinning and shape-memory recover; D. C. Dunand, D. Mari; Metallurgical and Materials Transactions A, Volume 27A, September 1996.
- [77]. Friction, lubrication and wear technology; Volume 18, ASM Handbook; ASM International, 1992, pp801.
- [78]. Friction, in tribology, friction and wear of engineering materials; I.M. Hutchings; Bodmin, Cornwall, 1992, pp. 22-35.
- [79]. Indentation behavior and wear resistance of pseudoelastic Ti-Ni alloy; R. Liu, D. Y. Li; Materials Science and Technology, 16 (2000), 328.
- [80]. The effect of particulate reinforcement on the sliding wear behavior of aluminum matrix composites; Roy, M., Venkataraman, B., Bhanuprasad, V. V., Mahajan, Y. R., Sundararajan, G.; Metallurgical Transactions A (USA), Volume 23A, no. 10, pp. 2833-2847, Oct. 1992.
- [81]. Density, Ultimate tensile strength and microstructure of a squeeze cast Al-11.8Si-3Mg-5Graphite composite; P. Balan, R. M. Pillai, K. G. Satyanrayana and B.C. Pai; Canadian Metallurgical Quarterly, Volume 33, No. 3, pp255-258, 1994.
- [82]. Performance of an Al/Si/Graphite particle composite piston in a diesel engine. (retroactive coverage); Krishnan, B. P., Raman, N., Narayanaswamy, K., Rohatgi, P. K.; Wear, Volume 60, no. 1, pp. 205-215, Apr. 1980.

- [83]. Powder metallurgy science; German, R. M.; Princeton, N.J., Metal Powder Industries Federation, C1984.
- [84]. Shape memory characteristics in powder metallurgy TiNi alloy; Kato, H., Koyari, T., Miura, S., Isonishi, K., Tokizane, M.; Scripta Metallurgica et Materialia; Volume 24, no. 12, pp. 2335-2340, Dec. 1990.
- [85]. Combustion synthesis of TiNi intermetallic compounds: part 1. Determination of heat of fusion of TiNi and heat capacity of liquid TiNi; H. C. Yi, J. J. Moore; Journal of Materials Science 24, (1989) 3449-3455.
- [86]. The formation of products of a self-propagating high temperature synthesis in Titanium--Nickel and Titanium--Cobalt alloys; V. I. Itin, A. D. Bratchikov, V. N. Doronin and G. A. Pribytkov; Izv. V.U.Z. Fiz., Volume 24, no. 12, pp. 75-78, 1981.
- [87]. Variations in wear resistance of pseudoelastic tribo-alloy as a function of pseudoelasticity and hardness; D.Y. Li and X. Ma ; J. Mater. Sci. & Tech., 17 (2000) 45.
- [88]. 55-Nitinol: the alloy with a memory--its physical metallurgy, properties and applications; C.M. Jackson, H. J. Wagner, R. J. Wasilewski; NASA-SP 5110, 1972, pp23-74.
- [89]. Structure property relationships in porous sintered steels; P. Beiss, M. Dalgic; Materials Chemistry and Physics 67 (2001) 37-42.
- [90]. Relationship between pore structure and fatigue behavior in sintered Fe-Cu-C; K. D. Christian, R. M. German; Int. J. Powder Metall., 31 (1995) 51-61.
- [91]. Cyclic deformation behavior of sintered pure and alloyed Iron; S. Klumpp, D. Eifler, O. Vohringer, E. Macherauch; Adv. Powder Metall. & Particulate Mat. 6 (1992), 347-361.

- [92]. Fatigue crack initiation in a porous steel; J. Holmes, R. A. Queeney; Powder Met., Volume 28, pp231-235, 1985.
- [93]. Effect of density on tensile strength, fracture toughness, and fatigue crack propagation behavior of sintered steel; N. A. Fleck, R. A. Smith; Powder Met., Volume 24, No. 3, pp121-125, 1981.
- [94]. The elastic moduli of heterogeneous materials; Zvi Hashin; J. Appl. Mechanics, Volume 29, pp143, 1962.
- [95]. Microstructure-property relationships of a high strength sintered steel; H. Danninger, D. Spoljaric, B. Weiss, J. Preitfellner; P-M Steels Advances in Powder Metallurgy. Volume 5. Publ by Metal Powder Industries Federation, Princeton, NJ, USA. pp 227-237.
- [96]. TiNi shape memory alloys prepared by normal sintering; Ning Zhang, P. Babayan Khosrovabadi, J. H. Lindenhovius and B. H. Kolster; Materials Science and Engineering, A150 (1992), 263-270.
- [97]. Fundamental aspects of hot isostatic pressing: an overview; H. V. Atkinson and S. Davies; Metallurgical and Materials Transactions A, Volume 31A, December 2000, pp 2981.
- [98]. Practical applications of hot isostatic pressing diagrams: four case studies; E. Arzt, M. F. Ashby, and K. E. Easterling; Metall. Trans. A, 1983, Volume 14A, pp. 211-221.
- [99]. Hot isostatic pressing diagrams: new developments; A. S. Helle, K. E. Easterling, and M. F. Ashby; Acta Metall., 1985, Volume 33, pp. 2163-2174.
- [100]. Crystal structure and a unique martensitic transition of TiNi; Wang, F. E., Buehler, W. J., Pickart, S. J.; J. Appl. Phys., V 36, No 10, Oct. 1965, pp3232-3239.

- [101]. Recent development of TiNi-based shape memory alloys in Taiwan; S. K. Wu, H. C. Lin; *Materials Chemistry and Physics* 64 (2000) 81-92.
- [102]. Crystal structure and internal defects of equiatomic TiNi martensite; Otsuka, K., Sawamura, T., Shimizu, K.; *Physica Status Solidi, A*, 16 MAY 1971, 5, 2, 457-470.
- [103]. Mechanism of the TiNi martensitic transformation and the crystal structure of TiNi-II and TiNi-III phases; Frederick E. Wang, Stanley J. Pickart, and Harvey A. Alperin; *J. Appl. Phys.*, Volume 43, No. 1, January 1972, pp97-pp111.
- [104]. Effects of hot rolling on the martensitic transformation of an equiatomic Ti-Ni alloy; H. C. Lin and S. K. Wu; *Materials Science and Engineering*, A158, (1992) 87-71.
- [105]. Transformation behavior of a $Ti_{50}Ni_{47}Fe_3$ alloy, I. Pre-martensitic phenomena and the incommensurate phase; C. M. Hwang, M. Meichle, M. B. Salamon and C.M. Wayman; *Philosophical Magazine A*, 1983, Volume 47, No. 1, 9-30.
- [106]. Transformation behavior of a $Ti_{50}Ni_{47}Fe_3$ alloy, II. Subsequent pre-martensitic behavior and the commensurate phase; C. M. Hwang, M. Meichle, M. B. Salamon and C.M. Wayman; *Philosophical Magazine A*, 1983, Volume 47, No. 1, 31-62.
- [107]. A study on the wire drawing of TiNi shape memory alloys; S. K. Wu, H.C. Lin, Y. C. Yen; *Materials Science and Engineering A215*, (1996) 113-119.
- [108]. Variation in erosion resistance of pseudoelastic TiNi alloy with respect to temperature; T. Zhang and D.Y. Li; *Mater. Science and Engineering. A*, 2000, accepted.
- [109]. Thermomechanical properties due to martensitic and R-phase transformations of TiNi shape memory alloy subjected to cyclic loading; H. Tobushi, S. Yamada, T. Hachisuka, A. Ikai, K. Tanaka; *Smart Materials and Structures (UK)*, Volume 5, no. 6, pp. 788-795, Dec. 1996.

- [110]. Structure formation in a Titanium-Nickel alloy of eutectic composition; V. P. Chepeleva, V. G. Delevi, E. D. Kizikov, L. V. Trunevich, and E. S. Cherepenina; *Sov. Powder Metall. Met. Ceram.*, Volume 23, no. 1, pp. 63-67, Jan. 1984.
- [111]. Tribological and corrosion behavior of aluminum alloy - silicon carbide metal matrix composites; Srinivasan, P. B., Rajiv, E. P.; *Bulletin of Electrochemistry (India)*, Volume 17, no. 5, pp. 197-202, May 2001.
- [112]. In situ stir cast Al-TiB₂ composite: processing and mechanical properties; Tee, K. L., Lu, L., Lai, M. O.; *Materials Science and Technology (UK)*, Volume 17, no. 2, pp. 201-206, Feb. 2001.
- [113]. Lower cost cast aluminum MMC process and products; Hunt, W.H. Jr., Schuster, D. M., Skibo, M. D., Smith, M. T., Herling, D. R.; *Minerals, Metals and Materials Society/AIME, State of the Art in Cast Metal Matrix Composites in the Next Millennium (USA)*, pp. 265-272, Oct. 2000.
- [114]. Synthesis of in situ Al-TiB₂ composites using stir cast route; Lu, L., Tee, K. L., Lai, M. O.; *Composite Structures (UK)*, Volume 47, no. 1-4, pp. 589-593, Dec. 1999.
- [115]. Wear behavior of TiNi shape memory alloys; D.Y. Li; *Script. Metall. Mater.*, 34, 195 (1996).
- [116]. New wear-resistant material: nano-TiN/TiC/TiNi composite; Y. Luo and D.Y. Li; *J. of Mater. Sci.*, 36 (2001) 4695-4702.
- [117]. The nature of reversible changes in M_s temperature of Ti-Ni alloys with alternating aging; Jinsong Zhang, Wei Cai, Xiaobing Ren, Kazuhiro Otsuka and Makoto Asai; *Materials Transactions, JIM*, Volume 40, No. 12 (1999), pp 1367-1375.

- [118]. Effects of precipitates on phase transformation behavior of Ti-49at%Ni film; Haobin Luo, Fenglan Shan, Yanling Huo, Yuming Wang; *Thin Solid Films* 339 (1999) 305-308.
- [119]. The effects of Ni₃Ti₄ precipitates on the R-phase transformation; Q. Chen, X. F. Wu and T. Ko; *Scripta Metallurgica et Materialia*, Volume 29, pp. 49-53, 1993.
- [120]. Microstructure and mechanical properties of neutron irradiated TiNi shape memory alloy; Y. Matsukawa, T. Suda, S. Ohnuki, C. Namba; *Journal of Nuclear Materials*, 271 & 272 (1990) 106-110.
- [121]. Effects of post-irradiation annealing on the transformation behavior of Ti--Ni alloys; A. Kimura, H. Tsuruga, T. Morimura, S. Miyazaki, T. Misawa; *Mater. Trans. JIM*, 34 Nov. (1993) 1076-1082.
- [122]. Restoration properties of neutron irradiated Ti--Ni shape memory alloys; T. Hoshiya, F. Takada, M. Omi, I. Goto, H. Ando; *J. Japan Inst. Met.* 56 (5), (1992) 502-508.
- [123]. Combustion synthesis of Ti--Pd and Ti--Ni--Pd high transition temperature shape-memory alloys; H. C. Yi, J. J. Moore; *Materials Science Forum*, 56-58, (1990), 735-740.
- [124]. Improvement of a Ti₅₀Pd₃₀Ni₂₀ high temperature shape memory alloy by thermomechanical treatments; D. Goldberg, Y. Xu, Y. Murakami, S. Morito, K. Otsuka, T. Ueki, H. Horikawa; *Scripta Metal. Mater.* 30 (1994). 1349-1354.
- [125]. High temperature shape memory effect of pre-deformation for Ti₅₀Ni₁₃Pd₃₇; Y. S. Li, Y. B. Jin, R. H. Yu; *Acta Metall. Sinica* 26 (1990) 113-116.